

**A novel method for determination of the filling
level within the feed frame of a rotary tablet press**

Dissertation

with the aim of achieving a doctoral degree

at the Faculty of Mathematics, Informatics and Natural Sciences

Department of Chemistry

Universität Hamburg

submitted by

Kym Patrick Dühlmeier

Hamburg 2019

Reviewer of the thesis:

Professor Dr. Claudia S. Leopold

Professor Dr. Hans-Ulrich Moritz

Professor Dr. Florence Siepmann

Thesis defense committee:

Professor Dr. Claudia S. Leopold

Professor Dr. Ralph Holl

Priv. Doz. Dr. Christoph Wutz

Date of thesis defense:

24th January 2020

Acknowledgements

This thesis was prepared at the University of Hamburg, Department of Chemistry, Division of Pharmaceutical Technology under supervision of Professor Dr. Claudia S. Leopold.

Foremost, I would like to thank Prof. Dr. Leopold for offering me this highly interesting research topic and for believing in me as a researcher as well as for giving me the opportunity to be a member of her research group. I want to express my deep gratitude for the interesting discussions, which guided me through my work as well as for the research freedom, which allowed me to work on my own ideas and projects and to develop myself personally and professionally.

Furthermore, I would like to thank Dr. Hüseyin Özcoban from Fette Compacting for the co-supervision of this work. I am grateful for the warm welcome I received during my progress reports in the Fette Compacting headquarter in Schwarzenbek. Dr. Hüseyin Özcoban motivated, inspired and supported me all the time. Moreover, I am grateful to Prof. Dr. Hans-Ulrich Moritz and Prof. Dr. Florence Siepmann for the evaluation of this thesis. Furthermore, I would like to thank Prof. Dr. Ralph Holl and Priv. Doz. Dr. Christoph Wutz for being members of the examination committee.

Furthermore, I would like to acknowledge my former and actual colleagues from the working group of Pharmaceutical Technology, especially for providing a great working climate and for the interesting discussions. I am grateful to all my friends for their understanding and patience during the last years.

Moreover, I dearly thank my family, especially my father, my mother and my sisters. You had a significant impact on this work, without you the next 222 pages would be empty.

Summary

Tablets are nowadays produced almost exclusively with rotary tablet presses. These presses usually regulate the compression force by the amount of die filling. Thus, the uniformity of many quality-relevant parameters of tablets depends on the uniformity of die filling which is carried out by special filling systems, the so-called feed frames, in which paddle wheels supply the powder to be compressed as homogeneously as possible to the dies. Because mass variations often occur during tablet production, which limit the production rate and/or lower the quality of the tablets, the functionality and performance of feed frames is the subject of current research. Therefore, the objective of this thesis was to gain a deeper understanding into the processes and phenomena occurring within feed frames, because the die filling process has a significant influence on the quality of tablets.

As so far, no suitable methods for the analysis of the powder supply for die filling within feed frames are available, a novel device needed to be developed. Therefore, the thesis mainly focused on the development and application of such a device for the analysis of the powder surface within feed frames. This device is supposed to enable an in-line monitoring of the powder filling level within feed frames and to provide several uniformity parameters for the characterization of the distribution behavior as well as the surface profiles of the powders within feed frames. The developed device consists of an instrumented feed frame, an electronic control system and software for sensor positioning, data acquisition, and evaluation.

The studies which were carried out in the present thesis deal among others with the suitability of the device for the monitoring of the filling level and the repeatability of the

measurement procedure. Furthermore, studies regarding the effect strengths of different process factors on the distribution behavior of powders within the feed frame and their effect on the tablet masses were conducted. The obtained data provides information on the causes of tablet mass variations in production processes and enables the optimization of tableting processes with regard to the uniformity of the final product.

It was demonstrated that the developed device is suitable for quantification of the filling level and the uniformity of the powder supply for die filling during tableting processes. Furthermore, it was shown that the tableting speed, the paddle wheel speed and the powders used for tableting all influence the filling level and the distribution behavior of the powders within the feed frame. In addition, a decrease of the filling level and a sudden refilling effect within the filling chamber of the feed frame have been observed at the end of tableting runs, which both may affect the tablet masses under certain process conditions. Moreover, initial distribution irregularities of the powders within the filling chamber were detected, which persisted through the tableting process and represent a possible cause of tablet mass deviations. In addition, evidence was found that a certain paddle wheel geometry (roundrod) may contribute to an improved inflow of powder into the filling chamber and may promote the mass uniformity of the tablets.

Zusammenfassung

Tabletten werden heutzutage fast ausschließlich mit Rundläufertablettenpressen hergestellt. Diese Pressen regulieren die Presskraft i.d.R. durch das Ausmaß der Matrizenbefüllung. Die Gleichförmigkeit vieler qualitätsrelevanter Parameter der Tabletten hängt damit von der Gleichförmigkeit der Matrizenbefüllung ab. Diese Matrizenbefüllung wird von speziellen Füllsystemen übernommen in denen Schaufelräder die Pressgüter den Matrizen möglichst gleichmäßig zur Verfügung stellen sollen. Da während der Tablettenherstellung häufig Massenschwankungen auftreten, wodurch die Produktionsleistung limitiert und/oder die Qualität der Tabletten herabgesetzt wird, sind die Funktionsweise und Leistungsfähigkeit von diesen Füllsystem Gegenstand aktueller Forschung. Die Zielsetzung dieser Arbeit war es daher mit geeigneten Methoden einen tieferen Einblick in Vorgänge und auftretende Phänomene im Füllsystem zu gewinnen, da der Matrizenbefüllungsprozess einen wesentlichen Einfluss auf die Tablettenqualität besitzt.

Da bisher keine geeigneten Messverfahren zur Analyse der Zurverfügungstellung von Schüttgütern in Füllsystemen verfügbar sind, entstand innerhalb dieser Arbeit ein Messsystem zur Pressgut-Oberflächenanalyse im Füllsystem, auf dessen Entwicklung und Anwendung sich die Arbeit fokussiert hat und auf welchem die durchgeführten Studien basieren. Das Messsystem ermöglicht eine Inline-Überwachung des Füllstands von Pressgütern in Füllsystemen, die Ausgabe mehrerer Gleichförmigkeitsparameter zur Charakterisierung der Pressgutverteilung und die Ausgabe von Pressgutoberflächenprofilen. Das Messsystem besteht aus einem instrumentierten Füllsystem, einer elektronischen Steuerung und Software zur Sensorpositionierung,

Datenerfassung sowie mehreren Auswertungsprogrammen für unterschiedliche Fragestellungen.

Die durchgeführten Studien befassten sich u.a. mit der Eignung des Messsystems zur Füllstandsüberwachung und der Reproduzierbarkeit des Messverfahrens. Des Weiteren wurden Studien zur Effektstärke unterschiedlicher Prozessfaktoren auf die Pressgutverteilung im Füllsystem und deren Auswirkung auf die Tablettenmassen durchgeführt. Die gewonnenen Daten geben Aufschlüsse über die Ursachen von Tablettenmassenschwankungen in der Produktion und ermöglichen die Optimierung von Tablettierprozessen hinsichtlich der Gleichförmigkeit des Produktes.

Es konnte gezeigt werden, dass das entwickelte Messsystem geeignet ist, während des laufenden Tablettierprozesses den Füllstand und die Gleichmäßigkeit der Zurverfügungstellung von Pressgut für den Matrizenbefüllungsprozess zu quantifizieren. Des Weiteren konnte gezeigt werden, dass die Tablettiergeschwindigkeit, die Schaufelradgeschwindigkeit und das verwendete Pressgut den Füllstand und die Pressgutverteilung im Füllsystem beeinflussen. Außerdem konnte eine Füllstandsabnahme sowie ein plötzlich auftretender Wiederauffülleffekt in der Füllkammer des Füllsystems zum Ende von Tablettierprozessen hin nachgewiesen werden, welche beide unter bestimmten Prozessbedingungen die Tablettenmassen beeinflussen können. Es konnten außerdem initiale Verteilungsunregelmäßigkeiten des Pressguts in der Füllkammer nachgewiesen werden, welche über den Tablettierprozess persistieren und eine mögliche Ursache für Tablettenmassenschwankungen darstellen. Zusätzlich wurden Hinweise gefunden, dass eine bestimmte Schaufelradgeometrie (Rundstab) zu einem verbesserten Zufluss von Schüttgut in die Füllkammer beitragen und die Massenhomogenität der Tabletten fördern kann.

List of Abbreviations

1D	One dimension
ADC	Analog to digital converter
ANOVA	Analysis of Variance
API	Active pharmaceutical ingredient
Av200	Avicel® PH 200
Av102	Avicel® PH 102
BUS	Binary unit system
CCC	Central composite circumference design
CCD	Central composite design
CCF	Central composite face centered design
cGMP	Current Good Manufacturing Practice
CMOS	Complementary metal-oxide-semiconductor
CPP	Critical process parameter
CQA	Critical quality attribute
DAC	Digital to analog converter
DAQ	Data acquisition
Destab	Destab® Calcium Carbonate 90SE Ultra 250
DoE	Design of experiments
EMA	European Medical Agency
Emc	Emcompress®
FDA	Food and Drug Administration
FFL	Foremost Fast Flo® Lactose 316
FIFO	First in first out
GMP	Good Manufacturing Practice
GPIO	General purpose input output
GUI	Graphical user interface
HPLC	High performance liquid chromatography
INT	Interspace
MUPS	Multiple unit pellet system

NIR	Near-infrared
OFAT	One factor at a time
PAT	Process Analytical Technology
PC	Personal computer
PE	Polyethylene
Ph. Eur.	European Pharmacopoeia
PMMA	Polymethylmethacrylate
PTFE	Polytetrafluoroethylene
PWR	Paddle wheel revolution
QbD	Quality by Design
S/N	Signal to noise
TDMS	Technical data management system
TTL	Transistor-transistor logic
USB	Universal serial bus
UV/Vis	Ultraviolet-visible
vF	Paddle wheel speed
VI	Virtual instrument
vT	Turret speed

Contents

Acknowledgements	III
Summary	IV
Zusammenfassung	VI
List of Abbreviations	VIII
Contents	X
1 Introduction	1
1.1 General aspects of pharmaceutical tablets	2
1.1.1 Powder flowability in context with pharmaceutical tableting	4
1.1.2 Characterization of the powder flowability	5
1.2 Production of tablets with high throughput rotary tablet presses	9
1.3 General aspects of feed frames	14
1.3.1 Operation principles of feed frames.....	14
1.3.2 Effects of feed frames on the bulk material.....	15
1.3.3 Instrumentation of feed frames.....	17
1.4 Pharmaceutical quality control with regard to QbD and PAT initiatives	19
1.5 Characterization of analytical techniques for process monitoring	21
1.6 Feedback systems in rotary tablet presses	24
1.7 General aspects of data acquisition systems	27
1.8 General aspects of rotary encoders	29
1.9 General aspects of laser triangulation	31
1.10 General aspects of data acquisition software	34
1.10.1 Prototyping of software with LabVIEW.....	35
1.11 Design of Experiments	38
1.12 Objectives of this work	44
2 Materials and Methods	45
2.1 Materials	46
2.2 General Methods	49
2.2.1 Powder characterization.....	49
2.2.1.1 Determination of the particle size distribution.....	49
2.2.1.2 Determination of the bulk and the tapped densities.....	49

2.2.1.3	Characterization of the powder flowability by the flow through an orifice.....	49
2.2.1.4	Characterization of the powder flowability by a ring shear cell tester.....	50
2.2.2	Technical equipment.....	52
2.2.2.1	Instrumented tablet press feed frame.....	52
2.2.2.2	Laser triangulator.....	53
2.2.2.3	Linear precision stage.....	55
2.2.2.4	Incremental rotary encoder.....	57
2.2.2.5	Data acquisition hardware.....	57
2.2.3	In-house written software.....	58
2.2.3.1	Data acquisition software.....	58
2.2.3.2	Data evaluation software.....	58
2.3	Specific methods for the off-line monitoring of the powder filling level.....	61
2.3.1	Tablet press off-line setup.....	61
2.3.2	Enclosurement of the filling chamber.....	62
2.3.3	Powder loading into the enclosed filling chamber.....	63
2.3.4	Experimental designs of the off-line experiments.....	65
2.3.4.1	Suitability of the developed device to monitor the powder filling level.....	65
2.3.4.2	Distribution behavior of powders within the enclosed filling chamber.....	67
2.3.4.3	Influence of the paddle wheel geometry on the powder distribution.....	68
2.4	Specific methods for the in-line monitoring of the powder filling level.....	70
2.4.1	Tablet press in-line setup.....	70
2.4.2	Simplification of the experimental feed frame setup.....	71
2.4.3	Experimental designs of the in-line experiments.....	75
2.4.3.1	In-line monitoring and determination of the factor influences on the selected responses.....	75
2.4.3.2	Comparison of the paddle wheel geometries.....	76
3	Results and Discussion.....	79
3.1	Suitability of the developed device to monitor the powder filling level.....	80
3.1.1	Evaluation of the powder characteristics.....	80
3.1.2	Evaluation of the mean powder surface profiles of Emc.....	82
3.1.3	Evaluation of the PWR filling levels of Emc.....	85
3.1.4	Conclusion.....	90

3.2	Distribution behavior of powders within the enclosed filling chamber.....	91
3.2.1	Characterization of the investigated powders.....	91
3.2.2	Comparison of the surface profiles of the investigated powders.....	92
3.2.3	Comparison of the PWR filling levels of the investigated powders.....	98
3.2.4	Conclusion.....	100
3.3	Influence of the paddle wheel geometry on the powder distribution.....	101
3.3.1	Comparison of the powder surface profiles.....	101
3.3.2	Factor influences on the filling levels	106
3.3.3	Conclusion.....	109
3.4	In-line monitoring of the powder filling level.....	110
3.4.1	Powder surface profiles during the tableting process.....	110
3.4.2	Filling level of the feed frame and the resulting tablet masses.....	114
3.4.2.1	Steady state PWR filling levels during the tableting runs.....	116
3.4.2.2	Decrease of the PWR filling levels during the tableting runs.....	123
3.4.2.3	Initial inhomogeneities in the powder filling levels.....	125
3.4.2.4	Factor influences on the feed frames' filling level and the tablet masses.....	128
3.4.3	Conclusion.....	131
3.5	Comparison of the paddle wheel geometries during tableting.....	133
3.5.1	Conclusion.....	139
4	References.....	140
5	Appendix.....	162
A	Supplementary data.....	163
A.1	Design matrix evaluation (Study 2.3.4.1).....	163
A.2	ANOVA of Emc PWR filling level (Study 2.3.4.1).....	172
A.3	Design matrix evaluation (Study 2.3.4.2).....	175
A.4	ANOVA of Emc PWR filling level (Study 2.3.4.2).....	178
A.5	ANOVA of Destab PWR filling level (Study 2.3.4.2).....	180
A.6	ANOVA of Av200 PWR filling level (Study 2.3.4.2).....	182
A.7	ANOVA of FFL PWR filling level (Study 2.3.4.2).....	184
A.8	ANOVA of Av102 PWR filling level (Study 2.3.4.2).....	186
A.9	Design matrix evaluation (Study 2.3.4.3).....	188
A.10	ANOVA of Av102 PWR filling level - flat rod paddle wheel (Study 2.3.4.3).....	191

A.11 ANOVA of Av102 PWR filling level - round rod paddle wheel (Study 2.3.4.3)...	193
A.12 Design matrix evaluation (Study 2.4.3.1).....	195
A.13 ANOVA of Av102 PWR filling level (Study 2.4.3.1).....	196
A.14 ANOVA of Av102 tablet mass (Study 2.4.3.1).....	198
A.15 ANOVA of Av102 tablet mass with nonsignificant factors (Study 2.4.3.1).....	200
A.16 ANOVA of Av102 tablet mass SD (Study 2.4.3.1).....	202
A.17 ANOVA of Av102 tablet mass SD with nonsignificant factors (Study 2.4.3.1).....	204
A.18 ANOVA of Destab PWR filling level (Study 2.4.3.1).....	206
A.19 ANOVA of Destab PWR filling level with nonsignificant factors (Study 2.4.3.1).....	208
A.20 ANOVA of Destab tablet mass (Study 2.4.3.1).....	210
A.21 ANOVA of Destab tablet mass SD (Study 2.4.3.1).....	212
B Curriculum vitae.....	214
C Conference contributions and publications.....	215
D Hazardous materials.....	217
E Declaration on oath / Eidesstattliche Versicherung.....	218

1 Introduction

1.1 General aspects of pharmaceutical tablets

Tablets with an estimated market value of more than 300 billion dollars per year and approximately 80 % of the total pharmaceutical production are the predominant dosage form for oral drug delivery [1]. In general, tablets are single-dose solid pharmaceuticals that are produced by compaction of powders or granules with tablet presses. The chemical, physical, microbiological, and thus, storage stability of tablets, their ease of handling during packaging and distribution as well as their cost-efficient manufacture are only some of the advantages of tablets compared to other dosage forms leading to their predominance on the market [2]. Moreover, coatings may be applied to tablets to facilitate the intake, to provide taste masking, to protect sensitive active pharmaceutical ingredients (APIs) against moisture or light, as well as to control drug release [3–7]. The possibility to apply imprinted codes indicating the tablet composition and the dose allow to unambiguously identify dosage forms, whereby the safety of the drug delivery system may be increased [8,9].

In addition to the API, tablets consist of a variety of excipients with different functions to either improve the tablet properties and/or the manufacturing process [10–12]. Common tableting formulations consist of fillers and binders (such as microcrystalline cellulose or lactose), lubricants (such as magnesium stearate), glidants (such as fumed silica) and disintegrants (such as croscarmellose sodium) [1,11,13–16]. These excipients are usually pharmacologically inert, but they may have an effect on drug release and therefore on the bioavailability which both may affect the performance of the pharmaceutical product [15,17]. Regarding the manufacturing process, the composition of the formulations may influence the flowability of the bulk material which often requires the adjustment of several process parameters [18,19]. Therefore, during formulation development suitable

excipients have to be selected for the quality assurance of the production process and the final product.

1.1.1 Powder flowability in context with pharmaceutical tableting

The flowability of powders is relevant for various productional operations of pharmaceutical tablets, such as storage, transport, blending and tableting process [20–25]. Regarding the tableting process, the flow behavior of the powder in the supply hopper, within the filling system and during the die filling process may be critical for the uniformity of the tablets [26,27]. Common problems that may occur during the mentioned process operations are flow disturbances and/or bridging with poorly flowing powders and segregation in the case of good flowing powders because of vibrations or shear stress [28–30].

The flowability of powders is influenced by many parameters [31–33]. Some of these are substance-specific, for example the chemical structure, the true density, the crystal lattice, the electrical conductivity, the electrostatic properties, the particle shape, size, and size distribution, the friability, the porosity, the surface roughness and activity, and the moisture content of the powder [2,34–38]. Additionally, the history of applied stress and the bulk density may influence the flow behavior [39,40]. Because of the complexity of the relationship between these factors and the flowability, it is almost impossible to describe the flow behavior of a powder based on all influencing factors sufficiently by a mathematical formula. Therefore, it is necessary for many processes to characterize the flow behavior of the bulk material experimentally.

1.1.2 Characterization of the powder flowability

A variety of techniques is available to characterize the flow behavior of powders [41–48]. In the European Pharmacopoeia (Ph. Eur.), the angle of repose, the flow through an orifice, and ring shear measurements are described as characterization methods for the powder flow behavior [49]. In addition to these pharmacopoeial methods, there have been introduced numerous other methods to characterize the flow behavior such as horizontally or vertically rotating cylinders and vibrating spatulas [41,50–53]. The suitability of a characterization method may vary depending on the production step, for which the flow behavior is investigated [54,55]. Several of these available methods are conventional methods with many parameters that may influence the measurement outcomes and therefore must be kept constant in the experimental setup. Regarding the flow through an orifice method, the geometry of the hopper, the material and roughness of the hopper surface, the powder filling level, the pre-consolidation of the powder within the hopper and the time period between filling and measurement are some of the parameters that may influence the outcome of the experiments [56–58]. However, because of the low costs, simple operation, short measurement time and the similarity to some pharmaceutical production steps, this method is principally suitable to get a first impression of the flow behavior of a powder but compared to other characterization methods the reproducibility is rather poor because of the variety of variables influencing the investigation of the flow behavior [53,59]. To determine the flow properties of powders, characterization methods which allow a defined handling of the powder samples prior to the measurements show a higher reproducibility and therefore should be preferred [60].

A defined handling of the powder samples may be carried out in uniaxial compression experiments (Fig. 1).

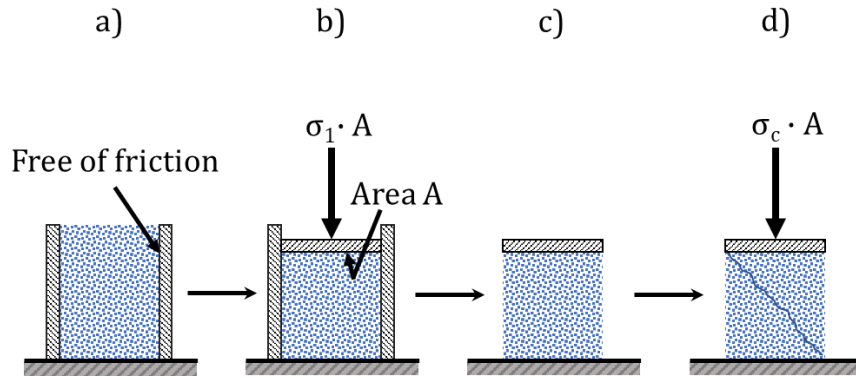


Fig. 1: Schematic illustration of the uniaxial compression experiment. The side walls are assumed to be free of friction. σ_1 : major principal stress, σ_c : unconfined yield strength.

In these experiments, a powder sample is densified and thus solidified in a mold, for example in a hollow cylinder, by a vertically applied stress σ_1 which is also referred to as major principal stress (Fig. 1a). The volume of the powder sample is reduced by the application of the major principle stress. Therefore, the process can also be referred to as compaction (Fig. 1b). The inner wall of the mold is assumed to be free of friction [61]. The more compressible the powder, the more pronounced the volume reduction [62]. The major principle stress thus simultaneously leads to a densification and a solidification of the powder sample (Fig. 1c). After removal of the mold, an increasing stress is vertically applied to the solidified powder sample (bulk solid) until the bulk solid breaks (fails) (Fig. 1d). This stress, which is also referred to as unconfined yield strength σ_c , is a measure of the flowability of the powder [63]. The breaking process of the bulk solid which is also referred to as "incipient flow" can be understood as plastic deformation under density decrease, because the distances of the individual particles increase in the area of the fracture surface [63]. As the bulk solid only fails at a sufficiently large vertical stress,

which is equal to the unconfined yield strength, there is a material-specific yield limit for the bulk solid. Only if this yield limit is reached the bulk solid starts to flow. However, this yield limit of the bulk solid is also dependent on its stress history, i.e. its previous consolidation: The higher the major principle stress, the higher the bulk density and the unconfined yield strength. Several measurements with different major principle stresses (σ_1) lead to value pairs (σ_1, σ_c). With these pairs a curve may be created with the major principle stress on the x axis and the unconfined yield strength on the y axis whereby the unconfined yield strength increases with increasing major principle stress. This curve is referred to as the flow function and may be used to quantify certain flow properties of powders. Powders with lower flow functions at the same major principle stress possess better flow properties [64].

Based on the principles of uniaxial compression experiments, instruments have been developed which are referred to as shear cell devices [65–67]. Because of the good reproducibility of the measurements, these devices have become a standard for the assessment of powder flow properties [68–71]. Ring shear cells have the advantage over other types of shear cells as they theoretically enable the investigation of an unlimited shear load because of the annularity of the shear cell [72]. This feature allows to detect changes in the flow behavior of powders which may occur over long time periods or distances, for example during transport through pipelines, as a result of shear loads acting on the powder [73,74]. Modern ring shear cell devices automatically carry out these measurements and report the results immediately. A typical ring shear cell device is shown in Fig. 2.

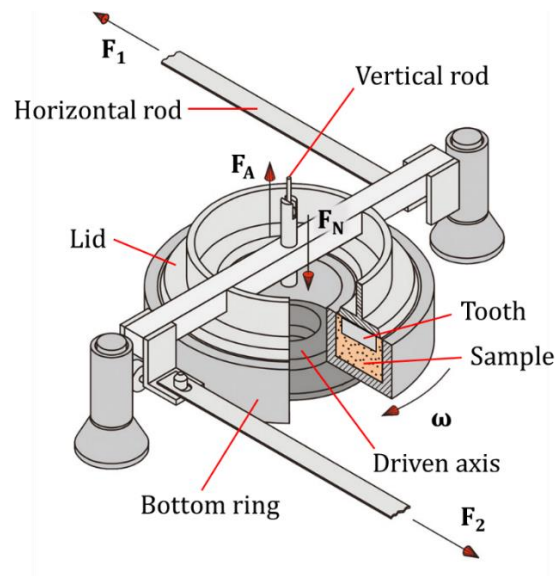


Fig. 2: Schematic illustration of a ring shear cell [63]. A vertical normal force (F_N) is transmitted centrally by a rod to the lid. The forces F_1 and F_2 , which result from the rotational movement (ω) of the bottom ring, are transmitted to sensors.

In ring shear cell devices, the powder sample is located within a bottom ring which is mounted on an electrically driven rotational axis. A lid which is not in contact with the side walls of the bottom ring is placed on top of the powder sample. Teethes are attached to the lid which dip into the powder sample to interlock the powder with the lid. A vertical normal force is transmitted centrally by a rod to the lid and is automatically varied during a series of subsequent measurements. Forces which result from the powder sample properties, the applied vertical normal force and the rotational movement of the bottom ring are transmitted to sensors by two horizontal rods attached to the lid. These forces are directly proportional to the shear stress which is acting on the bulk solid because of the shear deformation caused by the rotational movement [63]. With this technique it is possible to characterize the flow properties of powders in different states of consolidation and to compare powders with each other, both with a high reproducibility [68,75].

1.2 Production of tablets with high throughput rotary tablet presses

The manufacturing of tablets is a multi-step process that may consist of the unit operations powder blending, granulation, compaction, tablet coating and packing (Fig. 3) [76].

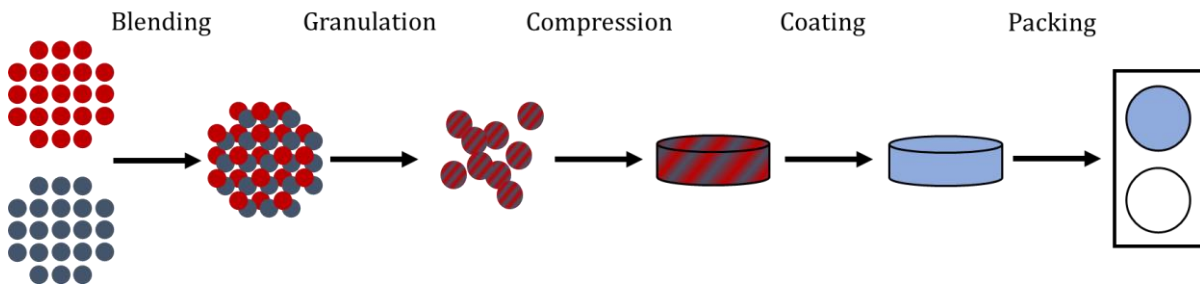


Fig. 3: Tablet manufacturing flow chart.

Nowadays, the processing from powders to tablets in an industrial scale is almost exclusively carried out on high-speed rotary tablet presses, which are able to produce up to 1.6 million tablets per hour [77].

The processing of the powder within these tablet presses can be subdivided into further single operations which are carried out at defined stations within the tablet presses, namely the filling station, the dosing station, the pre-compression station, the main compression station and the ejection station which are all located around a rotating die table (Fig.4). This die table contains the dies, i.e. the moles in which the powder is compressed into tablets. Pairs of punches which each consist of an upper and a lower punch rotate with the die table and thus with their corresponding die. Thereby, the upper and the lower punches are moved up and down by sliding cams to the desired positions at the operational stations of the tablet press.

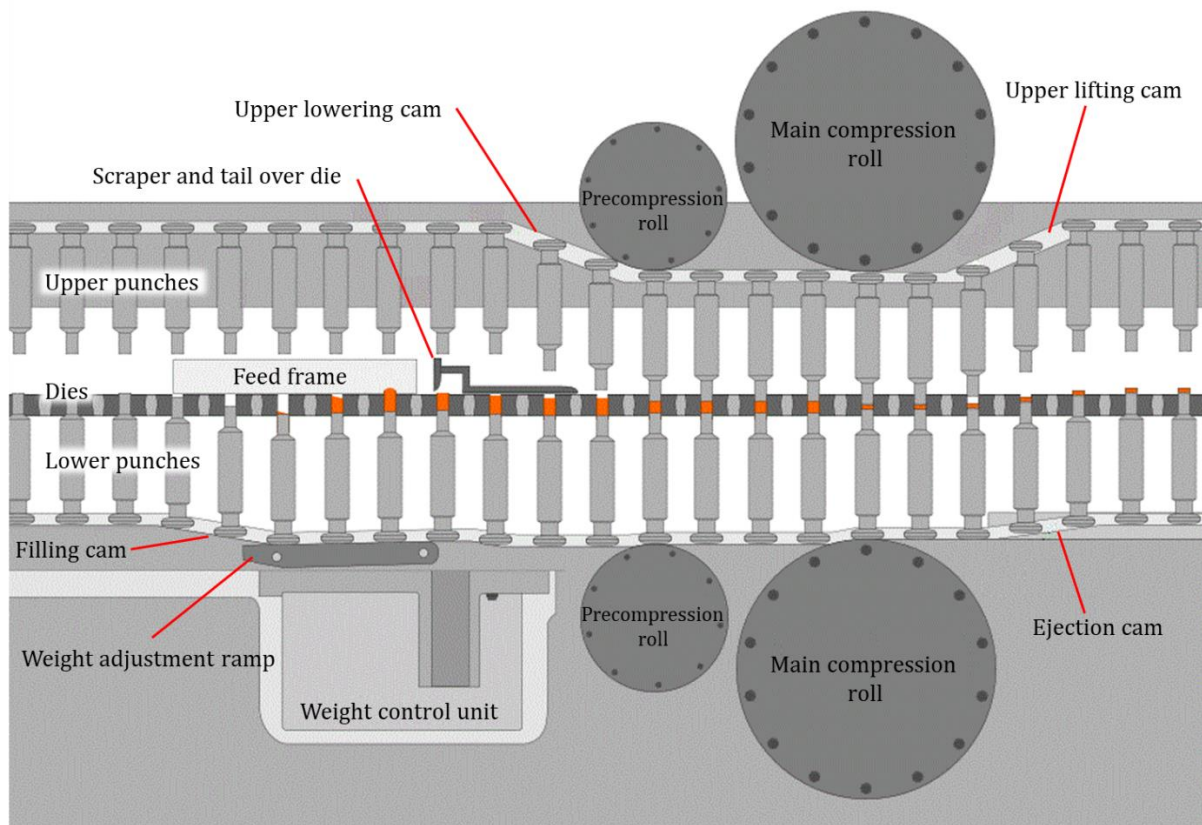


Fig. 4: Schematic illustration of the processing of bulk material within a rotary tablet press modified from [78].

The production process within the tablet press starts at the filling station:

1. *Filling station:* A die with the corresponding pair of punches is moved by the rotation of the die table to the filling station. Within the filling station, the lower punch, which up to this point was co-planar to the top-edge of the die is pulled down by a sliding cam, the so-called filling cam [79]. The downslide of the lower punch takes place below the filling chamber of the feed frame which provides the bulk material required for die filling. The downslide of the lower punch causes a suction effect within the die, by which a portion of the bulk material which is located within the die filling area of the filling chamber is filled into the die. Thereby, the die filling process is enhanced as hardly any air needs to be removed

from the die and thus the possible maximum tableting speed increases [80]. During this filling process the die is first overfilled by moving the lower punch below its final filling depth position which is controlled by the weight adjustment ramp at the end of the filling process of the die at the dosing station [81].

2. *Dosing station:* Within the dosing station of the feed frame, the lower punch is lifted by the weight adjustment ramp to reach the final filling depth whereby a portion of the bulk material is ejected from the die. This step is intended to promote the uniformity of die filling and thus the uniformity of the resulting tablet mass [82,83]. The excess bulk material is used for the filling processes of the subsequent dies because the ejection of the bulk material takes place within the dosing chamber which is connected to the filling chamber and allows a redistribution of bulk material between both chambers [84,85]. After the ejection of the material, a final dosing step is carried out by a scraper which removes bulk material from the dies planar to the die table, whereby the final amount of bulk material to be compacted is determined [84]. Because of centrifugal forces additional bulk material may be ejected from the dies between the scraper and the pre-compression station, by which the standard deviation and absolute mass of the resulting tablets may be affected [81]. The excessive powder, which is scraped of the dies is directed into a channel which is located within the die table. In this channel, the bulk material rotates together with the die table and is therefore redirected to the filling station. A lifter located in front of the filling system collects the bulk material and feeds it back into the filling system, by which the material is recycled [84]. This mechanism results in significant savings of bulk material.
 3. *Pre-compaction and main compaction:* During the described filling process of the dies, the upper punches are constantly pulled up and thereby moved along the
-

filling system. As soon as the dies leave the filling station, the upper punches are lowered by the upper lowering cam and inserted into their corresponding dies, whereby the orifices of the dies are closed and the bulk material is enclosed within the dies. The dies are now moved with the corresponding pair of punches to the pre-compression station, where both punches are pushed by the pre-compression rolls into the direction of the die center where pressure is exerted on the bulk material. The intention of a pre-compaction is mainly to remove air from the bulk material and to additionally solidify the bulk material directly after the filling process of the dies [86]. At high tableting speeds and thus a rapid compression of the bulk material may lead to “capping” or “lamination” of the tablets, which are common tablet defects occurring during tablet manufacture resulting for example from expanding air within the tablets after the compression step of the bulk material [87,88]. Within the main compression station, the maximum pressure is applied onto the bulk material by the compression rolls which regulate the hardness of the resulting tablets [88]. The position of the compression rolls which push the punches into the dies is usually constant in rotary tablet presses, whereby the applied compression force is regulated by the amount of powder in the dies [89].

4. *Tablet ejection:* After the compaction process the upper punches are lifted by the upper lifting cam and subsequently the lower punches are lifted by the ejection cam, whereby the tablets are pushed out of the dies [90–92]. The produced tablets are released from the lower punches by a scraper and directed along the scraper to a discharge chute for exiting the tablet press [93]. These discharge chutes may be instrumented for example with switches, by which the tablets with defects may be sorted out.
-

Commonly, between 6 and 100 dies are implemented in die tables of rotary tablet presses. A low number of dies is suitable for lab scale operations, galenic development, whereas high numbers of dies are preferred for production scale and up scaling. The number of implemented dies corresponds to the number of tablets produced per die table revolution if the tablet press is a so called single-sided tablet press. To increase the production capacity, tablet presses may be manufactured with larger die tables and/or with two production lines per die table. These machines are referred to as double-sided rotary tablet presses. In the case of double-sided rotary tablet presses, two tablets are produced per revolution and per die as these machines have two filling, dosing, pre-compression and main compression stations whereby only the half of a die table revolution is required for a complete processing from powder to tablets. These tablet presses allow a significantly increased production rate of tablets and/or a reduction of various problems related to high tableting speeds, because the turret speed may be reduced which still results in a sufficient production rate of tablets [81].

1.3 General aspects of feed frames

The feed frame is one of the major factors of influence on the uniformity of the tablet mass and it is the last component in the production process in which the bulk material is freely movable before it is separated by die filling and finally compressed into tablets [81]. In contrast to eccentric presses with stationary dies and a moving filling device, the filling devices in rotary tablet presses remain in position whereas the dies are moving [94]. The supply of bulk materials to these filling devices is usually guaranteed by a vertical pressure onto the bulk material within the hopper above the filling device, which is usually caused by gravitation. In addition, metal sheets or screw conveyors may be installed inside the hopper to assist the flow of the bulk material to the feed frame and/or to regulate the feed rate to the feed frame [95,96].

1.3.1 Operation principles of feed frames

Different types of filling devices are available on the market with different operational principles of die filling (Fig. 5). For instance, a centrifugal filling device is implemented in the IMA-Comprima tablet press (IMA Group, Ozzano dell'Emilia, Italy) which is positioned in the center of the press and fills the dies by a lateral opening in the dies through centrifugal forces acting on the bulk material [97,98]. This filling method offers advantages at high turret speeds and poorly flowing bulk materials and is particularly designed for high throughput tableting. However, these filling devices require special dies with a lateral opening and are not compatible with multi-tip tooling which is used to produce mini tablets.

Another type of filling device is the rotatable starwheel which is considered for multilayer tableting. These devices remain in position but rotate in their own axis and thereby supply the different bulk materials through different orifices to the dies. However, this method

of multilayer tablet production is only suitable for small batches, as a mass production of multilayer tablets preferably is carried out with rotary tablet presses equipped with multiple filling stations, in which one filling station is responsible for the supply of bulk material to only one of the tablet layers. The most common type of feed frame used nowadays is the chamber feed frame. Depending on the manufacturer, this feed frame may consist of one or more chambers in different dimensions and arrangements, which usually include paddle wheels in a variety of geometries [82]. This type of feed frame was investigated in this thesis because of its predominance on the market.

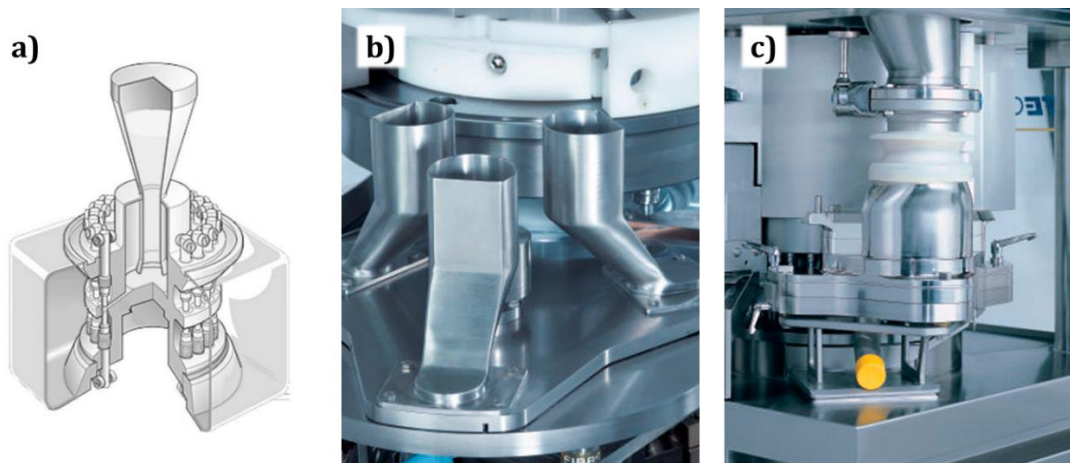


Fig. 5: Filling devices of rotary tablet presses: a) centrifugal filling device, b) rotatable starwheel, c) chamber feed frame [77,99].

1.3.2 Effects of feed frames on the bulk material

The paddle wheels within the chamber feed frames exert a shear stress on the bulk material, which differs depending on the paddle wheel geometry, the rotational speed of the paddle wheels and on the residence time of the powder within the feed frame [100,101]. The major effects of the applied shear stress are particle attrition, particle segregation, over-lubrication, and pre-compression, which all might influence the flow behavior of the bulk material into the dies and therefore the quality of the tablets [101–

103]. Depending on the paddle wheel geometry, paddles can have different distances to the ground plate, which may therefore lead to a different extent of attrition or grinding of the bulk material. Especially if granules or pellets are part of the bulk material, for example in multiple unit pellet systems (MUPS), such attrition effects in particular on coated pellets may unintentionally affect the drug release profiles of the tablets. For these applications special paddle wheels are available, which only cause slight particle attrition [101].

In addition to particle attrition, the shear stress which is applied to the bulk material in the feed frame may also lead to an over-lubrication, i.e. a too intense distribution of lubricants within the bulk material resulting from the intermixing by the paddles [103–105]. The concentration and distribution of lubricants in the bulk material can be considered as a critical quality attribute (CQA) as they may influence the hardness, friability, disintegration time and drug release of the produced tablets [106,107]. The lubricants reduce the wettability of the tablets, whereby the disintegration of the tablets is delayed in comparison to tablets with a low amount of lubricant and/or a low degree of lubricant distribution [106,108,109]. Moreover, the higher the degree of distribution of the lubricants within the bulk material, the tablet hardness decreases because certain particle interactions which promote a consolidation of the particles, e.g. cohesion forces, are formed to a less extent [109,110].

To prevent over-lubrication, the lubricants which are required to release the tablets from the dies and from the punch surfaces, i.e. to counteract sticking of the tablets to the dies and tablet punch surfaces are added to the bulk material in a last short blending process. Thereby, the lubricant is only distributed within the outer layers of the bulk material [76]. If the lubrication process leads to a lubricant distribution which can be considered as

close to over-lubrication, the bulk material may become over-lubricated by the shear stress during its residence time within the feed frame. Therefore, the total shear load within the feed frame has to be considered during tablet formulation development and during the lubrication process of the bulk material. These considerations are necessary to guarantee the quality and conformity of the tablets which may otherwise become out of specification regarding their quality attributes.

To keep the shear load of the bulk material low, the rotational speed of the paddle wheels should be selected to be as slow as possible, to avoid negative effects of the feed frame on the bulk material and the resulting tablets [111–113]. However, if the paddle wheel speed is too slow the supply of the bulk material for die filling becomes insufficient and the standard deviation of the tablet masses may increase [81]. The rotational speed of these paddle wheels is still determined empirically or by expensive preliminary tableting experiments because of an insufficient process understanding. So far, a general mathematical relationship between the complex flow behavior of the bulk material and the dynamic processes within the feed frames has not been developed to calculate an optimal rotational speed of the paddle wheels [47]. To determine an optimal rotational speed of the paddle wheels and/or to select an optimal geometry of the paddle wheels based on experimental data it is therefore necessary to gain a better understanding of the effects on the behavior of the bulk material within the feed frames.

1.3.3 Instrumentation of feed frames

To determine the drug content of the bulk material and/or to detect segregation effects within the feed frame, techniques for process monitoring within the feed frame have already been developed [114]. For example, near infrared (NIR) spectroscopy has been successfully applied to feed frames of tablet presses for real-time monitoring of the

homogeneity of the bulk material [112,115–117]. Moreover, instrumentation may be used to predict the residence time distribution of the bulk material within feed frames [118]. However, there is no device available yet for monitoring the distribution of the bulk material within feed frames. In the literature it was shown that a correlation exists between the chambers' filling level and a baseline shift of the spectra obtained by NIR probes [119]. Baseline shifts however, are complex events and they are susceptible to disturbances if used as variable for accurate distance measurements. For example, if the bulk material is altered, bands may occur at the wavenumber which was selected for the distance calculation. In this case, another wavenumber has to be selected which might possibly result in a different correlation between the baseline shift and the filling level. Therefore, a more universal technique is desirable to monitor the behavior of the bulk material within the feed frame.

1.4 Pharmaceutical quality control with regard to QbD and PAT initiatives

The production environment of pharmaceuticals is highly regulated by Good Manufacturing Practice frameworks (GMP) which were established in the pharmaceutical industry by regulatory authorities such as the Food and Drug Administration (FDA) and the European Medicines Agency (EMA) [120–122]. These frameworks are intended to specify the minimum requirements for an adequate manufacturing process to ensure product quality and patient safety by regulating critical aspects of the industrial environment such as personnel responsibilities and qualifications, equipment and facility standards, as well as analytical standards, packaging, labeling, distribution and documentation [120–124].

Because of these frameworks, the pharmaceutical industry is more strictly regulated compared to other branches of industry regarding changes of manufacturing processes and operational parameters, as these are usually accompanied by a periodic renewal of the approval by the regulatory authorities [125,126]. Thereby, the actual product quality and patient safety may be ensured by the authorities, but such a regulation may also impair improvements of the production processes and associated quality control procedures by the manufacturers [127–129].

To modernize pharmaceutical manufacturing, in 2004 the FDA introduced two initiatives: the ‘Pharmaceutical cGMPs for the 21st Century: A Risk-Based Approach’ [130] and ‘Guidance for Industry: PAT - A Framework for Innovative Pharmaceutical Development, Manufacturing, and Quality Assurance’ [129]. These initiatives and related guidelines [131] are intended to optimize the regulatory frameworks of pharmaceutical manufacturing and to facilitate innovations in pharmaceutical processing [127]. The

quality of the products as well as the production efficiency may therefore be more easily adjusted to the current state of science and technology and innovations are not excessively limited by regulatory restrictions [127,129,130].

In context with the PAT and QbD concepts, the FDA promotes the implementation of process analyzers that allow a continuous monitoring of the desired product attributes and process parameters instead of solely testing the end product quality [129]. A design space of process parameters may therefore be established to define a range of the process parameters in which a desired product quality can be ensured [126,132]. To set up such a design space and to control the process based on this framework, the real-time monitoring of relevant factors, such as the supply of bulk material for die filling, might be beneficial as it may be used to correlate the obtained information with the process parameters and quality attributes of the final product. The robustness of tableting processes may be improved by real-time monitoring, as it may be integrated within feedback loops to adjust critical process parameters (CPPs) based on the information obtained by the implemented process analyzers.

1.5 Characterization of analytical techniques for process monitoring

Traditionally, quality control has been performed off-line (Fig. 6a) by drawing small numbers of samples from the production stream and analyzing them subsequently in spatially separated laboratories [121,126,128]. For instance, to monitor the API content of tablets, a common method is to quantitatively dissolve the API of a tablet in a defined volume of a suitable solvent and subsequently to determine the API concentration in the solution by HPLC-UV/Vis. This procedure has been shown to be suitable for the quantitative determination of the API content in tablets. However, the procedure is destructive and therefore cannot be used in- or on-line within manufacturing processes to adjust the API content. In addition, because of the time-consuming determination of the API content in a tablet, HPLC-UV/Vis is unsuited for a real-time content control during tablet manufacturing. Therefore, such analytical methods are not implemented in feedback mechanisms [133–135].

To realize efficient real-time or near real-time monitoring of different CQAs during tablet manufacturing, analytical techniques are required which allow a straightforward sampling and a fast determination of the respective CQA, to allow an adjustment of the relevant process parameters within an acceptable time period [129,134]. This real-time process monitoring may be attained by analytical tools that allow at-line, on-line, or in-line measurements rather than off-line data acquisition [129,136]. A schematic illustration of the different types of monitoring is shown in (Fig. 6).

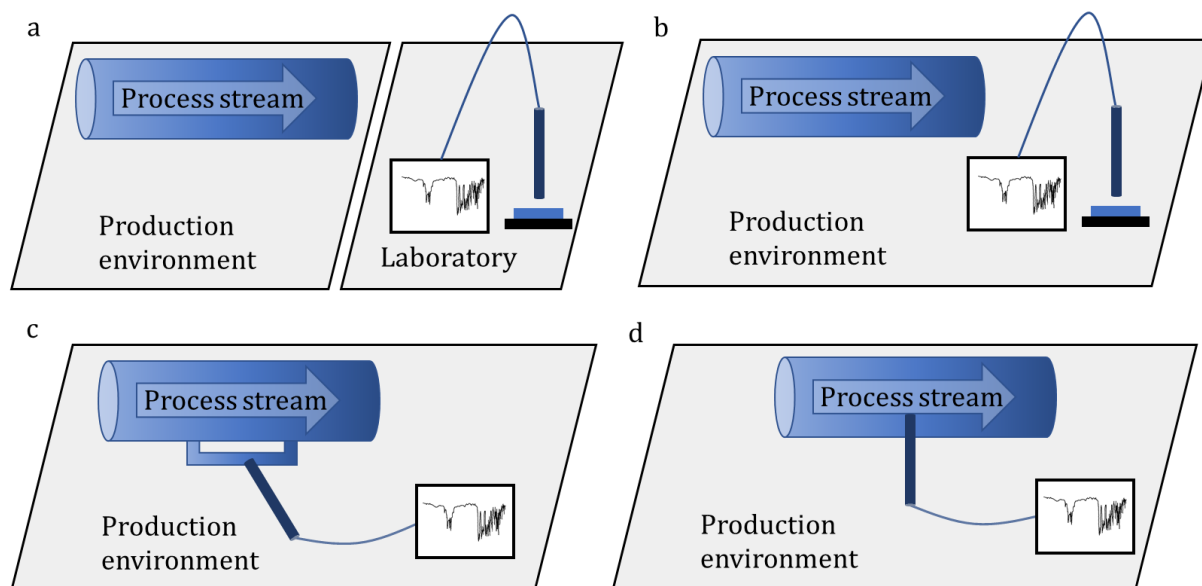


Fig. 6: Schematic illustration of the different types of process monitoring. (a) off-line, (b) at-line, (c) on-line, (d) in-line.

In the case of at-line measurements, the samples are removed from the process and analyzed in the production environment within the time course of processing [129]. The reaction time for readjustment of process parameters after detection of an insufficient product CQA is markedly shorter compared to off-line quality control and may therefore allow an adjustment the process if the specific CQA is still within the range of specification. An example for at-line measurements is the hardness testing of tablets, which may be drawn from the discharge chute of the tablet press. If the determined tablet hardness is too low, a readjustment of the compression force is possible, as these devices may provide a direct feedback to the tablet press.

During on-line measurements, samples are temporarily separated from the process stream, directed to an analytical device via a sampling by-pass and are fed back into the process after data acquisition [129]. During in-line process monitoring the sampling probe is directly placed into the machine and measures the material attributes directly

within the process [129]. Therefore, on-line and in-line monitoring differ essentially from the off-line and at-line measurements by the time required for receiving the desired information on the process parameters or material properties. On-line and in-line measurements therefore allow a continuous monitoring of processes and are potentially suitable for an automation of the product analysis and/or the adjustment of process parameters [134]. Therefore, a variety of sensors is nowadays implemented in modern high-speed rotary tablet presses to monitor and/or regulate the process by feedback mechanisms and control loops [89,137–140].

1.6 Feedback systems in rotary tablet presses

Nowadays the use of electronic control technologies is standard in many productional operations and essential for the robustness of many processes [141]. Regarding rotary tablet presses, some examples for such technologies are the control of the turret speed and/or the automatic separation of tablets which are out of specification from the production process by an air switch.

The turret speed of the tablet press may be considered as a CPP because it affects a variety of CQAs of the tablets such as the tablet masses and their corresponding standard deviation [81]. The turret speed is generated by a torque motor, which requires a certain power supply to reach the target speed [142,143]. The required power is proportional to the torque, which varies depending on the process conditions, such as the type of the mounted die table, the type and number of punches and the compression forces within the compression stations of the tablet press. Considering an energy conversion efficiency of 100 % by the engine, the relationship between torque M (Nm), rotational speed n (1/s) and the required power P (W) is shown in Eq. 1.

$$P = 2\pi \cdot M \cdot n \quad (\text{Eq. 1})$$

The actual turret speed is recognized by a rotary encoder, the functionality of which is described in more detail in chapter 1.8. The rotary encoder transmits the information on the actual turret speed to components of the data acquisition hardware of the tablet press. Based on the encoder information, the adjustment from the actual speed to the target speed of the die table is carried out by regulation of the power supply of the torque motor. In addition to the angular velocity of the turret, the encoder also provides information on the angular position of the turret and thus on the positions of the individual dies. In

addition to rotary encoders, compression force sensors are also implemented as standard in modern rotary tablet presses [144]. These sensors contain a Wheatstone bridge with strain gauge, whereby information on the maximum compression force of each single tableting event within the main compression station is obtained by an electronic signal. Because of the simultaneous acquisition of the compression force and the angular position of the die table, each compression force signal can be assigned to an individual tablet. The combined data processing of both sensors can be used to separate tablets by an air switch from the production batch, if deviations in the compression force occur, for example because of insufficient die filling with bulk material which is accompanied by exceeding the limit of the compression force [145]. For this mechanism to function successfully, the air switch has to be activated with a time delay referring to the time point of exceeding the compression force limit. This activation delay is integrated in the feedback mechanism of the software compounds but must be adapted to the individual production conditions. In particular, the actual turret speed, the position of the air switch and the tablet sliding properties in the discharge chute are main factors influencing the optimal time delay of air switch activation. By this feedback mechanism, at least with respect to homogeneous blends, tablets with API content deviations resulting from irregular die filling may be separated directly from the production batch.

These feedback mechanisms demonstrate how effective in-process control mechanisms may be for the safety and robustness of production processes, and these 100 %-controls in production processes are of particular importance. However, the described feedback loop for the separation of tablets does not allow the detection of content deviations, which are caused by inhomogeneous bulk materials. Far more complex technologies are required to determine the content of individual tablets in-line and without destruction

[8]. In this context, in-line technologies are developed, which are mainly based on spectroscopic methods [128,146–150]. For example, NIR techniques can be used to determine the API content by quantification of the absorption of a specific wave number by the API [128]. In addition, UV or NIR imaging methods are developed to quantify APIs on tablet surfaces and thereby assess the total API content and/or the API distribution within the tablets [151–155]. However, these techniques as well as the correlation of the compression force with the API content of the tablets is impaired, as for example segregation effects caused by vibrations of the tablet press, whereby the composition of the tablet surface may not be representative for that of the inner layers of the tablets [156]. The top and bottom surface of tablets may also differ in their composition because of segregation effects [157]. Factors which influence the correlation of the API content on tablet surfaces with the total API content in the tablets must be considered during development of PAT systems.

Although the final and in-line quality control of the API content by surrogate parameters (NIR/UV imaging of tablet surfaces or the compression force) provide an estimation of the process quality, an optimized and robust tableting process is ultimately crucial regarding the quality of the resulting tablets. To optimally adjust a tableting process, a comprehensive understanding of this process is required.

One reason for API content deviations of individual tablets are irregularities of the individual die fillings [158]. The investigation of factors influencing the die filling process is a major focus of this work. Thereby a better understanding of tablet mass variations and therefore API content deviations is expected by which options for an optimization of the production process of the tablets may be identified. For this purpose, the feed frame was instrumented with a newly developed data acquisition device.

1.7 General aspects of data acquisition systems

Data acquisition is the process of sampling signals that reflect real world physical conditions and the subsequent conversion of the resulting signals into digital numeric values that can be processed by a computer [159]. A data acquisition system can be illustrated schematically by a general basic structure shown in Fig. 7.

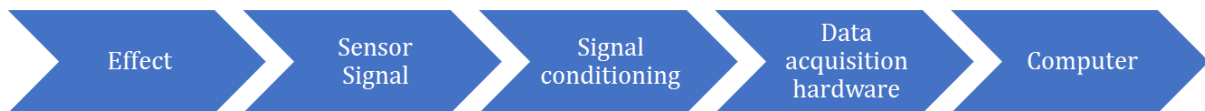


Fig. 7: Schematic illustration of a data acquisition system.

The sensor is receptive to the non-electrical variable (Effect). Physical or chemical effects are used to transform the non-electrical variable into an electrical signal. The signal conditioning circuits convert the output signal of the sensor into a "meaningful" electrical signal, i.e. a signal which is suitable for the next stage operation [160]. The signal conditioning contains electronic components such as amplifiers, filters, resistance change circuits (e.g. Wheatstone bridges), and/or electronic components for error compensation [160]. Inside the data acquisition hardware, the incoming signals are typically digitized and transformed into appropriate interface signals for digital processing [160]. The hardware typically includes components such as multiplexers, amplifiers or analog digital converters (ADCs) [160].

Depending on the application, different computers, such as PCs, microcontrollers or other digital signal processors with corresponding peripherals, can be used for digital processing, analysis, presentation of results or generation of return values [160]. Because of the rapid development computing technology, these elements of data acquisition systems may nowadays have high computing power. Therefore, complex computational

algorithms may be used to evaluate process data in real time and adjust or intervene within the process based on the return values and commands which are passed through physical channels of the controller to peripheral process control elements.

These circuits may be simple, e.g. the activation of relays by a GPIO channel of the microcontroller, which may be used to regulate circuits of larger voltages or currents. However, more complex information can also be passed on to peripheral components via different data transmission protocols (BUS systems) [161]. Thus, by serial and binary data transmission from microcontrollers to circuits further processing steps or actions based on the transmitted information may be carried out.

Before assembling a data acquisition system, the technological requirements of the data acquisition hardware have to be determined. The number and type of signals which have to be acquired, any necessary signal conditioning, the need for synchronous or simultaneous detection, the frequency content of the measured variables, the permissible measurement uncertainty, the duration of the measurements and any necessary online calculations must be considered during the selection of suitable hardware [160].

1.8 General aspects of rotary encoders

Rotary encoders are sensors with which lengths, positions, speeds and angles can be determined [162]. Basically, one may distinguish between absolute encoders and incremental encoders. With absolute encoders, the position information is obtained based on a unique code information. As a result, no initial referencing is required with these sensors before measurements and therefore the actual position value is returned immediately. Absolute encoders can further be subdivided into singleturn encoders that detect movements with an angle of up to 360° and multiturn absolute encoders that can detect positions over several revolutions.

In contrast to absolute encoders, incremental encoders must be referenced before measurements, as in a currentless state a change of the angular position of the rotational axis is not detected. One option of referencing is a zero impulse, which is emitted once per revolution at a specific angular position by the encoder. Encoder increments may be generated via sliding contacts, photoelectrically or magnetically. In the case of magnetic incremental encoders, the material of the measuring scale consists of a magnetic code which is applied to a hard ferrite ring, the so-called pole ring. A sensor which is placed statically in front of the rotating pole ring recognizes the alternating north and south poles on the pole ring. In the evaluation electronics of the sensor head, called interpolation box, the magnetic signals are converted into digital electronic impulses commonly in 5 V TTL format. A logic gate in the data acquisition hardware interprets the signal as "high" (logic 1) as soon as the signal level exceed 2 V or as "low" (logic 0) as soon as the signal level falls below 0.8 V. Usually encoders possess 2-3 channels, namely the A, B and Z channel, whereas the Z channel is the zero or circumference impulse. The digital impulses A and B are phase-shifted by 90° whereby the +/-sign of the phase shift depends on the direction

of the movement of the pole ring. Each edge change of A or B is registered by a time period counter in the data acquisition unit as a counting step. With the signal A appearing first, the meter reading of the counter increases, while it decreases with the signal B appearing first. Depending on the resolution of the encoder, i.e. on the number of pulses per revolution, the number of pulses is converted into a corresponding change of the angular position, which allows within a temporal reference the determination of an angular velocity [163]. There are different modes for the edge count (Fig. 8) [164]. In X1 mode, only the rising edge of a channel is counted, in X2 mode, the rising edges of both the A and B channels are counted, while in X4 mode, which shows the highest spatial resolution, both the rising and falling edges of both channels are counted. Depending on which mode was selected, the conversion into a rotating position can be expressed by Eq. 2:

$$\text{Rotation angle (}^\circ\text{)} = \frac{\text{Edge Count}}{x \cdot N} \cdot 360^\circ \quad (\text{Eq. 2})$$

where N is the number of pulses generated by the encoder per revolution and x is the mode (1, 2, 4).

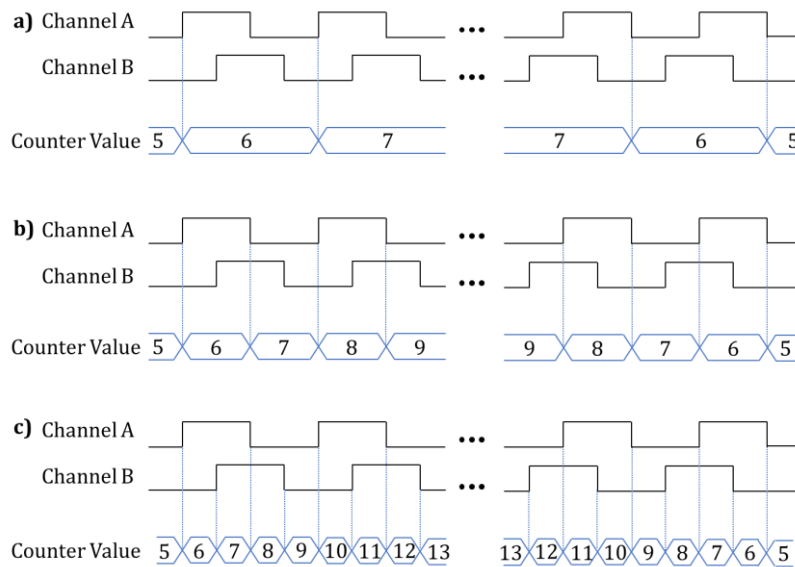


Fig. 8: Schematic illustration of the different modes of edge count: a) corresponds to X1, b) corresponds to X2, and c) corresponds to X4.

1.9 General aspects of laser triangulation

Several principles are known with which displacements of objects can be measured [165–170]. The displacement of an object to be measured, as well as the required precision of the measurements and the physical properties of the object, limit the appropriate measuring techniques [166]. The displacement measurements, which are presented in this study, are in the low millimeter range and can be realized by optoelectronic displacement sensors such as laser triangulators [171,172].

Laser triangulators are sensors for the determination of changes in the distance between the sensor and a target object and have been used in the industry for decades in a wide variety of fields [173–176]. Because of the individual measurement requirements many different sensors are available on the market. The most important differentiative features are the resolution, the measuring range and the measuring frequency of the sensor, as well as the parameterization options in the associated software [177,178].

Laser triangulation, by means of the geometrical measurement of triangular relationships with a laser beam can be explained as follows (Fig. 9): A beam emitted from a laser produces a light spot on a diffuse surface [179,180]. A portion of the light is scattered from the surface and projected onto a detector by a converging lens [181]. The detector usually consists of a spatially resolving CCD/CMOS chip, which is positioned at an inclined angle to the laser beam. If the surface is moved, the light spot is shifted along the path of the laser beam and thus the image of the light spot on the detector is also shifted. The displacement of the image (D_i) on the detector corresponds to the displacement of the surface (D_s) [182]. Even though the dusty environment inside a feed frame is challenging for optical distance measurements, a successful implementation of optical triangulation sensors even under these harsh conditions appears possible [183].

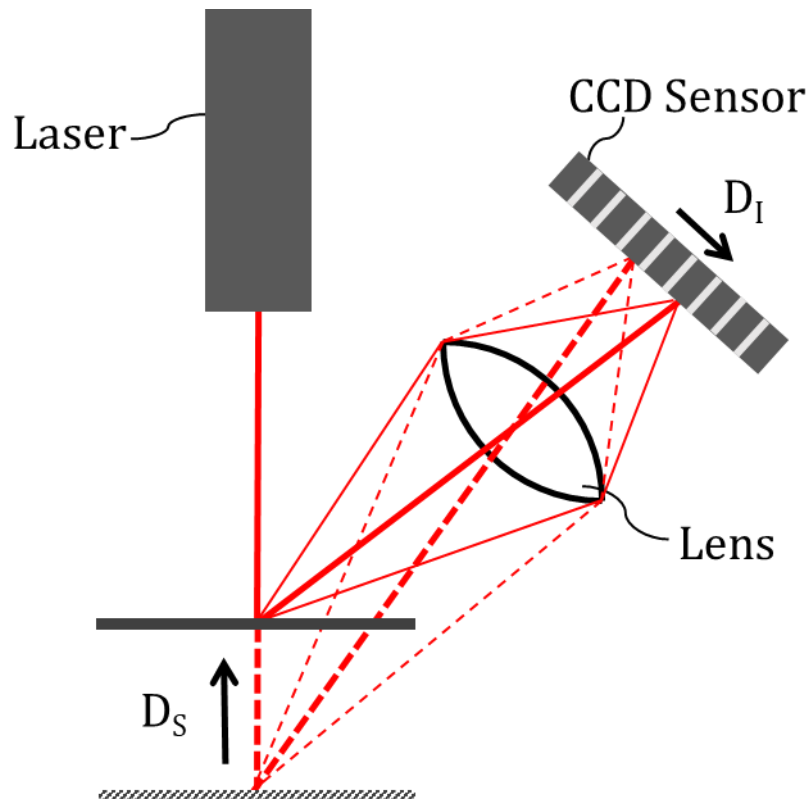


Fig. 9: Principle of laser triangulation.

If light impinges on a transparent plane-parallel plate, refraction occurs at each of the two interfaces [184]. The path of the laser beam follows Snell's law of refraction (Eq. 3):

$$n_1 \sin(\alpha_1) = n_2 \sin(\alpha_2) \quad (\text{Eq. 3})$$

where n is the refractive index and α angle of incidence.

The extent of the parallel shift depends on the angle of incidence, the thickness of the plate and the material of which it is made. The emerging beam is shifted parallel to the incident laser beam, if the media on both sides of the plate are of the same density (Fig. 10).

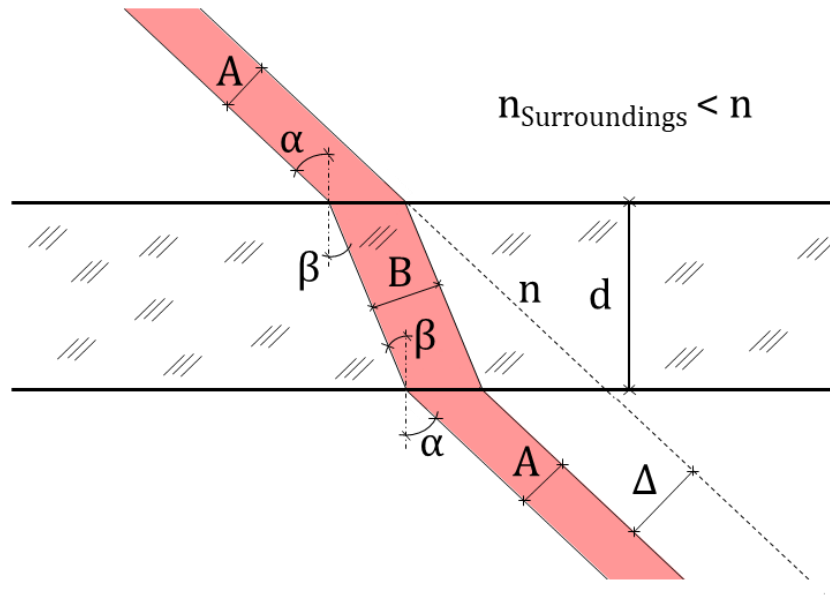


Fig. 10: Parallel shift of a laser beam if passing through an inspection window.

The parallel shift (Δ) increases, if the thickness (d) of the plate, the angle of incidence (α) and/or the refractive index (n) of the plate increases, which can be described by Eq. 4:

$$\Delta = d \cdot \sin(\alpha) \cdot \left(1 - \frac{\cos(\alpha)}{\sqrt{n^2 - \sin^2(\alpha)}} \right) \quad (\text{Eq. 4})$$

In the experimental setup of the present work, the laser beam emitted from the laser triangulator vertically enters the plane plate and passes straight through it, because its angle of incidence is zero. However, the diffusely reflected laser spot undergoes a parallel shift as it is detected by the triangulation principle at a lateral angle to the plane parallel plate by a video chip. The resulting signal shift was considered during signal processing and was compensated for by scaling of the signal within the software of the developed measuring system.

1.10 General aspects of data acquisition software

The functionality of a computerized measuring instrument requires certain software components that enable the communication of the electronic components with each other and the processing of the generated data. The operating system forms the basis for loading, executing, pausing and terminating the used applications. It is an assortment of computer programs for the management of the computer's system resources, e.g. the Random Access Memory, hard drives, input and output devices, and for the provision of these resources for the used applications (e.g. data acquisition and evaluation software) [185]. For communication with the individual electronic components of the computer and thus also with the data acquisition hardware, drivers for the hardware of the system are necessary. These drivers usually communicate directly with their associated hardware components and thus exchange control and data signals over a physical hardware communication bus. Furthermore, the hardware drivers offer the operating system and/or the programmer a standardized interface with which the hardware can be addressed in the same standardized manner as similar hardware from other manufacturers or with another electronic design. Depending on the hardware interface, these hardware drivers can be very complex and are therefore usually offered by the manufacturers of the electronic component together with the hardware. The application programmer therefore does not have to know the exact design of the electronic hardware nor does he need to understand the complex hardware-related binary communication protocols of the components to program applications. The operating system with hardware drivers offers the programmer less complex and thus understandable and easy to program interface (virtual machine) compared to the much more complex underlying machine [186].

The application software required for the present work has to solve the tasks of acquiring, analyzing and presenting the measurement data as well as controlling the components of the measuring device. A variety of programming languages are available to formulate the required data structures and algorithms. These programming languages differ mainly in their syntax, i.e. the pattern in which statements are formulated. So-called higher-level programming languages use an abstract and problem-oriented expression that is easy to understand for humans and can be automatically translated into machine language. Depending on the application, some programming languages are therefore better suited than others, as they have been optimized for a problem-oriented approach.

1.10.1 Prototyping of software with LabVIEW

The software components developed in this thesis are realized / programmed with LabVIEW. LabVIEW is a graphical programming language with which program codes may be generated by a selection of graphical elements, so-called virtual instruments (VIs), and their structuring is performed in a graphical block diagram by data flow oriented wiring of the VIs [187]. The basic idea of LabVIEW and its principle of graphical programming is to structure software for measuring instruments similar to their electrotechnical structure [188]. This development approach of the measuring instrument software offers advantages but also has disadvantages [189]. With LabVIEW, the graphical user interface of the software (front panel), the communication with the hardware and the algorithms of the data evaluation can be developed according to this principle. In addition, the developers of LabVIEW also provide data acquisition (DAQ) hardware for which the pre-built LabVIEW program code blocks are optimized, eliminating compatibility issues between hardware and software [160].

LabVIEW offers a library of input and control elements as well as visualization elements. These elements on the front panel are linked to corresponding elements in the block diagram, from which data can be transferred to the front panel in the case of visualization elements, or as variables in the case of input elements to the program code.

In the block diagram the program code is formulated by wiring the VIs together. Accordingly, the VIs correspond to objects or functions and have wiring connections through which input parameters are passed to the VIs and/or output parameters are returned from the VI. Wiring errors in the program code can be sometimes recognized directly. For example, if an incorrect data type is transferred, the corresponding wire immediately displays an error. Furthermore, the visualized data flow can be slowed down to find erroneous links in a program sequence.

A disadvantage of programming with LabVIEW is that a program code may become confusing for the programmer during development. The wiring of the VIs can take up much space in the block diagram and thus can make it hard to understand the data flow in the program code. Another disadvantage of programming with LabVIEW is the complicated translation into text-based programming languages. Many programming languages behave like dialects of a common language and can therefore be translated into one another by simple changes in the syntax. However, in the case of the translation from LabVIEW to text-based languages, a completely new program code has to be developed that may only have the data flow structure in common with the LabVIEW program code [190]. If it is intended to use a different programming language than LabVIEW in the further development of the instrument prototype, this effort of translation should be considered in the development process.

Nonetheless, LabVIEW allows a relatively simple development of software for measurement instruments with a user-friendly graphical user interface (GUI) and good compatibility with the data acquisition hardware. Therefore, LabVIEW was selected as the programming language in the present work.

1.11 Design of Experiments

Design of experiments (DoE) is used in many industrial branches, for instance, in the development, optimization and robustness testing of manufacturing processes [126,131,191–195]. These processes can be described by the influencing factors as input variables and the responses as output variables (Fig. 11) [196].

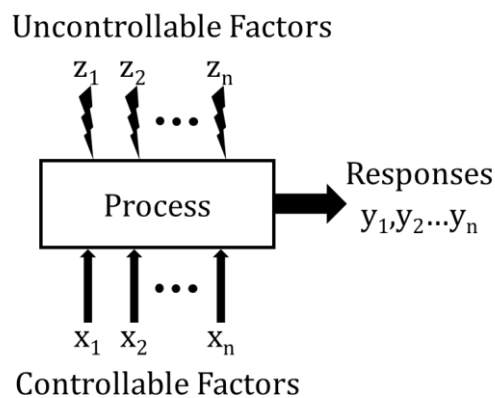


Fig. 11: Schematic illustration of a process with uncontrollable (z) and controllable (x) factors as input variables and responses (y) as output variables.

If the influences of several factors on a response need to be investigated, experiments in which only one factor is varied per experiment (OFAT experiments) are obsolete, as no interactions with the other factors may be detected, which might possibly show a crucial influence on the investigated process. Instead of OFAT experiments with a limited gain of information, in DoE experiments several factors are varied simultaneously and the overall effect on the response is measured. Based on the entire experimental design space, the effect of each factor on the response as well as factor interactions can be recognized. From a certain number of factors on, it is also possible to skip experiments, which results in time and cost savings, but may reduce the information of the experimental design. In the case of high numbers of factors, it is therefore advisable to determine main and minor factors empirically prior to the creation of an experimental design and possibly exclude

factors which, in comparison to the major factors, probably have only a low influence on the response and may unnecessarily increase the number of experiments.

Although the expected polynomial of a response surface is usually unknown, the strengths of factors are initially determined by two-level full factorial experimental designs or two-level fractional factorial experimental designs (Fig. 12) [197]. In these designs, all factors are varied on only two levels, which are referred to as low level (-1) or high level (+1). These levels which circumscribe the design space, must be selected carefully, because if the high and the low level are too close to each other depending on the S/N-ratio, effects of these factors on the response might not be detected. Likewise, extreme levels should be avoided, as at these levels unrepresentative effects may occur.

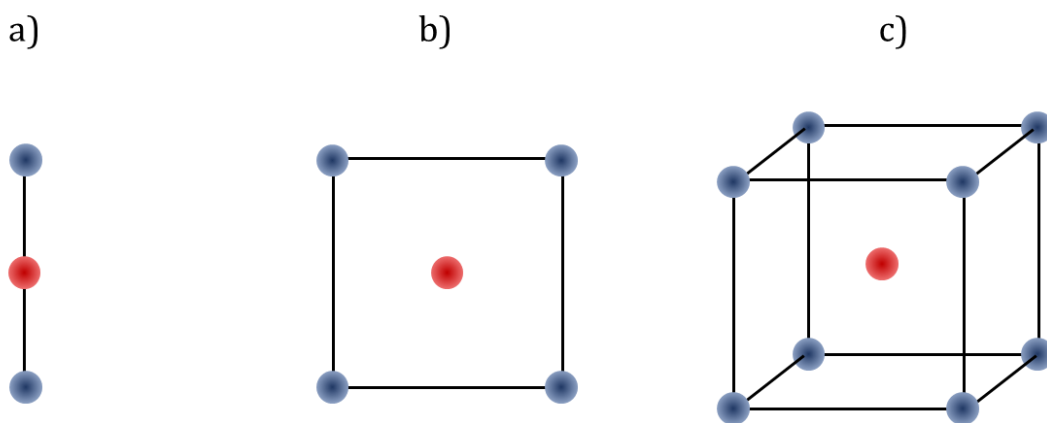


Fig. 12: Examples of factorial designs with additional center points: a) two-level-one-factor (OFAT), b) two-level-two-factors, and c) two-level-three-factors. The blue dots represent the factorial points whereas the red dots represent the additional center points.

The choice of appropriate levels is crucial for the validity and the success of the experiments and require process understanding by the scientist. All other factors which are not included in the experimental design must be kept constant. If they cannot be kept

constant and are therefore disturbances, they have to be monitored because they may falsify the determination of the actual factor effects on the responses.

However, these experiments are only suited to estimate the factor influences within the range of the investigated factor levels if these influences are linear. To check the factor influences for linearity, two-level full and two-level fractional experimental designs can easily be augmented by center point experiments as long as all investigated factors of the screening remain in the experimental design. These experimental points are located at the center of the design space and may also be used to determine the S/N-ratio of a response which corresponds to the mean of measurements divided by its standard deviation. Therefore, these center point experiments are repeated several times, whereas the remaining factorial point experiments are only carried out ones. To estimate the significance of the factor influences within the entire design space, the standard deviation of the center point responses is applied to the factorial point responses. This approach might be criticized, as a process is often more stable at the center point than at the factorial points. If the deviation of the actual response values at the center point exceeds the standard deviation of the response surface model a lack of fit is significant. In this case it may be assumed, that the influence of the investigated factors on the response cannot be described by a linear model and additional terms have to be added to fit the model to the actual relationship between the investigated factors and the response. Therefore, additional experimental design points have to be added, to determine a response surface with a higher polynomial. For example, a suitable augmentation of an experimental design to determine quadratic terms of the response surface are star points, resulting in so-called central composite designs (CCDs) (Fig. 13). These designs are referred to as composite designs because they are built of three blocks, namely the already described factorial experiments (corners) of the two-level factorial design, replicated center points, and star

points which are symmetrically arrayed to the factor axis. These star points may be located at different distances to the center point resulting e.g. in central composite circumference designs (CCC) or central composite face centered designs (CCF).

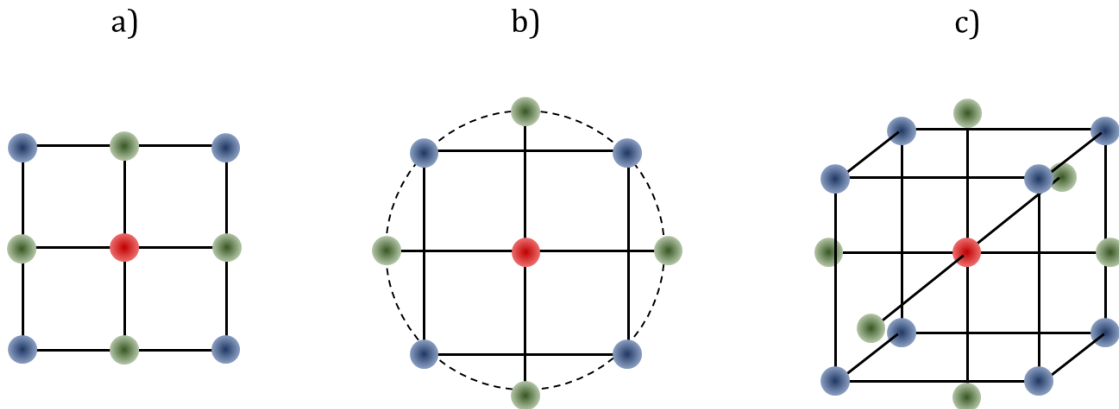


Fig. 13: Examples of central composite designs (CCDs). a) two-factorial face centered design (CCF), b) two-factorial circumference design (2^2 -CCC), and c) three-factorial circumference design (2^3 -CCC).

In CCCs, the star point and corner experiments approximate the surface of a sphere, hence these design spaces are symmetrical. As the star points in CCCs are located outside the low and the high settings of the factors, the factors are investigated at five different levels which allows an estimation of quadratic terms with high rigor.

In CCF designs however, the star points are located plane to the factorial points whereby the star point and corner experiments approximate a surface of a cube which may also be considered as a symmetrical design space. Although these designs only result in three levels of each factor, they still support quadratic terms because they contain a sufficient number of experiments. On the one hand, CCF designs may be of advantage compared to CCCs, because factor levels that are plane to the factorial points are often easy to adjust in processes and the results of the experimental points may also be easily interpreted by the

scientists. On the other hand, CCF designs might be inferior to CCC designs as CCCs comprise a larger volume of the design space than CCFs, if the same settings of the low and the high level of the factors are applied in both experimental designs. Moreover, the investigation of five different factor levels also allows a better capture of strong curvatures by which even a cubic response behavior might be modeled. Therefore, CCCs should be preferred over CCFs, unless an extension of the design space beyond the factorial points is impossible.

However, CCDs are only suitable for a limited number of factors, as CCDs with too many factors result in an immense number of experiments. Therefore, these experimental designs should be avoided if more than approximately 5 factors (resulting in at least 26 experiments) have to be investigated. Moreover, these experimental designs are not always applicable, because the factors are not allowed to have constraints within the experimental design space. Alternatives to these symmetrical designs which allow the investigation of high numbers of factors are non-symmetrical optimal designs. Computer algorithms determine the optimal distribution of the design points within the design space, either to optimize the estimates of the specified model coefficients (D-optimal) or to optimize the prediction variance around the model (IV-optimal). These designs can also be augmented stepwise to any polynomial and allow constraints of the factors which are considered within the distribution of the design points within the design space. Because of the non-symmetric distribution of the factor levels, individual runs cannot be interpreted by the scientist, which is a disadvantage of these designs.

However, the planning and performing of experiments with the DoE approach offers many advantages compared to OFAT or unfocussed trial and error experiments. It is an organized approach with which the scientist is guided to perform a structured set of

experiments, which is adequate for the selected objective. Experience showed that DoE requires fewer experiments than any other approach. As all experiments belong to an experimental plan, they are mutually connected in a logical and theoretically favorable manner. Thus, with the implementation of the methodology of DoE more useful and precise information on those factors which significantly influence a response may be assessed by the investigation of the joint influence of all factors and by a defined number of experiments [126,131,191-195,198].

1.12 Objectives of this work

Rotary tablet press feed frames are supposed to ensure a uniform die filling and, thus, to guarantee the weight and content uniformity of the resulting tablets. Therefore, a constant bulk availability and flow within the feed frame is crucial and has to be assured by the feed frame design and the operating conditions. As there is no instrument available yet to monitor the powder availability and/or the powder distribution within feed frames, one aim of the present thesis was to investigate whether the filling level within the feed frame may be quantified by laser triangulation combined with the angle recognition of the paddle wheel via rotary encoder. It was also investigated, if it is possible to detect differences in the distribution behavior of powders within the filling chamber of the feed frame with the newly developed device. For this study five powders with different flowabilities were selected.

Further aims of this thesis were to investigate if the powder filling level inside the feed frame is affected by the feed frames' paddle wheel speed and/or by the turret speed and whether the filling level affects the resulting tablet masses while filling the respective dies. For this study, two tableting excipients one with poor flowability and one with excellent flowability, were selected.

Moreover, the influence of two different paddle wheel geometries on the distribution behavior of a powder within the filling chamber was investigated. Furthermore, these paddle wheels were compared regarding their influence on the resulting tablet masses during the tableting process. For this study one tableting excipient with poor flowability was selected.

2 Materials and Methods

2.1 Materials

In the present work, 5 different excipients, namely Emcompress® (Emc; JRS PHARMA, Rosenberg, Germany), Destab® Calcium Carbonate 90SE Ultra 250 (Destab; Particle Dynamics, Saint Louis, USA), Avicel® PH102 and Avicel® PH200 (FMC BioPolymer, Wallingstown, Ireland) further referred to as Av102 and Av200, respectively, and Foremost Fast Flo® 316 (FFL; Foremost Farms, Penny Lane, USA) were selected. These powders were selected because of their different powder characteristics resulting in different flow properties and/or presumably different distribution behaviors within the tablet press feed frame.

Emc is a water-insoluble functional filler for wet granulation and direct compression which consists of calcium phosphate dihydrate. Emc offers improved flow for many powder blends [199,200]. It served in this study as a model powder for an excellently flowing material with a high bulk density and a low cohesivity.

Destab is a co-processed filler/binder for tablets, which consists mainly of calcium carbonate and approximately 10 % of pregelatinized starch. It shows fast densification and excellent flow properties which makes it suitable for high speed tableting [201]. Destab is used in this study as a model for an excellently flowing material with a lower density compared to Emc. Destab was lubricated with 3% of magnesium stearate by a drum hoop mixer (Erweka, Offenbach, Germany) for 7 min. The high percentage of lubricant was selected because of sticking problems at the punch surfaces with Destab observed in preliminary tableting experiments.

Av102 consists of microcrystalline cellulose and is one of the mostly used fill-binders and may be used to produce very hard tablets [202]. In the literature, Av102 is described as a reference standard for a powder with a flow behavior between acceptable and poor

during high speed direct tableting [71]. Consequently, plain Av102 tablets show a higher standard deviation with regard to their tablet masses compared to excellently flowing powders. Av102 showed no problems with respect to sticking to the punch surfaces or discharge from the dies during tableting and may therefore be compressed without any lubricant.

Av200 consists of microcrystalline cellulose and possesses an excellent flowability [202,203]. The powder was selected, because it differs from Av102 mainly by the particle size and may therefore be used for comparative purposes of both powders.

FFL is a product composed of a spray-dried mixture of crystalline and amorphous lactose monohydrate. FFL is used primarily for direct compression of tablets and in capsule filling [204]. Moreover, it is used for high throughput tableting as a filler/binder. It has better flow properties than Av102 despite a comparable mean particle size. It is therefore intended to serve as reference material for Av102 to compare the distribution behavior within the feed frame of different powders with similar particle size distributions but significantly different flow behaviors.

Scanning electron micrographs of the investigated powders at 500x magnification are shown in Fig. 14. The Emc particles show a rough surface whereas the Destab particles show a smooth surface and a spherical shape. The small particles between the larger particles of Destab may exert a ball bearing effect within the powder by which the flowability may improve. The particles of Av102 and Av200 consist of agglomerates of crystalline microneedles and amorphous cellulose and show a rough surface by which the flowability is decreased. Both powders differ mainly by their particle size distribution. FFL shows smaller particles in comparison to Emc, Destab, and Av200 and contains triangular crystals with a very smooth crystalline surface. The smooth crystalline surfaces

improve the flowability by reducing particle interactions compared to amorphous surfaces which are larger.

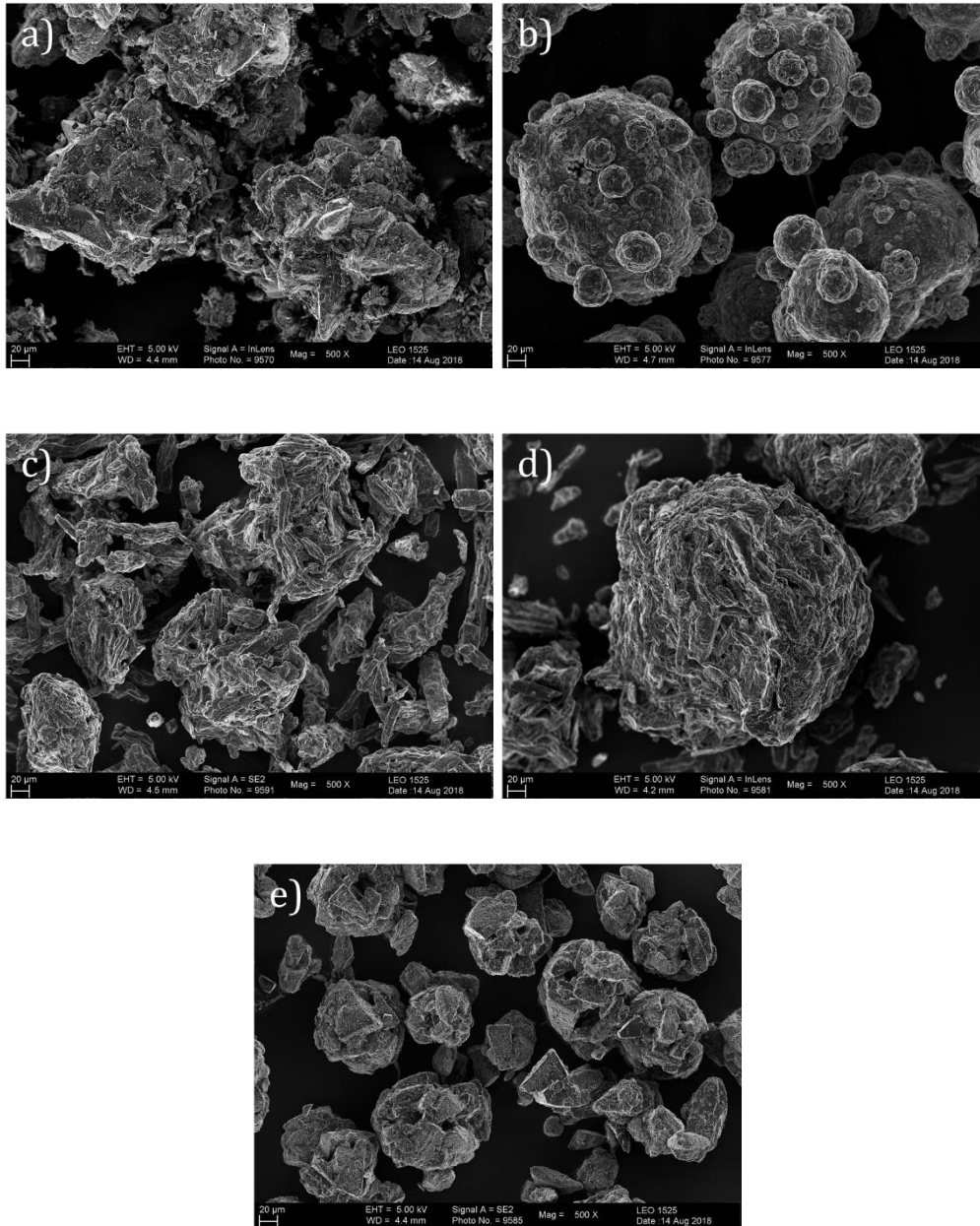


Fig. 14: Scanning electron micrographs of the powder particles at 500x magnification of (a) Emc, (b) Destab, (c) Av102, (d) Av200, (e) FFL.

For the tableting experiments magnesium stearate (Caesar & Loretz, Hilden, Germany) was selected as lubricant [16]. It is the most commonly used lubricant for tablets [205].

2.2 General Methods

2.2.1 Powder characterization

2.2.1.1 Determination of the particle size distribution

The particle size distributions of the powders were determined via laser diffraction (Study 3.1: HelosVR /RodosVR; Study 3.2: HelosKR /RodosKR, Sympatec, Clausthal-Zellerfeld, Germany). Compressed air of 1.5 bar was used to disperse the powders. All experiments were performed in triplicate.

2.2.1.2 Determination of the bulk and the tapped density

As the powders differ in their bulk density and compressibility, the powder bulk density was determined by filling a 250 ml measuring cylinder through a funnel with approximately 200 ml of the respective powder and subsequently determination of the respective mass of the powders by an analytical balance. The experiments were carried out in triplicate.

Tapped densities of the investigated powders were determined in a 250 mL graduated cylinder, mounted on a tapping machine (STAV 2003J, Engelsmann, Ludwigshafen am Rhein, Germany). About 100 g of powder were used to determine the tapped volume after 1250 taps (V1250). Each sample was measured in triplicate.

2.2.1.3 Characterization of the powder flowability by the flow through an orifice

In the flow through an orifice method, the time required for the Emc powder (100 g) to flow through a stainless-steel funnel with a 10 mm orifice was measured using a powder flowability tester (BEP2, Copley Scientific, Nottingham, United Kingdom) before and after each experiment of the study 2.3.4.1. Each sample was measured in triplicate.

2.2.1.4 Characterization of the powder flowability by a ring shear cell tester

A ring shear cell tester (RST-XS, Dietmar Schulze, Wolfenbüttel, Germany) with a 70 ml shear cell was used to perform powder flow testing with all investigated powders at pre-shear normal stresses of 1, 2.5 and 5 kPa. The shear cell was first overfilled with powder and then the excess powder was gently removed using a spatula to obtain a powder surface coplanar with the top of the two walls of the shear cell. The experiments were performed immediately after the excess powder was removed from the shear cell. To determine a yield locus, the powder samples were sheared to failure under five gradually increased normal stresses, which were lower than the pre-shear normal stress (Table 1). The sixth shear point was a repetition of the first one (the lowest normal stress). If the difference in the maximum shear strength between the first and sixth shear points was less than 5 %, changes in the powder properties because of shear testing were considered to be negligible [68,206]. The major principal stresses (σ_n) and the unconfined yield strengths (f_c) were obtained from each corresponding yield locus by drawing two Mohr's circles according to the standard procedure. By plotting f_c versus σ_n , the flow function profile of a powder sample was obtained.

Table 1: Overview of the stresses used for characterizing the flow properties of the powders. (#0-#6 represents the sequence of the normal stresses which were applied to the samples)

Pre-shear normal stress (kPa)	Normal stress used for yield loci (Pa)					
#0	#1	#2	#3	#4	#5	#6
1	330	448	565	683	800	330
2.5	825	1119	1413	1706	2000	825
5	1650	2238	2825	3413	4000	1650

2.2.2 Technical equipment

2.2.2.1 Instrumented tablet press feed frame

The novel instrument for the measurement of the filling level in the filling chamber of the feed frame is based on a 3-chamber feed frame (Fill-O-Matic®, Fette Compacting, Schwarzenbek, Germany) and is shown in Fig. 15. By mill-cutting parts of the chassis, space for the required technical equipment and an additional inspection window was created. The window material consists of 10 mm thick polyethyleneterephthalate modified with glycol (Vivak®, Bayer Material Science, Germany). To ensure a reproducibility of the sensor installations some connectors and spacers were added and fastened to the chassis.



Fig. 15: Instrumented feed frame.

2.2.2.2 Laser triangulator

For measurement of the powder surface level a laser triangulator, i.e. an ultra-high speed and high accuracy laser displacement sensor was chosen (LK-H052, Keyence, Osaka, Japan), controlled by a main controller unit (LK-G5001P, Keyence, Osaka, Japan). Technical specifications for both may be found in the respective data sheets. The location of the laser triangulator was chosen to be placed as close as possible to the die filling area. Sensor-internal parameters for determination of the displacement signal were identified by preliminary experiments. Settings which generate minimum noise of the displacement signal under extreme measuring conditions with a sufficiently high signal frequency were selected. The displacement signal was generated stepwise: At the frequency of 50.0 kHz, the light intensity peak used for triangulation was determined within the charge-coupled device (CCD) chip video signal. Assuming the peak farthest away from the sensor head to represent the powder bed surface signal, all other peaks regardless their intensities were ignored. To prevent turbid or dusty layers on the window surface or the window itself from erroneously being detected as powder surface, a restriction of the measuring range excluding the window was implemented within the video signal. Out of 15 following signals a median was determined. Consequently, the signal output frequency was reduced from 50.0 to 3.3 kHz. In case of a signal error resulting either from the diffuse reflected light intensity falling below its specified minimum, exceeding the maximum of the peak width, or the measuring range e.g. the powder bed being pressed against the inspection window, the last valid signal is hold until errorless signal conditions are regained. The processing steps inside the sensor led to a signal output delay of 570 μ s. This delay was compensated for by a rotational speed-dependent offset between encoder and distance signal in the evaluation software.

The scaling of the measured displacement signal to an analog output signal in voltage was set by a sensor system-related software (LK-Navigator 2, Keyence, Osaka, Japan) and transferred to the controller internal memory. Because laser distance measurements via triangulation through a window are distorted by Snell's law of refraction [207], a calibration model in terms of correction of the distortion was set up. Therefore, a reflector simulating the powder bed and fastened to a linear precision stage next to the feed frame's inspectional window and laser triangulator was installed, to determine the distortion by refraction. Initially, the parallel shift of the laser beam resulting from passing the window material was compensated by resetting the zero displacement position. Subsequently, the reflector was moved in 5.00 mm steps up to 15.00 mm and the corresponding displacement values were collected. Calibration was repeated three times, the mean being taken for scaling the signal. The displacement signals and the distance values correlate linearly. Eq. 5 was used to convert the displacement signals to the distance values:

$$S = 1.02042 \cdot d + 3.9333 \cdot 10^{-3} \quad (\text{Eq. 5})$$

where S is the displacement signal and d the distance value (mm)

Because of the analog signal transmission an attenuation of the signal occurs between signal amplifier and analog input module. Therefore, defined amplifier output voltages were set and the signal attenuation was determined by reading out the resulting voltages in the analog input channel of the data acquisition hardware. Eq. 6 describes the relationship between the analog output voltage of the signal amplifier and the voltage resulting at the data acquisition hardware:

$$AI = 0.99903 \cdot AO + 2.86667 \cdot 10^{-4} \quad (\text{Eq. 6})$$

where AI is the input voltage of the acquisition hardware and AO the output voltage of the signal amplifier.

Both equations were used to convert the input voltages into distance values with an interface software (Measurement and Automation Explorer, National Instruments, Austin, USA) which connects the applied hardware with the in-house programmed software used for data acquisition.

2.2.2.3 Linear precision stage

The laser triangulator was mounted to a linear precision stage (LPTM-30-50, OWIS, Staufen, Germany) to enable investigations of the powder behavior at different pitch circles inside the filling chamber. A spindle axis, actuated by a two-phase step motor moves the stage within a range of 50 mm on a linear axis at a speed of 4 mm/s. Before starting the experiments, the stage position was calibrated by moving the stage to a zero position defined by activation of hall sensors inside the stage chassis. The position of the stage is then controlled by counting the steps of the motor. This is implemented by a stage-related control unit (PS 10, OWIS, Staufen, Germany). A control unit-related DLL file (ps10.dll, OWIS, Staufen, Germany) was used to read out the real time position of the stage and to adjust the position of the stage by operational elements at the front panel of the developed data acquisition software. Deviations of the ideal alignment of the linear stage (Euler angles) and therefore the laser triangulator to paddle wheel rotational axis were determined by measurements of paddle wheel- and ground plate signals in an empty feed frame. These deviations were taken into account in the evaluation software and thereby compensated.

The distances between the stage positions, i.e. the positions for monitoring the powder surface and the center of the paddle wheel rotational axis were selected to be 45, 59, and 73 mm (Fig. 16). The lowest level of the stage position (45 mm), referred to as R45 throughout this work is the deepest possible position for measurements inside the filling chamber, limited by the feed frame's chassis and the sensor's size. The highest level of the

stage position, referred to as R73 is located 28 mm farther outside from R45. Up to R73 a triangulation to the ground plate is possible. Beyond R73, the laser spot on the ground plate is hidden by the feed frame's sidewall. Thus, measurements beyond R73 are only possible if the feed frame is filled with powder.

Because of the circular geometry of the filling chamber, the powder surface profiles obtained at different radiuses with the flat rod paddle wheel correspond to different circular arcs i.e. distances inside the paddle wheel interspaces. In this study, the interspace surface profiles of the powders obtained at R45, R59, and R73 correspond to 18.5, 28.8, and 33.1 mm of distance between the paddles.

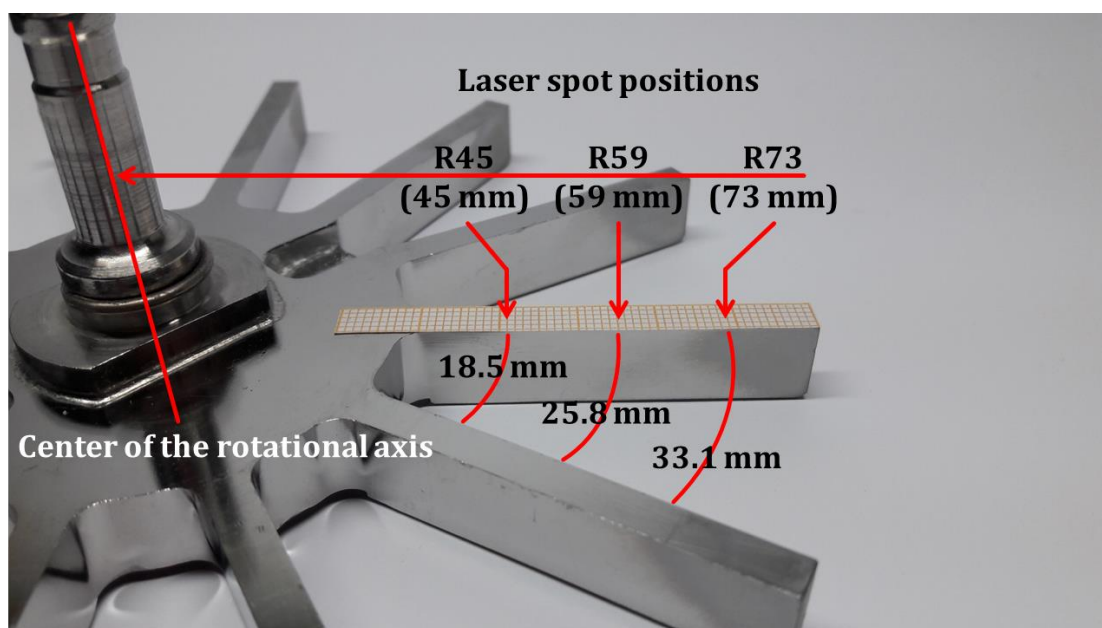


Fig. 16: Flat rod paddle wheel with the stage positions for monitoring the powder surface.

2.2.2.4 Incremental rotary encoder

For monitoring the angular position of the paddle wheel inside the feed frame a bearingless magnetic incremental rotary encoder was mounted (Fig. 15). The system consists of a magnetic ring and a sensor head (8.RI50.048.2000.112 and 8.LI50.1111.1064, Fritz Kübler, Villingen-Schwenningen, Germany). The system generates 4096 pulses and a zero pulse per revolution. TTL signals of the A-, B- and Z-channel are counted in X4 mode (the rising and falling edges were counted). Further technical specifications of both, the magnetic ring and the sensor head may be found in the respective data sheets.

2.2.2.5 Data acquisition hardware

The hardware used for data acquisition consists of a 4-slot high speed backplane (NI cDAQ-9174, National Instruments, Austin, USA) equipped with 4 integrated 32-bit counters and a USB connector for the data transmission. The first slot was equipped with a 4-channel differential analog input module (NI-9215, National Instruments, Austin, USA) which is capable to simultaneously sampling the analog input in 16-bit ADC-resolution within a range of ± 10 V and up to 100,000 signals per s. The second slot is equipped with an 8-channel, 100 ns bidirectional digital module (NI-9401, National Instruments, Austin, USA). Each channel is compatible with 5 V TTL signals. Further technical specifications may again be found in the respective data sheets.

2.2.3 In-house written software

2.2.3.1 Data acquisition software

The data acquisition and the adjustment of the stage position was performed by an in-house written software script (LabVIEW, National Instruments, Austin, USA). The software allows to acquire distance values of the laser triangulator, the stage position and the angle position of the encoder. Because of a shared sample clock and start trigger, the sampling tact and rate of these tasks which acquire these values are concerted and synchronized. A producer-consumer architecture inside the software prevents a data loss out of a FIFO-buffered queue before streaming the data to a technical data management system file, referred to as TDMS file. All channels apart from the stage position were stored in a 1D-array data format at a frequency of 2 kHz. The data of the stage position was stored only once per s to prevent an enlargement of the raw data files.

2.2.3.2 Data evaluation software

The evaluation of the raw data was performed by an in-house written software script (LabVIEW, National Instruments, Austin, USA). The software evaluates defined parts of the raw data TDMS files and stores the results and evaluation setting information in a newly created TDMS evaluation file.

The developed software consists of two algorithms, which were optimized for each of the two investigated paddle wheels. For the experiments containing the round rod paddle wheel the round rod algorithm was used; for the experiments containing the flat rod paddle wheel the flat rod algorithm was used.

Both algorithms return the powder surface level data in a format that corresponds to one (or multiple layered) complete paddle wheel revolutions, which are referred throughout the studies as “powder surface profiles”, as they represent only a cross-section of the total

powder surface, i.e. only the distance of the powder surface to the ground plate of the filling chamber at the respective monitoring position. If unintended deviations in the data subset length occur, for example by speed variations of the paddle wheel or, even worse, by false zero impulses of the encoder, the affected paddle wheel revolutions were excluded from the evaluation process. If the output is a powder surface profile of several revolutions, it corresponds to the arithmetic mean of the powder surface profiles of the individual paddle wheel revolutions. In addition to this average powder surface profile, the software calculates the standard deviation of the individual powder surface profiles. Furthermore, a single value, referred to as the “PWR filling level” throughout the studies, is calculated from the powder surface profile which corresponds to the arithmetic mean of the powder surface profile values, i.e. the arithmetic mean of the powder surface distances to the ground plate of the chamber after one or multiple paddle wheel revolutions. Moreover, the flat rod algorithm calculates 12 mean filling levels of the 12 individual paddle wheel interspaces, referred to as ‘INT filling levels’ throughout the studies, which correspond to the arithmetic mean of the distance of the powder surface to the ground plate of the filling chamber of the individual paddle wheel interspaces.

Both algorithms differ in the handling of paddle signals, which appear if a paddle passes the measuring position of the laser triangulator. The algorithm used with the flat rod paddle wheel deletes the respective data containing the paddle signals such that the paddles do not influence the calculation of the powder surface profile and thus the filling level. Moreover, a filter is implemented in the flat rod algorithm that reduces powder dust artefacts which may occur in the signal behind a preceding paddle because of powder which is shifted across a paddle. This phenomenon was reduced by an automatic exchange

of the artefact signals by the respective minimum value measured inside the paddle wheel interspace.

The algorithm used with the round rod paddle wheel replaces the signals of the round rods drawn high. It uses the values of the powder surface level measured to the left and to the right of the round rods drawn high to replace 50 % of the signals from these rods by the last value of the powder surface level measured to the left and 50 % by the first value of the powder surface level measured to the right. If a change in the powder level occurs below the round rods drawn high, it appears as a “step”. The low-drawn rods of the round rod filling wheel, which are always below the powder surface except for very low powder filling levels are not considered in the algorithm. The algorithm of the flat rod filling wheel does not consider powder, which is located below the flat rods. However, the filling levels of both algorithms are comparable, as both algorithms use only the powder surface to calculate the PWR filling level.

2.3 Specific methods for the off-line monitoring of the powder filling level

2.3.1 Tablet press off-line setup

In the present work a rotary tablet press 102i (Fette Compacting, Schwarzenbek, Germany) with a maximum tableting rate of 324000 tablets per hour was used (Fig. 17). However, in the off-line experiments, i.e. experiments within the enclosed filling chamber, the tablet press served only as a power unit to drive the paddle wheel within the filling chamber of the feed frame.



Fig. 17: Rotary tablet press 102i (Fette Compacting) with a maximum tableting rate of 324000 tablets per hour.

2.3.2 Enclosure of the filling chamber

The feed frames' filling chamber was enclosed for the offline experiments by closing all orifices, namely the dosing chamber, the partition plate orifice, the sealing segment and the outflow orifice with lids made of different materials (Fig. 18). These lids consisted of polytetrafluoroethylene (PTFE), polymethylmethacrylate (PMMA) and polyethylene (PE). The enclosure of the chamber was necessary to keep the factor level powder mass constant during the offline experiments.

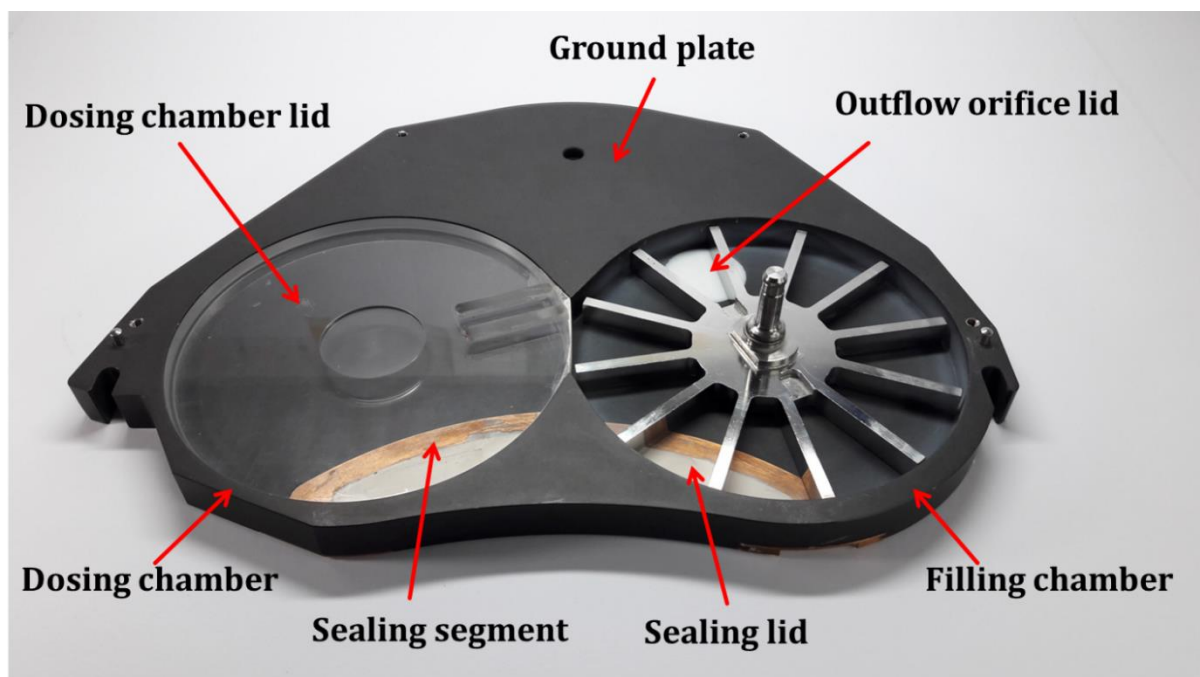


Fig. 18: Ground plate of the feed frame with different lids.

2.3.3 Powder loading into the enclosed filling chamber

To make sure that the amount of powder is inserted quantitatively into the filling chamber, the drill-hole of the standard inspection window was used for filling (Fig. 19). Therefore, a closeable orifice made of PTFE was implemented. The powder was inserted by a removable copper-pipe. To achieve a sufficient uniformity of powder distribution, 5.83 % (corresponding to 7 of 120 g of Emc) of the final amount of powder were first inserted into the chamber and the paddle wheel was rotated counterclockwise for 720 degrees. Subsequently, another 5.83 % of the final amount of powder were inserted and the paddle wheel was rotated clockwise again for 720 degrees such that the space between paddle wheel and ground plate is mostly filled with powder. Finally, the interspaces between the paddles were filled with equal portions of the remaining powder. Only into the first interspace 1.67 % (corresponding to 2 of 120g of Emc) of the final amount more powder were inserted compared to the remaining interspaces, because during the rotation of the paddle wheel (in 30 degrees steps) a part of the powder will redistribute leading to a decrease of the filling level inside the first interspaces. The rotation of the paddle wheel was controlled by real-time monitoring of the angle position by an in-house programmed software. This procedure leads to an expectable uniformity of powder distribution and was sufficient for the studies. To ensure that the correct total amount of powder was loaded into the filling chamber, the powder was collected and weighed again after each experiment.

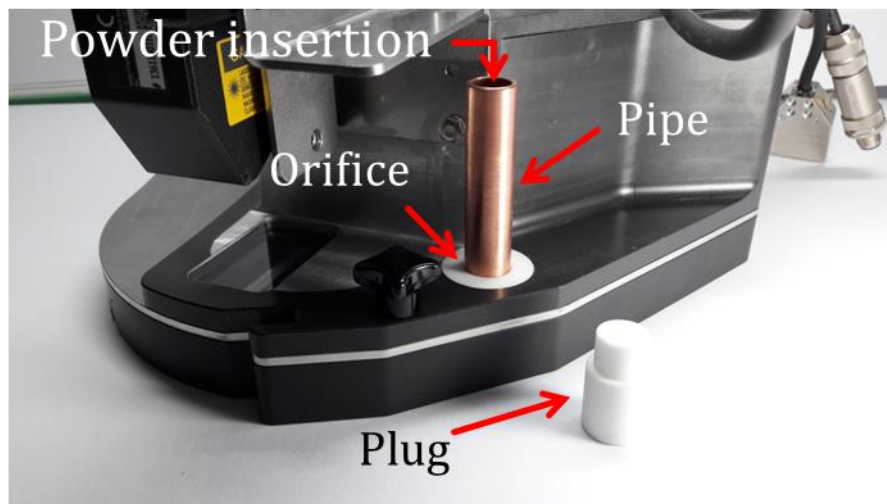


Fig. 19: Location of powder insertion.

2.3.4 Experimental designs of the off-line experiments

2.3.4.1 Suitability of the developed device to monitor the powder filling level

A factorial-lattice design with 75 experiments, each determined in triplicate was used to assess the suitability of the developed device to monitor the powder phenomena taking place inside the feed frame. This study was conducted with Emc. The influence of three factors, namely the 'powder mass' inside the chamber, the 'paddle wheel speed', and the 'monitoring position' of the powder surface were investigated. Both, the 'powder mass' and the 'paddle wheel speed' were varied at five levels whereas the 'monitoring position' was varied only at three levels. These levels have been selected by preliminary experiments. The experimental runs that included an identical amount of powder were carried out in a standardized sequence without refilling the chamber for each experimental run again with powder except for the repeat experiments (Fig. 20). The sequence started at the lowest level of paddle wheel speed, subsequently the paddle wheel was accelerated to next higher level until the highest level of the paddle wheel speed was reached. On each level of the paddle wheel speed the laser was shifted along all positions for monitoring before the paddle wheel was accelerated to the next higher level. The experimental design was planned and statistically evaluated using the Design Expert® software (Stat-Ease, Minneapolis, USA). The design matrix evaluation for the response surface quadratic model resulted in a variance inflation factor of 1.0 for all terms of the model indicating that coefficients are well estimated even if multicollinearities occur. Additionally, the experimental design provides high degrees of freedom for lack of fit and pure error which ensures a valid lack of fit test. The entire design matrix evaluation for the used experimental design can be found in the supplementary data section.

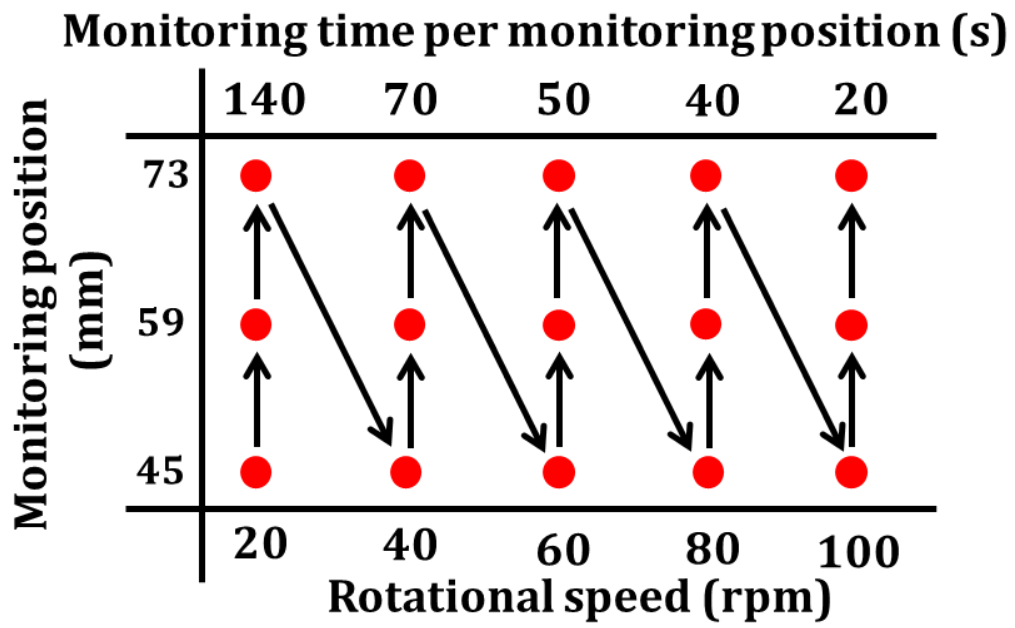


Fig. 20: Illustration of the experimental sequence. The points represent the respective amount of Emc powder (80, 100, 120, 140, or 160g).

2.3.4.2 Distribution behavior of powders within the enclosed filling chamber

A factorial-lattice design with 225 experiments was used to compare the behaviors of the powders within the filling chamber. The influence of four factors, namely the categorical factor 'type of powder', further referred to as 'powder', the numerical factors 'powder volume within the filling chamber of the feed frame' further referred to as 'powder volume', the 'rotational speed of the paddle wheel', further referred to as 'paddle wheel speed', and the 'laser spot position for monitoring the powder surface within the filling chamber of the feed frame', further referred to as 'monitoring position' were investigated. The factors 'powder' and 'paddle wheel speed' were examined at five levels whereas the factors 'powder volume' and the 'monitoring position' were examined at three levels. The levels of the paddle wheel speed were selected to be 20, 40, 60, 80, and 100 rpm whereas the monitoring positions were selected to be R45, R59, and R73. The levels of the factor 'powder volume' were selected to be 116, 139, and 162 ml for all powders corresponding to the determined bulk densities of 100, 120, and 140 g of Emc. These levels turned out to be suitable in study 2.3.4.1. The experimental runs that included identical amounts of powder were carried out in the standardized sequence described in study 2.3.4.1. The experimental design was planned and statistically evaluated using the Design Expert® software (Stat-Ease, Minneapolis, USA).

2.3.4.3 Influence of the paddle wheel geometry on the powder distribution

To compare the influence of two different paddle wheel geometries on the distribution behavior of powders in the filling chamber (Fig. 21), a response surface experimental design was developed with the software Design expert® (v. 8.0.7.1, Stat Ease, Minneapolis, USA), which contains the categorical factor 'paddle wheel geometry' as well as the numerical factors 'powder mass', 'paddle wheel speed' and 'monitoring position'. This study was conducted with Av102. The factor 'powder mass' was adjusted to three levels (38, 46, and 54 g of Av102), the factor 'paddle wheel speed' to 5 levels (20, 40, 60, 80, and 100 rpm) and the factor monitoring position to 3 levels (R45, R59, and R74). Of each experimental run 30 subsequent filling wheel revolutions were recorded and the PWR filling level generated via the algorithms described in chapter 2.2.4 was used as response. The design matrix evaluation of the response surface quadratic model may be found in the supplementary data section. Experimental runs with the same factor level of powder mass were carried out in the standardized sequence which is described in study 2.3.4.1.

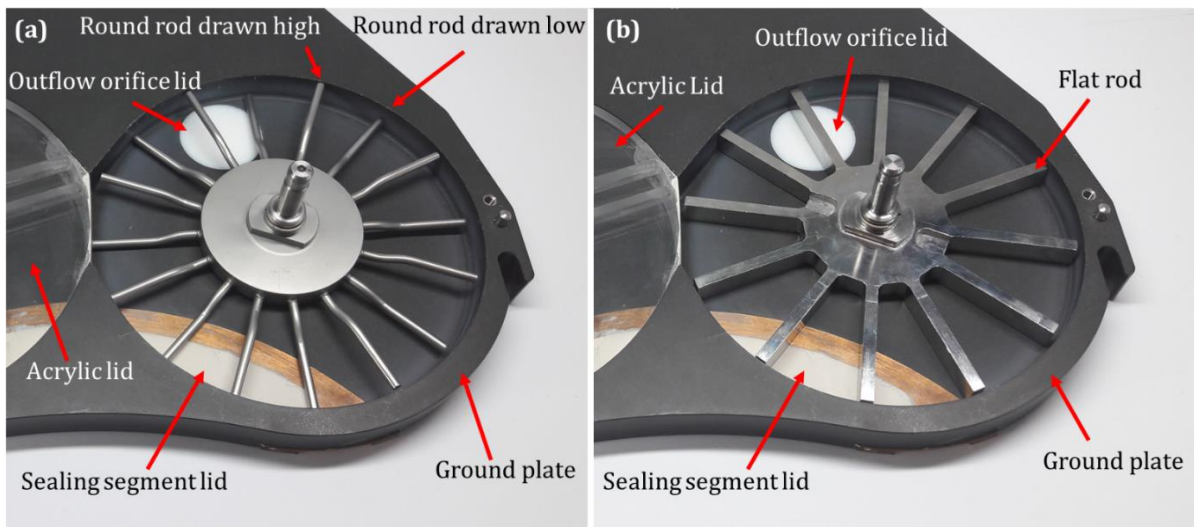


Fig. 21: Images of the filling chamber of the feed frame; (a) round rod paddle wheel with a total of 16 rods (paddles), which are alternately drawn high or low and (b) flat rod paddle wheel with a total of 12 rods (paddles), which do not differ geometrically. The dosing chamber is deactivated by an acrylic lid.

2.4 Specific methods for the in-line monitoring of the powder filling level

2.4.1 Tablet press in-line setup

For the in-line experiments, i.e. the monitoring of the powder filling level during tableting, the rotary tablet press (Fette 102i, Fette Compacting, Schwarzenbek, Germany) was equipped with 30 pairs of punches (8 mm diameter, faceted). A filling cam of 12 mm was used to slide the lower punches downwards for filling the dies with powder. The filling depth adjustment was set to the minimum possible level of 0.5 mm (11.5 mm final filling depth). During commercial tablet production, a scraper behind the feed frame collects and transports excessive powder into a channel in the die table, which redirects the powder into the feed frame with a lifter. In the present experimental setup, a scraper behind the feed frame removes excessive powder from the tableting process by moving protruding powder through a pipe into a collecting container. This modification from a commercial production process prevents protruding powder from an increase of the degree of die filling and / or an increase of the powder filling level inside the feed frame behind the monitoring position of the powder surface level. With regard to a commercial production process, the redirection of powder by a lifter in the feed frame and / or in the dies might affect the relationship between the determined filling levels and / or the distribution parameters and the die filling. This effect of the redirected powder on this relationship has to be considered, if results obtained with the presented device are interpreted. The distance of the punches within the compression station of the tablet press was adjusted individually for each tableting run to achieve sufficiently hard tablets (breaking point of the tablets greater than 80 N), providing an adequate mechanical stability for the collecting and weighing procedure.

2.4.2 Simplification of the experimental feed frame setup

The die feeding system used in the tableting experiments consists of a hopper which delivers powder through gravity to the distributing chamber of the instrumented feed frame (Fig. 22). The distributing chamber is located above the filling and dosing chamber and moves powder by a paddle wheel (distributing wheel) through an orifice inside the partition plate, which separates the distributing chamber from the dosing and filling chamber, to the filling chamber. To simplify the experimental setup and thus the correlation between the measured powder filling level inside the filling chamber and the resulting tablet masses the dosing chamber was closed by the acrylic lid. In Fig. 23 the implementation of the acrylic lid and the difference between the commercial production setup and the experimental setup is shown. This modification of a commercial production process is intended to increase the influence of the filling level on the resulting die filling, which means that the effect of the filling level on the die filling might be less pronounced in commercial processes in which the dosing chamber is a component of the process setup. The feed frame configuration with the enclosed dosing chamber was only investigated for scientific purposes in this study because the dosing chamber with its dosing wheel is an essential component of the feed frame and is of particular importance for the manufacturing of tablets [208].

For determination of the powder filling level the position of the laser spot inside the filling chamber was adjusted at R59 and kept constant over all experiments (Fig. 24). The experiments of the study 2.3 led to the conclusion that this spot is particularly suitable for the measurement of the powder surface level. If the monitoring position is further outwards, dust artefacts may reduce the accuracy of the measurements. Additionally, in the edge region of the chamber, the powder filling level is relatively high under most

process conditions and the powder is partially pressing against the chamber's ceiling, so that variations of the powder surface may be more difficult to detect in the edge region than in the inner region of the chamber. In contrast, if the monitoring position is located too deep inside the chamber, the correlation of the filling level at this position with the filling level in the edge region of the chamber, where the die filling takes place, becomes more inaccurate.

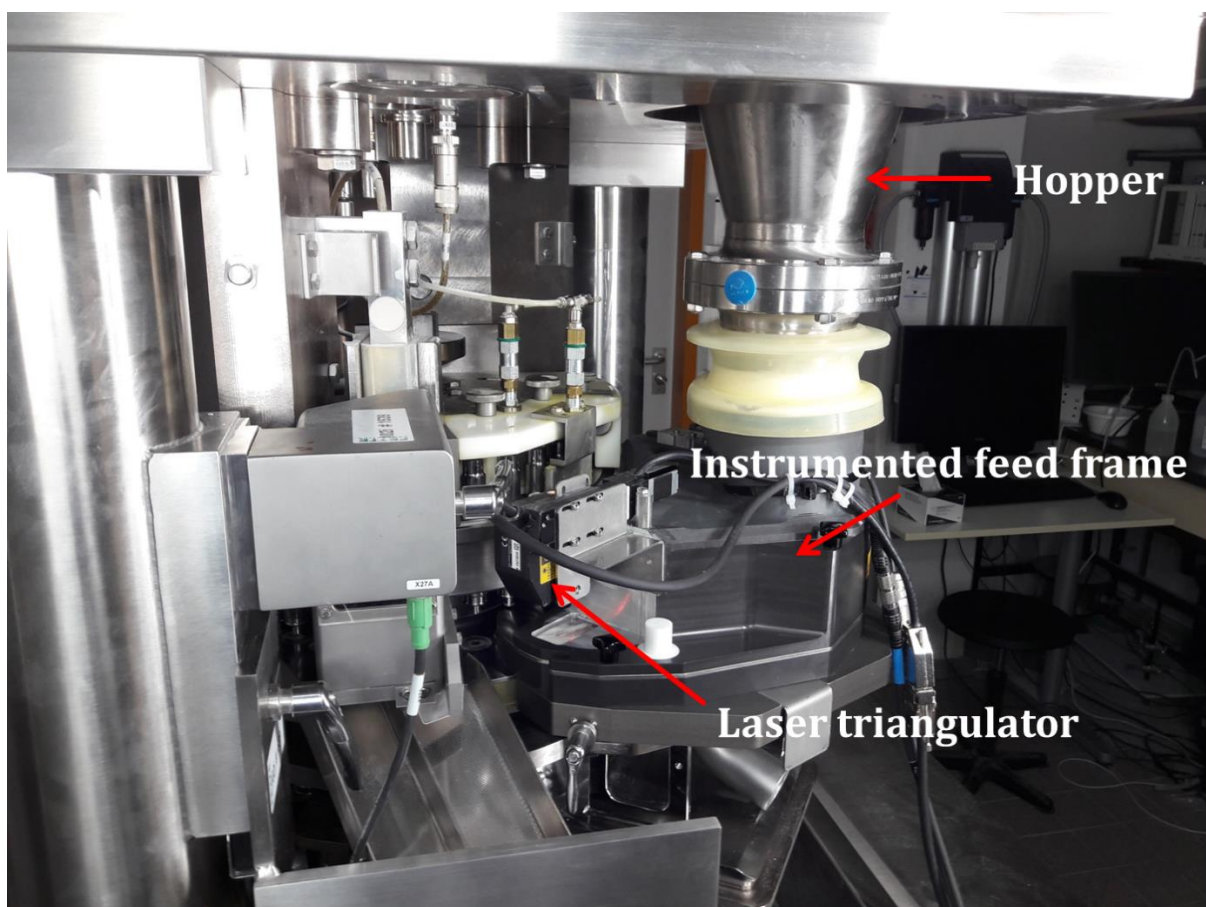


Fig. 22: Photograph of the rotary tablet press Fette 102i with instrumented feeding system.

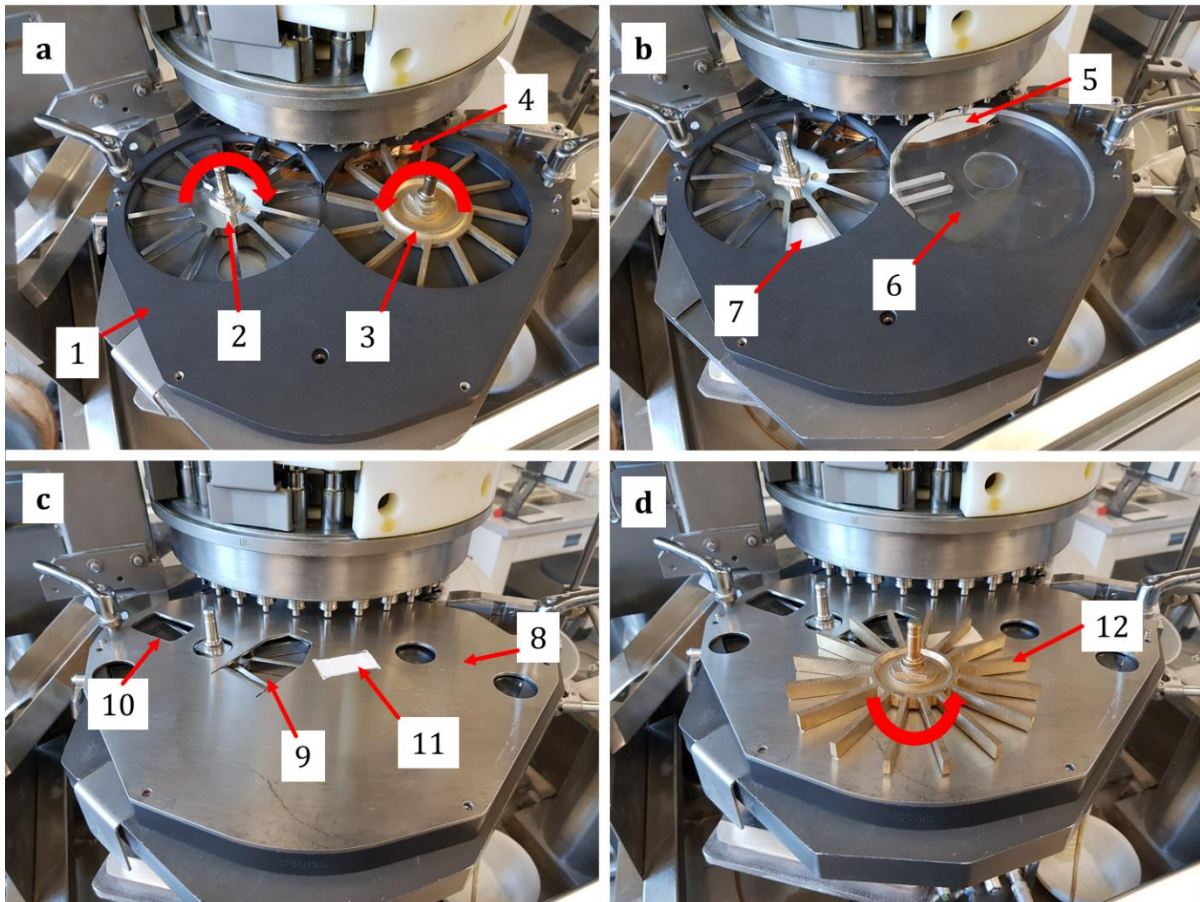


Fig. 23: Components of the feed frame. (a) Production typical construction: ground plate 1, flat rod paddle wheel 2 within the filling chamber (chamber height 15.3 mm and chamber diameter 170 mm), dosing wheel 3, and sealing segment 4. (b) Modified construction for the experimental setup of this study: sealing segment 5 partially closed by filling compound within the region of the dosing chamber up to the filling chamber, an acrylic lid 6 filling the dosing chamber, and a lid 7 made of PTFE covering the outflow orifice. (c) partition plate 8 with the partition plate orifice 9 through which the powder enters the filling chamber, the inspection window 10 used for monitoring the powder surface within the filling chamber, and a second partition plate orifice which delivers powder from the distributing chamber into the dosing chamber closed by filling compound 11. (d) distributing wheel 12, placed onto the partition plate to show its

position within the feed frame (paddle height 12.5 mm, paddle width 5 mm, wheel diameter 178 mm, and chamber diameter 180 mm).

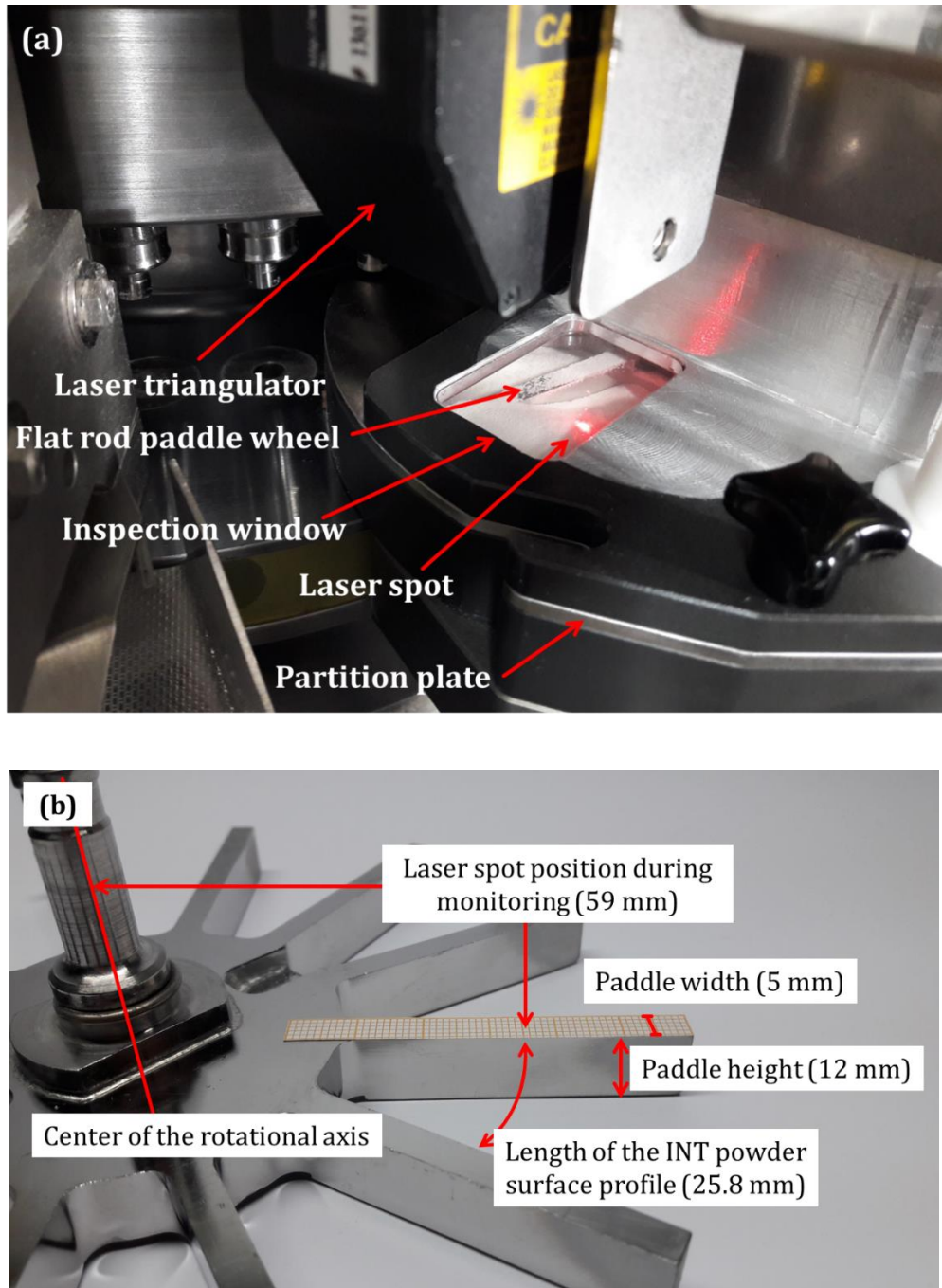


Fig. 24: Photographs of (a) instrumented feed frame within the tablet press with position of the laser spot for monitoring of the powder surface within the feed frame (R59) and (b) flat rod paddle wheel with the laser spot position during monitoring of the powder surface.

2.4.3 Experimental designs of the in-line experiments

2.4.3.1 In-line monitoring and determination of the factor influences on the selected responses

A two-level full factorial design with additional center points was developed to investigate whether the turret speed, the feed frames' paddle wheel speed or the powder itself affect the PWR filling level inside the feed frame and furthermore if variations in the PWR filling level are accompanied by changes in the corresponding tablet masses. The factor turret speed was varied between 20, 60 and 100 rpm, while the factor paddle wheel speed which applies to both, the filling and the distributing wheel, was varied between 20, 40 and 60 rpm. The maximum level of the factor paddle wheel speed was selected to be 60 rpm, because measurements at even higher paddle wheel speeds might be accompanied by signal artifacts, caused by powder which is pushed over the paddles. According to the determined bulk densities of the powders either 2.0 kg of Av102 or 3.4 kg of Destab were filled into the tablet press feeding system resulting in an approximately equivalent powder filling level within the hopper above the feed frame for each experimental run. The turret and the feed frame were accelerated simultaneously, i.e. no pre-run of the feed frame was carried out to prevent an initial accumulation of powder inside the feed frame. A center point experiment with 2.0 kg of Av102 at a turret speed of 60 rpm and a paddle wheel speed of 40 rpm was carried out in triplicate to investigate the reproducibility of the measurements. As the reproducibility of the responses was determined only with Av102 in triplicate, all findings regarding the effects of the factors refer to Av102. Destab as an ordinal categorical factor was used only to detect the trends of these effects, i.e. the impact of an improved powder flow behavior on the discovered effects. During tableting, a variable number of tablets per sample time point (every 30 s after the start of a tableting run) were collected manually by cups. From these cups, 20 tablets were randomly drawn

and weighed immediately after completion of an experimental run with an analytical balance (Mettler Toledo, Columbus, USA). However, for the DoE only the samples collected after 60 s were used. The experimental design was planned and statistically evaluated using the Design Expert® software (Stat-Ease, Minneapolis, USA). The design matrix evaluation of the model (full factorial main effects) resulted in a variance inflation factor of 1.0 for all terms of the model indicating that coefficients are well estimated even if multicollinearities occur. However, because of the low degrees of freedom for both lack of fit and pure error of the experimental design, a valid lack of fit test may not be guaranteed. The entire evaluation of the design matrix for the used experimental design is attached to the supplementary data section.

2.4.3.2 Comparison of the paddle wheel geometries

To investigate whether the geometry of the paddle wheel within the filling chamber of the feed frame affects the resulting tablet mass, an OFAT experimental design was selected that covers only the process parameter paddle wheel geometry (round rod or flat rod paddle wheel geometry). The experimental feed frame setup which is described in chapter 2.4.2 was used. The tableting experiments were carried out at a turret speed and a paddle wheel speed of 60 rpm.

By adjusting the compression rolls located within the compression station of the tablet press, a punch distance of 2.7 mm in the compression station was reached, resulting in a sufficient tablet hardness, providing an adequate mechanical stability of the tablets for the collection and weighing procedure.

The experiments described in study 2.4.3.1 showed that the filling chamber is considerably full under the chosen experimental conditions on a 102i tablet press. To achieve a lower filling level within the filling chamber, the partition plate orifice through which the powder flows into the filling chamber was downsized by attaching a stable adhesive tape (Fig. 25).

The purpose of downsizing the partition plate orifice was to increase the influence of the paddle wheel on the filling process of the dies by preventing a nearly filled up filling chamber and thus an oversupply of powder from overlapping effects of the wheel geometry on the die filling process. However, without downsizing the partition plate orifice and with an accessible dosing chamber which both affect the powder behavior within the feed frame, the influence of the paddle wheel geometry on die filling may be reduced and therefore the possible application of the developed model on commonly used feed frame setups is limited because the obtained results are affected by the use of only one chamber on the bottom stage of the feed frame and the downsized partition plate orifice.

Before starting each tableting run, 2 kg of Av102 were filled inside the hopper above the feed frame. After starting the tableting process, a variable number of tablets per sample time point (every 20 s after the start of a tableting run) were collected manually by cups. From these cups, 10 tablets were randomly drawn and weighed immediately after completion of an experimental run with an analytical balance (Mettler Toledo, Columbus, USA).

The powder surface within the filling chamber was monitored continuously over the entire experimental run time by laser triangulation at R59. Both, the experiment

containing the round rod paddle wheel as well as that containing the flat rod paddle wheel were carried out in triplicate.

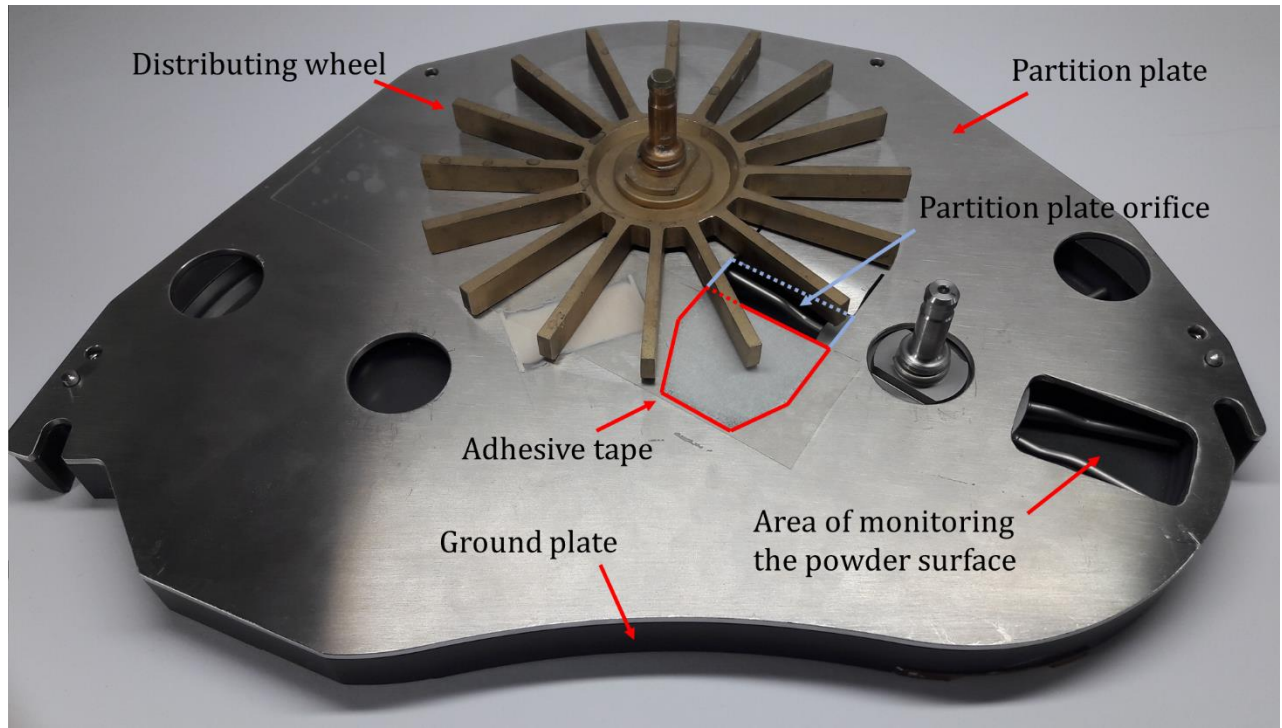


Fig. 25: Image of the partition plate separating the distributing chamber from the filling and dosing chamber. The distributing wheel is located at its usual position in the feed frame. The partition plate orifice is decreased with an adhesive tape.

3 Results and Discussion

3.1 Suitability of the developed device to monitor the powder filling level

3.1.1 Evaluation of the powder characteristics

The powder volumes which were determined from the bulk and tapped densities as well as the average particle size of the investigated powder samples did not change significantly over the course of the experiments. However, slight changes in the powder flow were observed. In Table 2 the results of the measurements of the powder properties of untreated Emc (Emc_{initial}) and Emc taken from the filling chamber after the applied shear stress by the experimental sequence (Emc_{shear}) are shown. These results allow the conclusion that the different degrees of shear stress applied to the powder before the powder surface profiles were recorded can be neglected in this study.

Table 2: Powder characteristics before and after the recording of the powder surface profiles. All experiments were carried out in triplicate.

Powder properties	Emc_{initial}	Emc_{shear}
Particle size d50 / d90 (μm)	220.75 (d50) / 347.17 (d90); 221.28 (d50) / 346.69 (d90); 223.4 (d50) / 347.79 (d90)	221.77 (d50) / 349.52 (d90); 225.47 (d50) / 348.14 (d90); 226.37 (d50) / 354.48 (d90)
Powder volumes V0/V1/V10/V500/V1250/ V2500 (ml/100g) (determined by the bulk and tapped densities)	110/108/106/96/94/92 110/108/106/96/94/92 110/108/106/96/94/92	110/108/106/96/94/92 110/108/106/96/94/92 110/108/106/96/94/92
Powder flow through an orifice (s/100 g)	8.13 \pm 0.05	8.6 \pm 0.1

3.1.2 Evaluation of the mean powder surface profiles of Emc

Throughout the evaluation process 225 mean powder surface profiles were created each out of 30 subsequent paddle wheel revolutions. In Fig. 26 three mean powder surface profiles exemplary for the monitoring positions R45, R59 and R73 at the center levels of the 'powder mass' and the 'paddle wheel speed' are displayed. The profile that was obtained at R73 is shown twice to illustrate the influence of the artifact filter which was implemented inside the flat rod algorithm. The standard deviations of the layered profiles are displayed as purple bands above and below the mean. The INT filling levels calculated separately for each of the twelve paddle wheel interspaces are displayed at the bottom of the respective interspace's profile. Results show a powder accumulation in front of the pushing paddles. Occasionally, a preceding powder avalanche was observed in front of a main avalanche.

An increase of the PWR filling level in the direction from R45 to R73 was observed at equal levels of the 'powder mass' and 'paddle wheel speed.' This increase of the filling level is probably reflecting centrifugal and shear forces caused by the rotational movement. In the present study no investigations were performed regarding a relationship between the profile shape and flowability of the powder. However, different flow properties might be reflected in the surface profile measured in the feed frame. The link between the powder characteristics, the powder distribution within the feed frame and the die filling process is among the most important relationships in context with the die filling process. However, in the present study the focus was on the development of the instrumented feed frame. This relationship will be investigated in the following studies.

Significant differences between the INT filling levels of the paddle wheel interspaces suggest that the distribution of the powder inside the chamber is inhomogeneous. This

might be caused by a deformation of the axis of the paddle wheel, which is presumably a result of production inaccuracies. Therefore, the distance to the ground plate of the individual paddles varies, which causes a different amount of powder to be captured by the paddles, which then accumulates to different degrees in front of the respective paddles. Transferred to a tableting process, the information on the inhomogeneity of the powder distribution inside the feed frame may be used to determine variations in powder availability for die filling which might cause tablet mass deviations.

At R73 high deviations of the signal behind the paddles indicate that redistribution effects occur between the interspaces. These artifacts result from powder shifts above the paddle and are intensified with increasing paddle wheel speed. This intensification is probably caused by mass inertia effects which become stronger at higher paddle wheel speed levels because of an increased powder acceleration. This hypothesis is supported by DEM simulations [209]. The powder which is shifted above the paddle remains at higher trajectories and therefore pretends a powder surface which is detected by the laser triangulator. Additionally, the duration of the measurements decreases if the paddle wheel is accelerated. The impact of these powder artifacts on the determination of the filling level was reduced by the software filter described in the method section.

Overall, the radiuses R45 and R59 show lower powder levels, less powder artifacts, and lower orbital speeds than the radius R73 which all support the smaller radiuses to be more suitable for a calculation of the true filling levels, particularly regarding a distortion by powder artifacts. Comparing evaluations with and without filtering out of powder artifacts, the calculated filling levels obtained at R45 and R59 are very similar. However, at R73 a strong reduction of the filling level by reducing the powder artifacts was observed. Because of the measurement method, no information on the powder density

inside the system is obtained. No investigations were performed on the penetration depth of the laser beam into the powder surface. Presumably, different powders or powder densities lead to different immersion depths or spot sizes of the diffuse reflected light. Both might influence the distance signal.

A challenge for a measurement by laser triangulation might be the blinding of the inspection window. Adhesive products may lead to adhering powder layers to the window surface and thus to turbidity of window. Moreover, a static charge of the inspection window by itself could cause adhesion of particles, in the worst case inside the optical path of the laser beam. However, in this study Emc did not impair measurements noticeably by blinding of the inspection window.

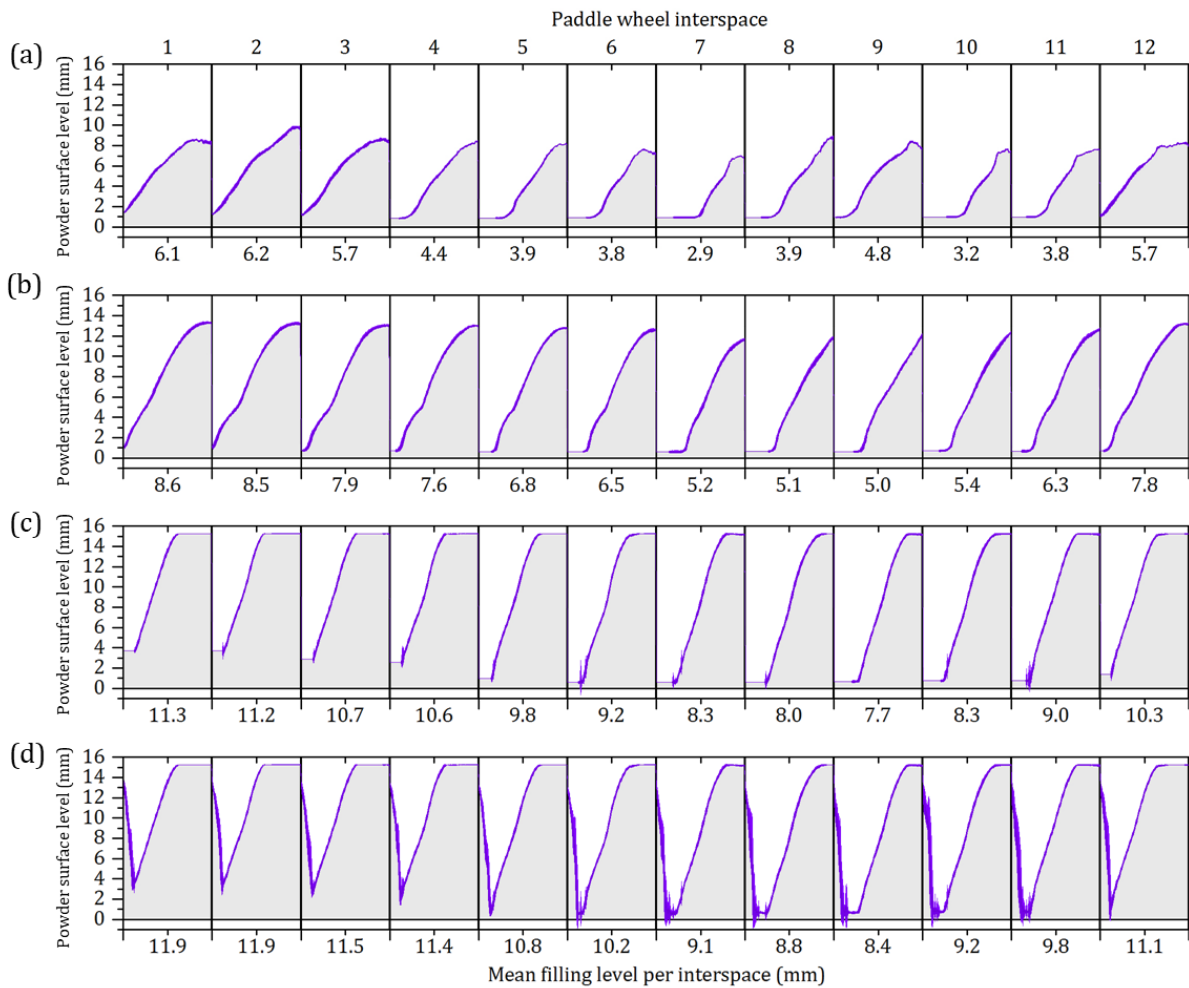


Fig. 26: Mean powder surface profiles ($n = 30$) of 120 g Emc at 60 rpm paddle wheel speed obtained at the monitoring positions: (a) R45, (b) R59, (c) R73, and (d) R73 without artifact filter.

3.1.3 Evaluation of the PWR filling levels of Emc

A quadratic model was selected to describe the effect of the investigated factors on the PWR filling level. According to the analysis of variance (ANOVA) the model explains 98.96% of the relationship between the factors and the response ($R^2 = 0.9896$). The F value of 3049 implies that the model is significant. There is only a 0.01% probability that such a high F value results from noise. However, there is still a significant lack of fit (LOF = 321.62), indicating that some differences between the actual and predicted values do

not result from noise; instead, there are other reasons why this might occur. In general, unconsidered effects or cofactors may lead to a lack of fit inside a modeling approach. Here, the cause might be the restriction of the increase in the filling level by the chamber's ceiling. If the powder reaches the chamber's ceiling or inspection window's surface, a further increase of the filling level is impossible.

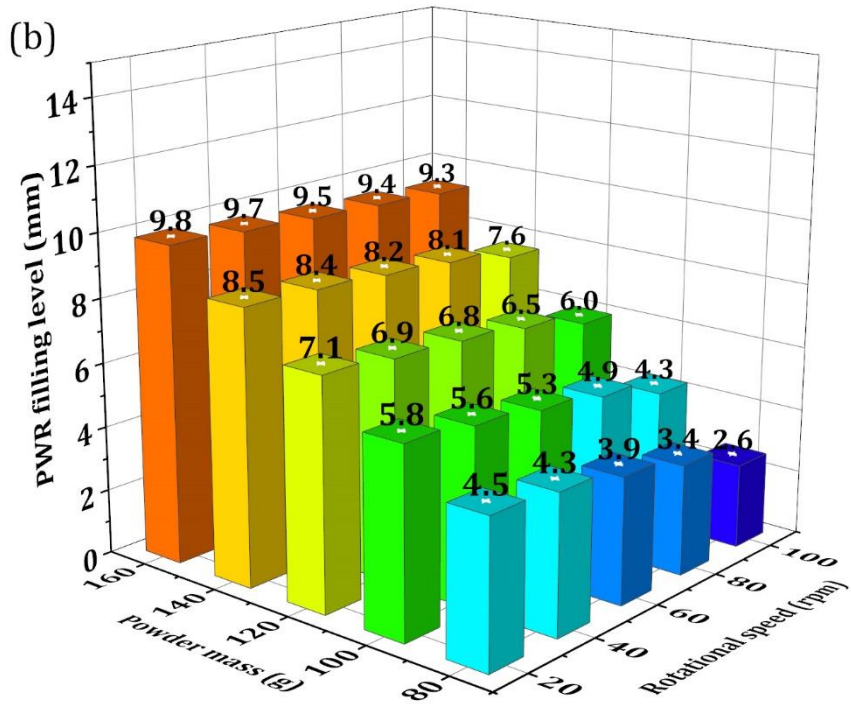
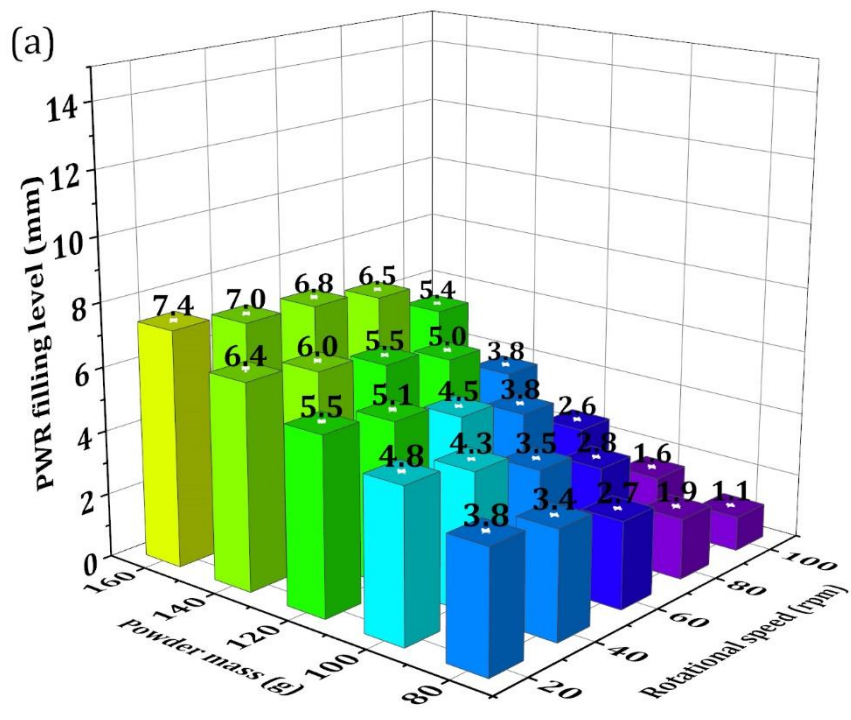
Despite the significant LOF the predicted R^2 of 0.9890 is in reasonable agreement with the adjusted R^2 of 0.9896 (difference < 0.2) and an adequate precision ratio of 233.91 (> 4 is desirable) indicate that the model can be used to navigate the design space. According to the ANOVA all terms of the model significantly influence the filling level (p values < 0.05). The factors 'powder mass' and 'paddle wheel speed' show a linear influence on the filling level. All factors interact with each other; the 'monitoring position' is the only quadratic term within the model.

Generally, the calculated PWR filling levels show expected trends. An increase of the powder mass inside the system leads to an increase of the PWR filling levels at all monitoring positions. The highest PWR filling levels were always observed at R73 regarding equal levels of the factors 'powder mass' and 'paddle wheel speed'. The paddle wheel speed affects the PWR filling level in different directions dependent on the 'monitoring position'. An acceleration of the paddle wheel results in a decrease of the PWR filling level at R45 and R59 but in an increase at R73. As already mentioned, the powder is shifted outward by the rotational movement of the flat rod paddles and accumulates at the chamber's side wall. The standard deviation of the PWR filling level was maximal 0.11 mm over all experiments and in average 0.02 mm which indicates a high reproducibility. In Fig. 27 the PWR filling levels at the three different monitoring positions are shown.

From the instrumental developer's point of view, the knowledge about the general filling conditions is necessary to find an optimal or universal spot for monitoring of different

production conditions. In the edge region of the chamber a high filling level is present at most process conditions which might lead to problems with regard to an accurate determination of usable filling level values. If further studies lead to the conclusion that an independent variation of the paddle wheel speed and the powder filling level within the feed frame turns out to be of advantage, it might be imaginable to build up a feedback loop to a valve above the feed frame that adjusts the powder inflow. Thereby, the powder acceleration within the feed frame may be varied independent of its powder filling level. Whether or not such a feedback mechanism is of advantage has to be discussed elsewhere.

Suitability of the developed device to monitor the filling level



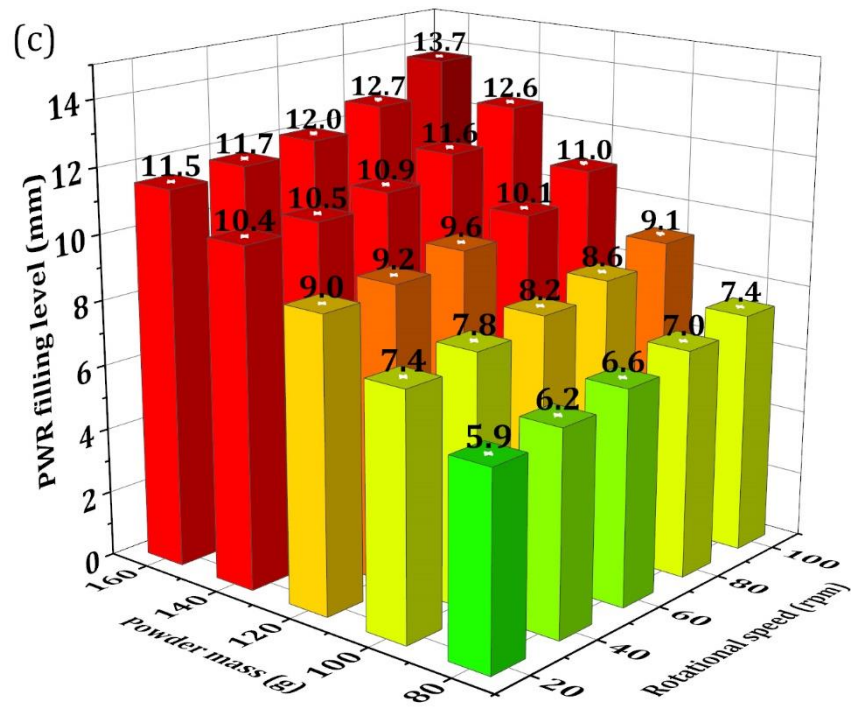


Fig. 27: PWR filling levels at the three monitoring positions (a) R45, (B) R59, and (c) R73. Means \pm SD, n = 3.

3.1.4 Conclusion

Laser triangulation combined with an angle recognition of the paddle wheel via rotary encoder may be used for monitoring of the powder filling level within rotary tablet press feed frames. This method is suitable for both, the characterization of the uniformity of the powder filling level between the individual paddle wheel interspaces as well as the rotational speed-dependent behavior of powders within the chamber. The resulting data might provide useful information for optimization of the paddle wheel speed and/or for selection of the paddle wheel design depending on the powder behavior within the filling chamber. Investigations on the inhomogeneity of the powder distribution might also be useful to better understand tablet mass deviations during production processes. However, blinding of the inspection window can be challenging with this device. Thus, there is a need to optimize the window surface in the future for example by choosing different window materials, surfaces, or tools against blinding.

3.2 Distribution behavior of powders within the enclosed filling chamber

3.2.1 Characterization of the investigated powders

The powders used for comparisons of the distribution behavior within the feed frame differ in the determined powder properties, namely the particle size distribution, bulk and tapped densities, and moisture (Table 3). Because of these and further properties of the powders, the flow functions which were determined by ring shear cell experiments differ between the investigated powders (Fig. 28). Regarding the flow functions which are predominantly governed by cohesion, Av102 shows the poorest flowability at all investigated major principal stresses in comparison to the other powders, whereas Destab shows the best flowability at a major principal stress of 2 kPa and Emc the best flowability at major principle stresses above approximately 5 kPa [210].

Table 3: Bulk densities, tapped densities, particle sizes and moisture of the investigated powders.

	Emc	Destab	Av200	FFL	Av102
Particle size d10/d50/ d90 (µm)	14.7/206.6/ 297.0	81.9/178.6/ 292.6	44.7/184.8/ 344.5	54.7/113.7/ 187.1	37.8/116.4/ 221.3
Bulk density (g/ml)	0.86	0.56	0.35	0.55	0.33
Tapped density (g/ml)	1.00	0.63	0.43	0.66	0.41
Moisture (%)	7.72	1.15	5.12	5.29	4.7

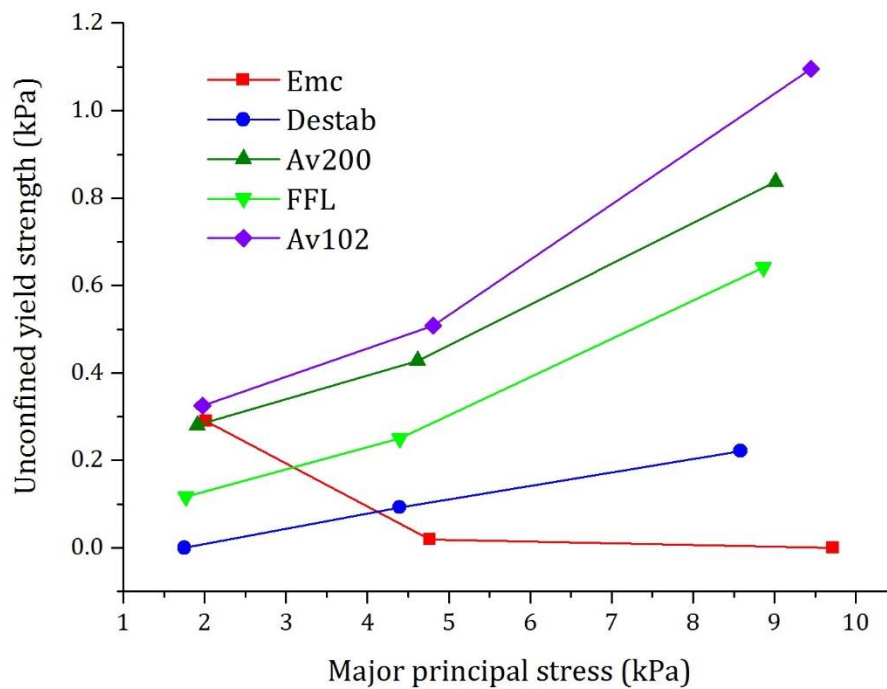


Fig. 28: Flow functions of the investigated powders.

3.2.2 Comparison of the surface profiles of the investigated powders

The determined powder surface profiles of the investigated powders appear to be relatively similar at 20 rpm rotational speed of the paddle wheel (Fig. 29).

At 60 rpm rotational speed, a clear differentiation between the shape of the Av102 powder surface profile and the other powder profiles, which furthermore show similar surface profiles, is possible (Fig. 30). In comparison to the surface profiles recorded at 20 rpm, a shift of the ratio between the location of the powders from the proximity to the ground plate to an arrangement closer to the paddle is obvious. One reason for the clear difference between the Av102 profile and the remaining powder surface profiles might be the cohesive properties of Av102, by which Av102 is prone to pre-consolidation by centrifugal forces which might result in a specific profile shape of the powder surface. The shape of the surface profile of Av102 shows a steep powder front which rises to the upper

edge of the paddles. In addition, it is noticeable that the Av102 profiles show the most distinct differences between the single paddle wheel revolutions, which manifest themselves by the increased standard deviation of the 30 profiles shown as a purple band around the mean powder surface profile (Fig. 30e).

At a paddle wheel speed of 100 rpm, all powders develop different shapes of their surface profiles (Fig. 31). This surface formation reflects the overall effect of all powder characteristics on the distribution behavior of the respective powder at the observed rotational speed and presumably does not result from only one single parameter of the powders. At 100 rpm, Av102 continues to show the highest standard deviation of the single profiles, followed by FFL. The FFL mean powder surface profile appears to develop a similar shape as Av102. Av200 reaches the highest powder surface levels within the paddle wheel interspaces while accumulating in front of the paddles at 100 rpm (Fig. 31c). It is good-flowing because of its large particles and has a low density compared to Emc which probably promotes the accumulation of Av200 in front of the paddles in contrast to Emc which is comparatively dense. Emc shows the lowest changes in the powder surface profiles over all investigated rotational speeds of the paddle wheel. Destab's surface profiles are very uniform over each of the 30 averaged revolutions of the paddle wheel and the surface shape appears to be only slightly affected by an increase in the rotational speed.

With respect to the die filling behavior of powders the informative value of the powder surface profiles might be very limited, as pronounced differences in the standard deviations of the tablet masses between powders are well known especially at low rotational speeds of the paddle wheel, while the powder profiles obtained in these

experiments appear relatively similar at low rotational speeds for all powders investigated in this study [81,211].

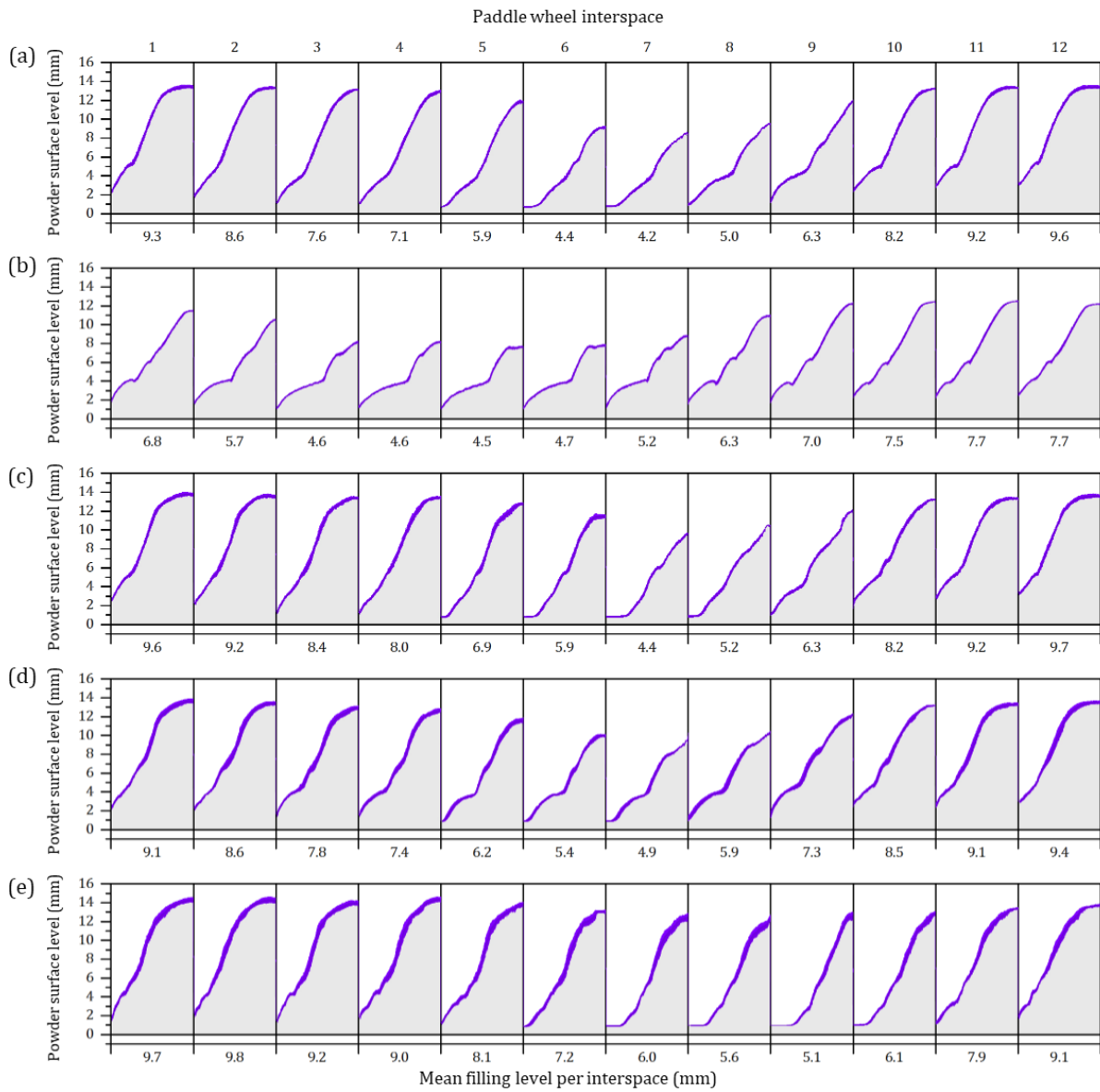


Fig. 29: Mean powder surface profiles of 30 continuing paddle wheel revolutions at 20 rpm rotational speed and the monitoring position R59 within the filling chamber of the feed frame of (a) Emc, (b) Destab, (c) Av200, (d) FFL, and (e) Av102. The standard deviation of the 30 individual powder surface profiles is shown as a purple band around the mean. The 12 mean filling levels per interspace (INT filling level) are shown below each mean powder surface profile.

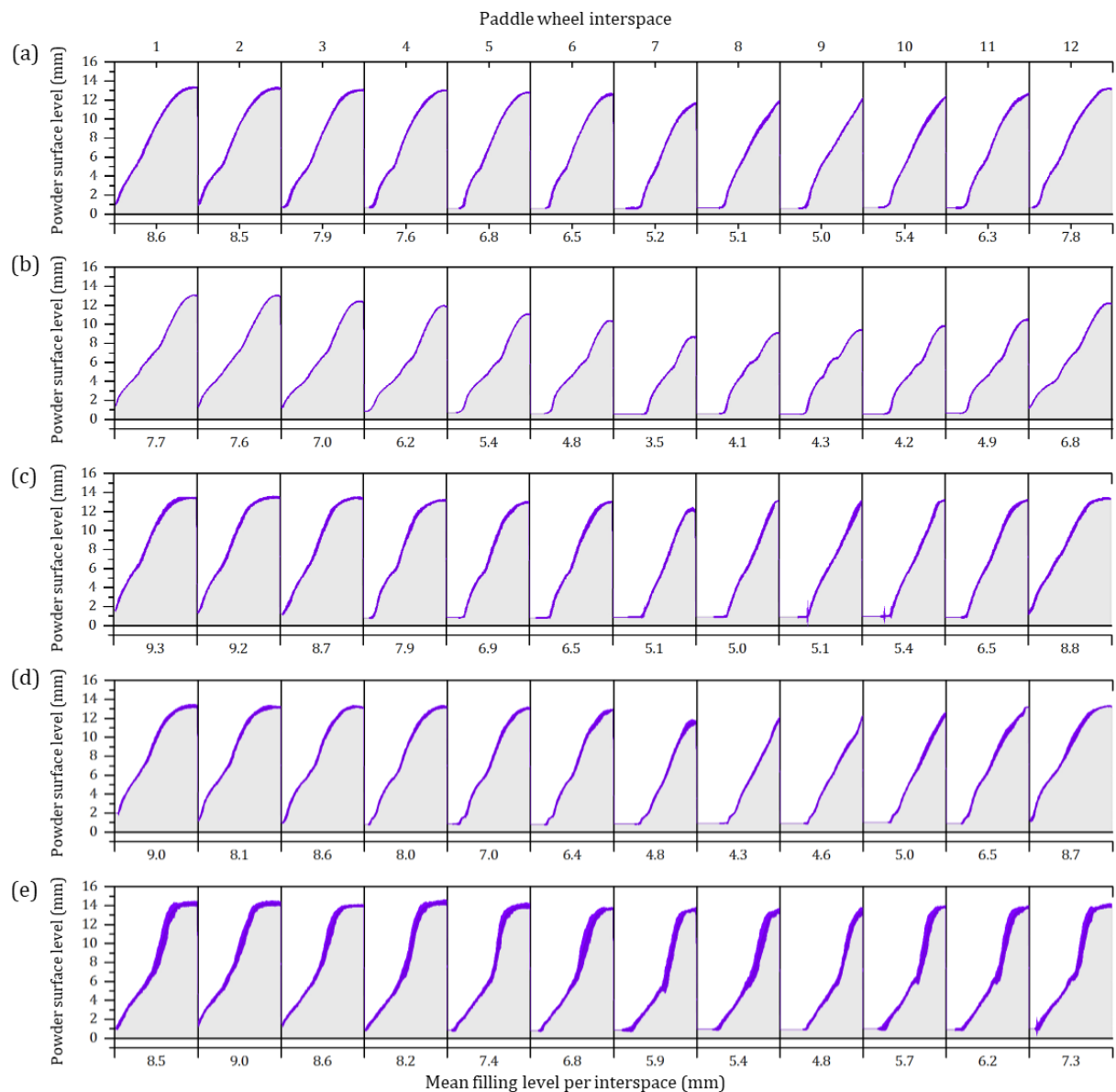
Comparison of the distribution behavior of different powders

Fig. 30: Mean powder surface profiles of 30 continuing paddle wheel revolutions at 60 rpm rotational speed and the monitoring position R59 within the filling chamber of the feed frame of (a) Emc, (b) Destab, (c) Av200, (d) FFL, and (e) Av102. The standard deviation of the 30 individual powder surface profiles is shown as a purple band around the mean. The 12 mean filling levels per interspace (INT filling level) are shown below each mean powder profile.

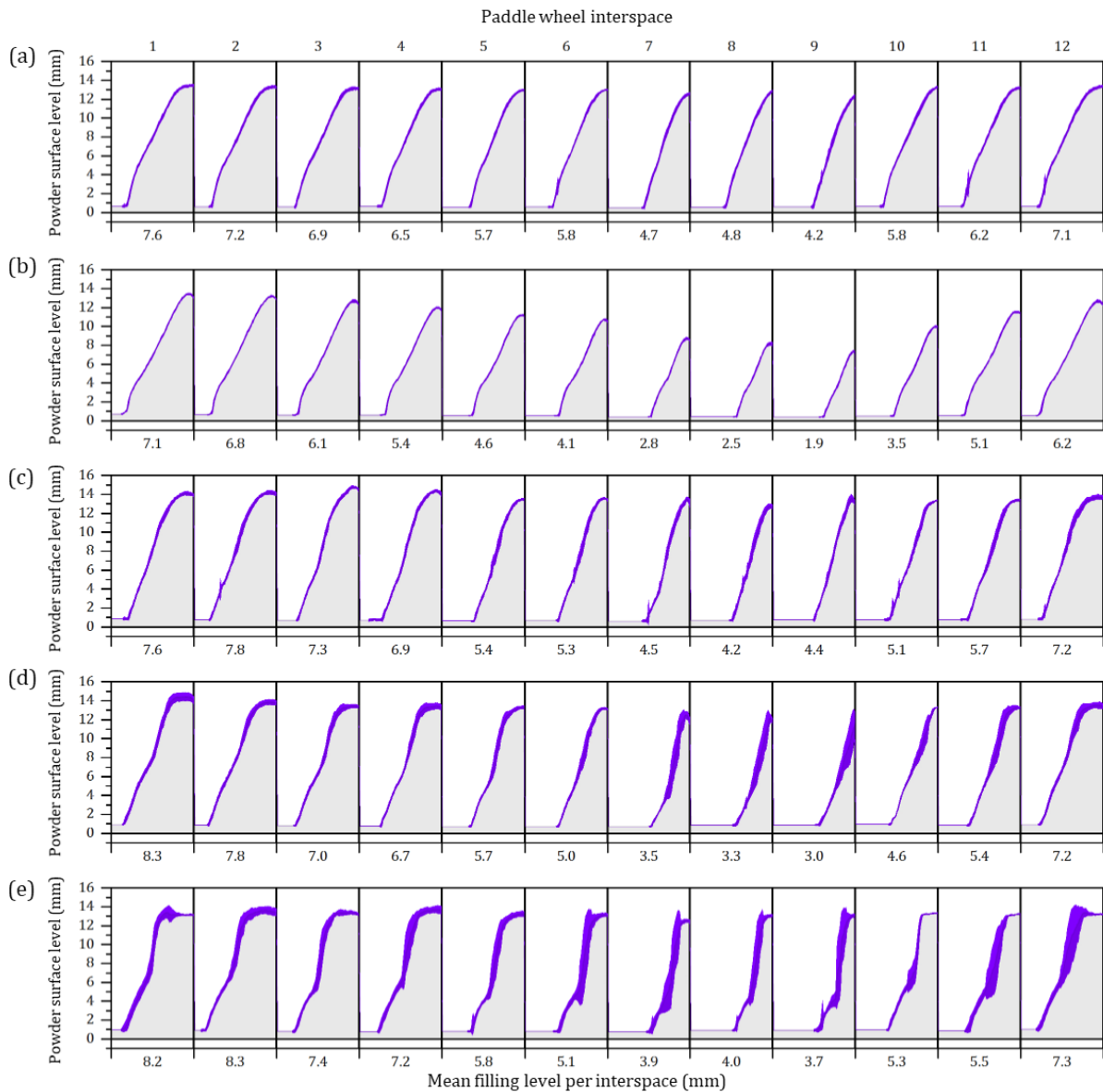


Fig. 31: Mean powder surface profiles of 30 continuing paddle wheel revolutions at 100 rpm rotational speed and the monitoring position R59 within the filling chamber of the feed frame of (a) Emc, (b) Destab, (c) Av200, (d) FFL, and (e) Av102. The standard deviation of the 30 individual powder surface profiles is shown as a purple band around the mean. The 12 mean filling levels per interspace (INT filling level) are shown below each mean powder profile.

3.2.3 Comparison of the PWR filling levels of the investigated powders

According to the two-way ANOVA, the paddle wheel speed, the monitoring position, and the powder volume affect the PWR filling level ($p < 0.05$). With all powders an increase in the paddle wheel speed leads to a rise of the PWR filling level at the monitoring position R73 and a drop of the filling level at the monitoring position R45. However, the type of powder might not affect the PWR filling level as the coefficient plots of the individual powders show only minor differences (Fig. 32). The influence of the paddle wheel speed on the PWR filling level of Emc may be less pronounced compared to the other powders which might be caused by its high density and associated inertia of the powder regarding a centrifugal shift. Moreover, the factor interaction of the paddle wheel speed and the monitoring position may be more pronounced with FFL compared to the other powders. However, these differences might be caused by deviations of the investigated individual powder volumes. The powder volumes might differ from those initially determined because of forces acting on the powders within the filling chamber which might result in a different extend of pre-consolidation of the different powders and therefore a deviation in the investigated powder volumes. A lower powder volume allows a more pronounced centrifugal shift within the defined chamber volume, because the percentage of the powder volume which is shifted centrifugally from R45 to R73 is higher.

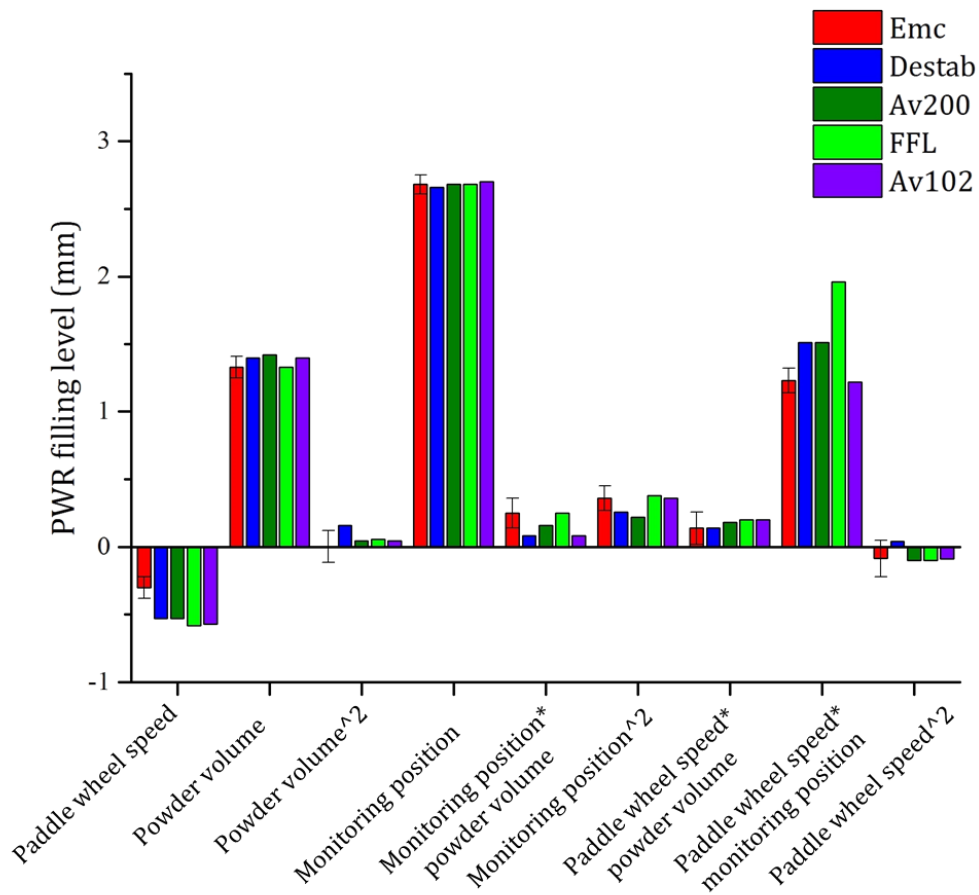


Fig. 32: Effect plot of the investigated factors paddle wheel speed (rpm), powder volume (ml), and monitoring position (mm) on the response PWR filling level of all investigated powders. Error bars are 95% confidence intervals.

3.2.4 Conclusion

The surface profiles of the investigated powders appear to be similar at 20 rpm paddle wheel speed whereas differences between the powders are observed with increasing paddle wheel speed. Therefore, the informative value of the powder surface profiles regarding the die filling behavior of powders may be limited, as pronounced differences between the standard deviations of the respective tablet masses are well known especially at low rotational paddle wheel speeds.

Regarding the PWR filling levels, the developed instrument was only able to detect minor differences between the rotational speed-dependent shift of the investigated powders into the edge region of the enclosed filling chamber despite their different flow functions. Therefore, it may be concluded that the flow function of a powder has only a minor effect on its redistribution behavior within the enclosed filling chamber. As the flow function of a powder provides information on the powder flowability which affects the relative standard deviation of the die fillings and therefore the tablet mass, the rotational speed-dependent redistribution behavior of powder within the enclosed filling chamber may not provide further information on the individual die filling behavior of powders.

3.3 Influence of the paddle wheel geometry on the powder distribution

3.3.1 Comparison of the powder surface profiles

The surface analysis of the Av102 powder with the laser triangulator allowed the generation of surface profiles with both paddle wheel geometries. The comparison of these powder surface profiles indicate that the different paddle wheel geometries cause significant differences in the distribution behavior of the powder within the filling chamber of the feed frame (Fig. 33).

The powder surface profiles obtained with the round rod paddle wheel show a wavy shaped powder surface. This shape is caused by the 8 low-drawn round rods which plow through the powder. Therefore, the round rods increase the powder surface height resulting from their displacement volume and thus increase the determined powder filling level to higher values. These round rods cause powders to accumulate in front of the rods until the rods finally plow through the powders, by which the powders are partially pushed forward. The powders thereby move into the direction of the rotational movement of the paddle wheel, whereby the supply of powders for the die filling process is ensured. By increasing the speed of the round rod paddle wheel, a change of the shape of the powder waves to a more symmetrical form and a broadening of the powder waves may be observed in the powder surface profiles (Fig. 34).

As already shown with the flat rod paddle wheel in study 3.2.2 the powder accumulates in front of the pushing paddles and forms a heap that rises towards the paddle. This accumulation of powder causes an increase of the powder availability for die filling within the paddle wheel interspaces into the direction to the pushing paddles. Thus, an inhomogeneous provision of the powders for die filling occurs while the paddle wheel interspaces move across the die filling area. In the interspace area in front of the pushing

paddle, comparably more powder is available, while within the interspace area behind the previous paddle less powder and/or probably less dense powder is present [209]. This factor of inhomogeneous powder distribution in the interspaces is likely to influence the uniformity of the die filling process, as the final filling of a die is presumably lower when leaving the filling area, if it was mainly exposed to the front area of an interspace during its filling whereas the filling of a die which predominantly took place in a rear interspace area with high powder availability might lead to a higher filling. However, no investigations on individual die filling processes were performed in this study but a combined evaluation of compression forces and corresponding powder surface profiles or paddle constellations related to individual die filling processes is conceivable.

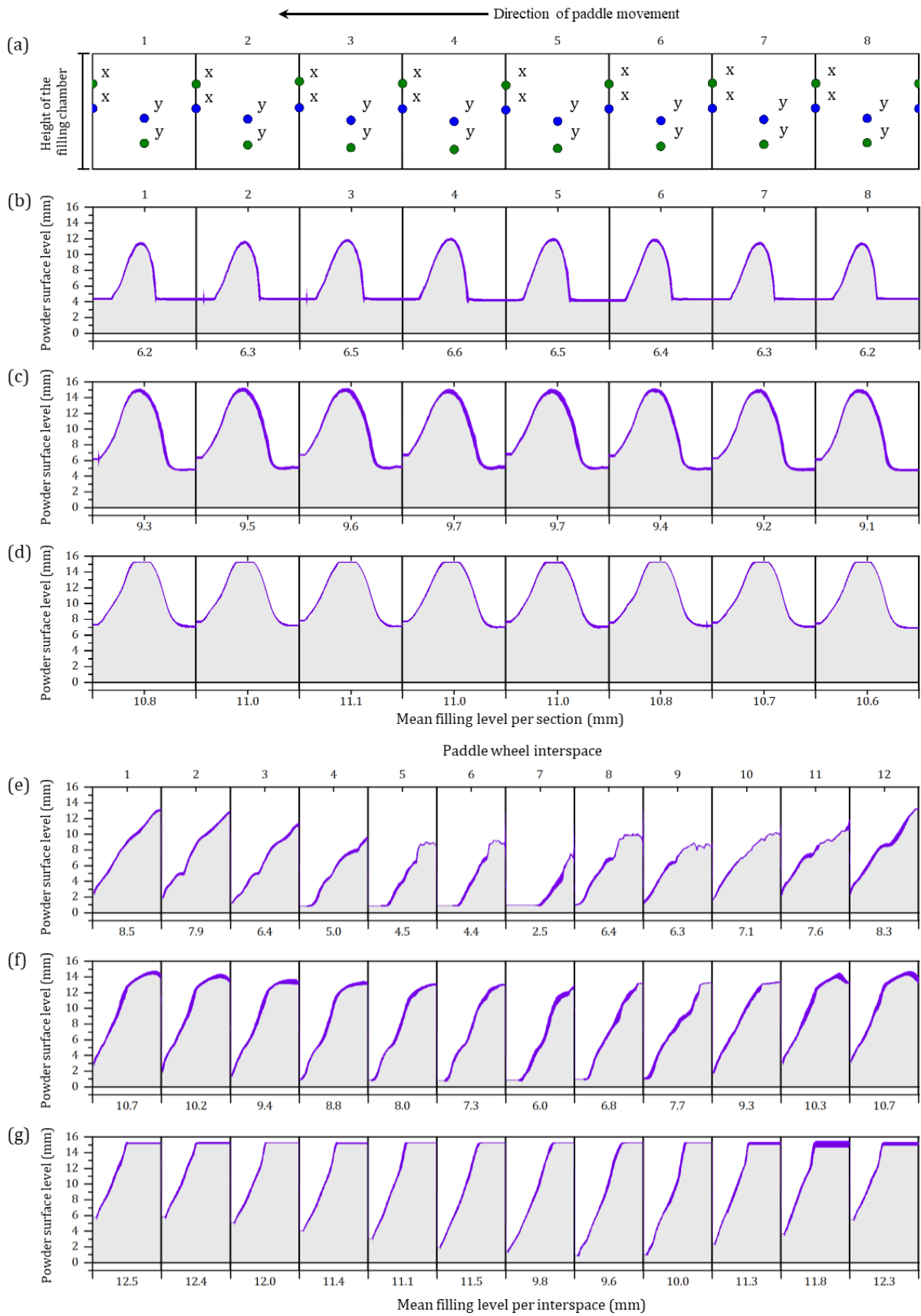


Fig. 33: (a) Illustration of the round rod positions at R45 mm distance (blue dots) and at 59 and 73 mm distance (green dots) to the center of the rotational axis applicable to (b), (c), and (d). Paddles drawn high are marked with an x whereas paddles drawn low are marked with an y. (b-g) mean powder surface profiles ($n = 30$) obtained over 30 s of monitoring 54 g of Av102 within the enclosed filling chamber of the feed frame at 60 rpm paddle wheel speed. Mean powder surface profiles were obtained at (b) 45 mm, (c) 59 mm, and (d) 73 mm distance to the center of the filling chamber in experiments with the round rod paddle wheel and at (e) 45 mm, (f) 59 mm, and (g) 73 mm distance to the center of the filling chamber in the offline experiments with the flat rod paddle wheel. The height of the filling chamber is 15.3 mm. The purple bands around the average profiles represent the standard deviations of the layered profiles.

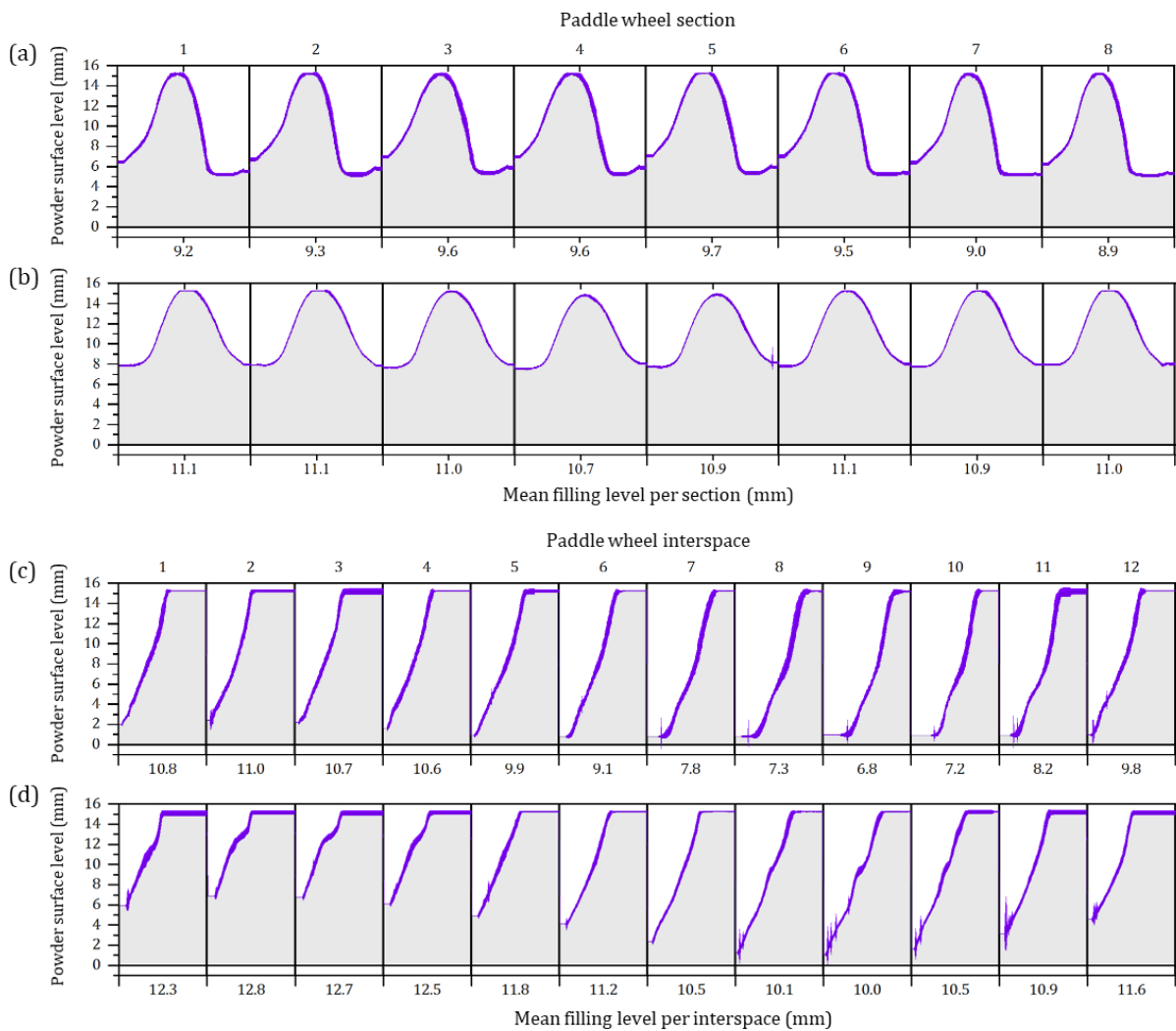


Fig. 34: Mean powder surface profiles ($n = 30$) obtained over 30 s of monitoring 46 g of Av102 at a distance of 73 mm to the center of the rotational axis at (a) 40 rpm and (b) 80 rpm rotational speed with the round rod paddle wheel mounted and (c) 40 rpm and (d) 80 rpm with the flat rod paddle wheel mounted within the enclosed filling chamber.

3.3.2 Factor influences on the filling levels

Despite the significantly different powder surface profiles of the two paddle wheels, which reflect the different effects of the paddle wheels on the powder, the respective resulting PWR filling levels are partially similar (Fig. 35). The corresponding ANOVA (please refer to the supplementary data section) shows that the response 'PWR filling level' is influenced by all investigated factors ($p < 0.05$), namely the geometry of the paddle wheel, the rotational speed of the paddle wheel, and the amount of powder within the filling chamber of the feed frame.

With both paddle wheel geometries an increase in the rotational speed leads to an increase in the PWR filling level at the measuring position located at a distance of 73 mm from the center of the filling chamber. This is mainly the result of the centrifugal and shear forces which cause a radial displacement of the powder to the edge region of the chamber. An increase in the powder mass within the filling chamber leads to an increase of the PWR filling level at all three measurement positions regardless of the paddle wheel geometry. At 45 mm distance from the chambers' center the PWR filling level does not fall below approximately 4.2 mm if the chamber is equipped with the round rod paddle wheel, whereas with the flat rod paddle wheel implemented, the PWR filling level does not fall below approximately 1.2 mm. This discrepancy in the maximum drop of the PWR filling level is probably caused by the different distances of the paddles to the ground plate and the plowing behavior of the round rod paddles. A residual powder layer remains on the bottom of the chamber which is not captured by the paddles. Additionally, the round rod paddles might lead to a minor centrifugal shift of powder because of the plowing behavior of these paddles compared to flat rod paddles.

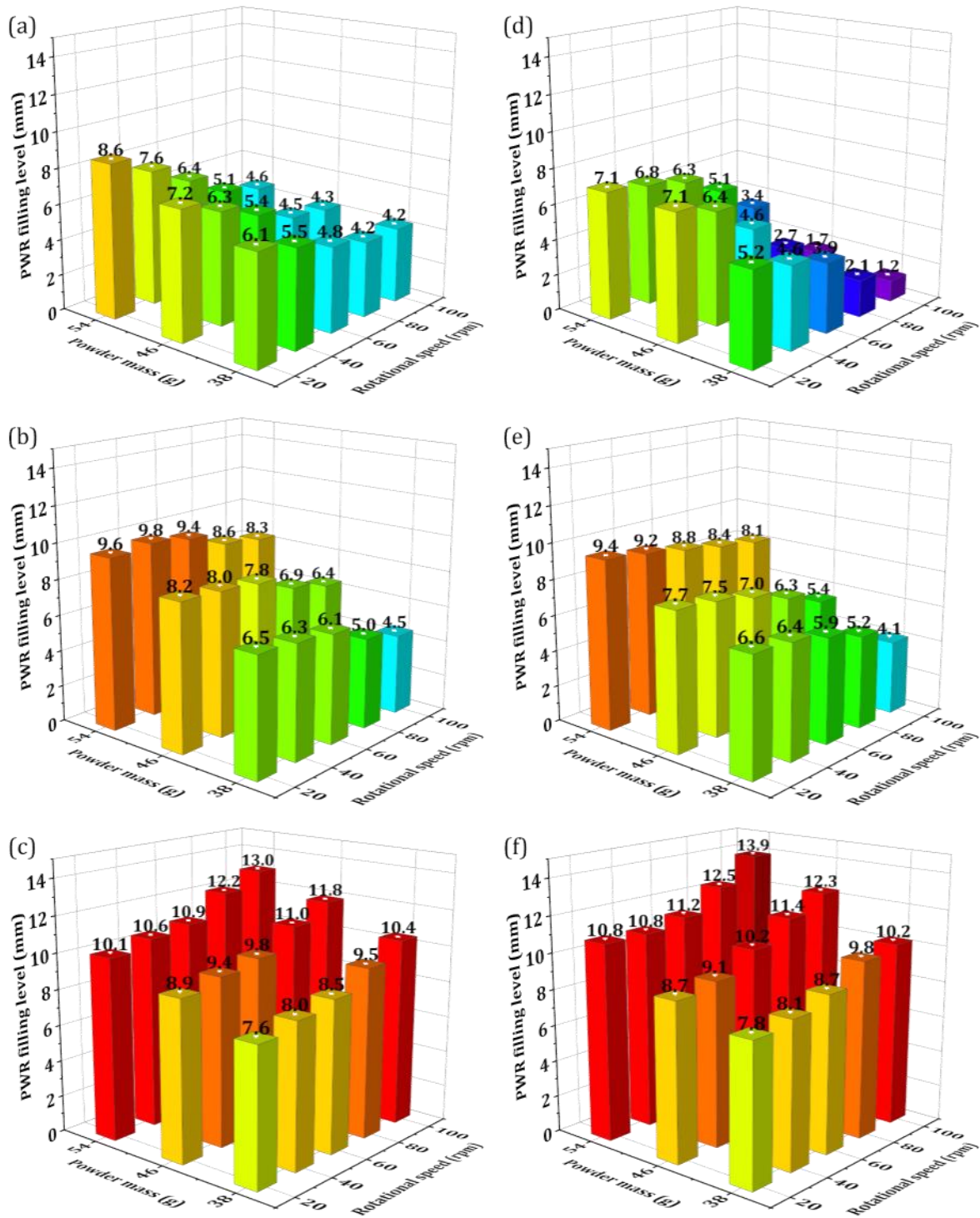


Fig. 35: Filling levels determined offline within the enclosed filling chamber at the three measurement positions for monitoring at a distance of (a) 45 mm, (b) 59 mm, and (c) 73 mm from the center of the chamber for the experiments carried out with the round rod

paddle wheel and at a distance of (e) 45 mm, (f) 59 mm, and (g) 73 mm from the center of the chamber for the experiments carried out with the flat rod paddle wheel. Means \pm SD, n = 30.

3.3.3 Conclusion

The surface analysis of the Av102 powder with the laser triangulator allowed the generation of surface profiles with both paddle wheel geometries. The analysis of the powder surface profiles measured in the enclosed filling chamber of the feed frame clearly showed, that the choice of the paddle wheel geometry has a significant influence on the distribution behavior of powders within the filling chamber.

3.4 In-line monitoring of the powder filling level

3.4.1 Powder surface profiles during the tableting process

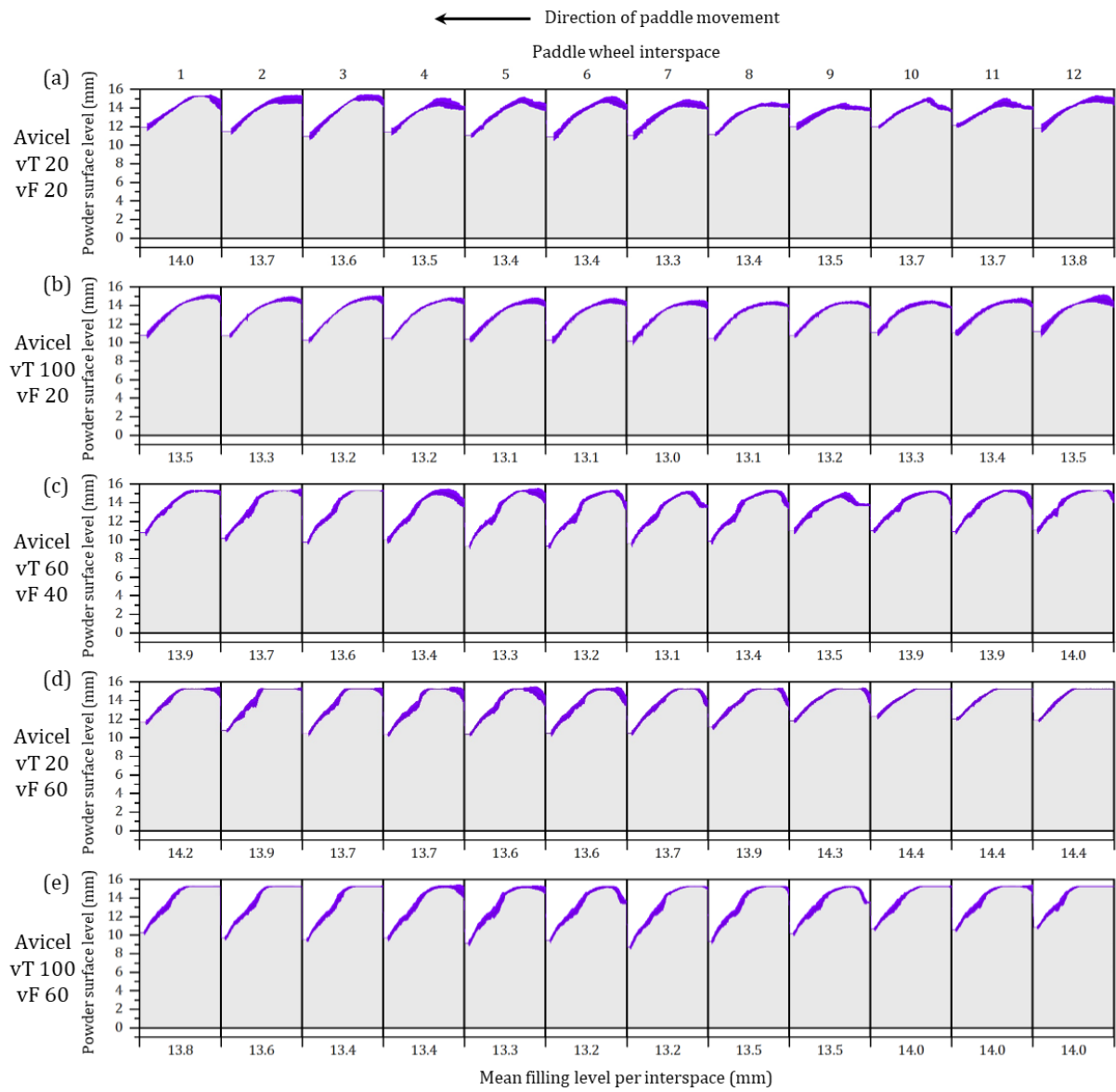
The mean powder surface profiles of Av102 and Destab which are shown in Fig. 36 resulted from an averaging process of the powder surface profiles of complete paddle wheel revolutions over 30 s of monitoring within the steady-state range of the PWR filling level, i.e. that of the powder supply for die filling. These profiles corresponded to 30 revolutions at 60 rpm, 20 revolutions at 40 rpm, and 10 revolutions at 20 rpm and represented the respective mean powder surfaces at 59 mm distance to the chambers' center. The purple band around the mean powder surface profile represents the standard deviation of the layered profiles. The measured powder surface profiles underwent only little changes over a long period of tableting and barely showed any artefacts. They therefore appear to be suitable for in-line monitoring of the filling level and the assessment of distribution phenomena of powders within feed frames.

The readily flowing Destab shows a very smooth and uniform powder surface, which changes much less over the averaged paddle wheel revolutions compared to the poorly flowing cohesive Av102, where the standard deviation between the individual paddle wheel revolutions is much higher. An increase of the powder surface in the direction of the pushing paddles indicates an uneven powder distribution inside the interspaces and thus deviations in the powder availability for die filling. Nevertheless, because of the displacement volume of the paddles the powder availability is presumably lowest at the locations of the paddles.

Within the interspaces Destab always rises steadily towards the paddles until reaching the ceiling of the chamber. Because of friction between the powder and the ceiling, a contact of the powder with the chambers' ceiling is probably accompanied by

redistribution above the paddle into the following interspace [209]. As a result, initial distribution inhomogeneity, which occurs if the feed frame is filled up with powder at the beginning of a tableting process may be compensated, because fuller interspaces lead to a more pronounced powder stream into the following interspace compared to the initially barely filled interspaces. The powder surface of Av102 occasionally lowered in the direction of the paddle after forming a small heap. It seems less prone to stream above the paddle (at least at the position of monitoring) and may be therefore less redistributed. This is probably caused by its cohesive properties and the resulting poor flowability. Also, the pushing paddle is compacting the powder which might result in a mechanically stabilizing effect for cohesive materials [66].

A decrease of the INT filling level is initially observed in the front region of the powder surface within the interspaces. Clearly, the powder accumulates in front of the pushing paddles, such that the powder-free area increases behind the preceding paddles. To increase the sensitivity of the determination of the INT and / or PWR filling level variances, i.e. inhomogeneities in the powder supply, it might be advantageous to separate the interspace profiles in a front and a back area. The front area of the interspace may be used to determine variances with higher amplitude. However, in the present study such a separation for the evaluation of the powder surface profiles was not necessary, as the influences of the factors could be determined without a separation of the interspace areas.



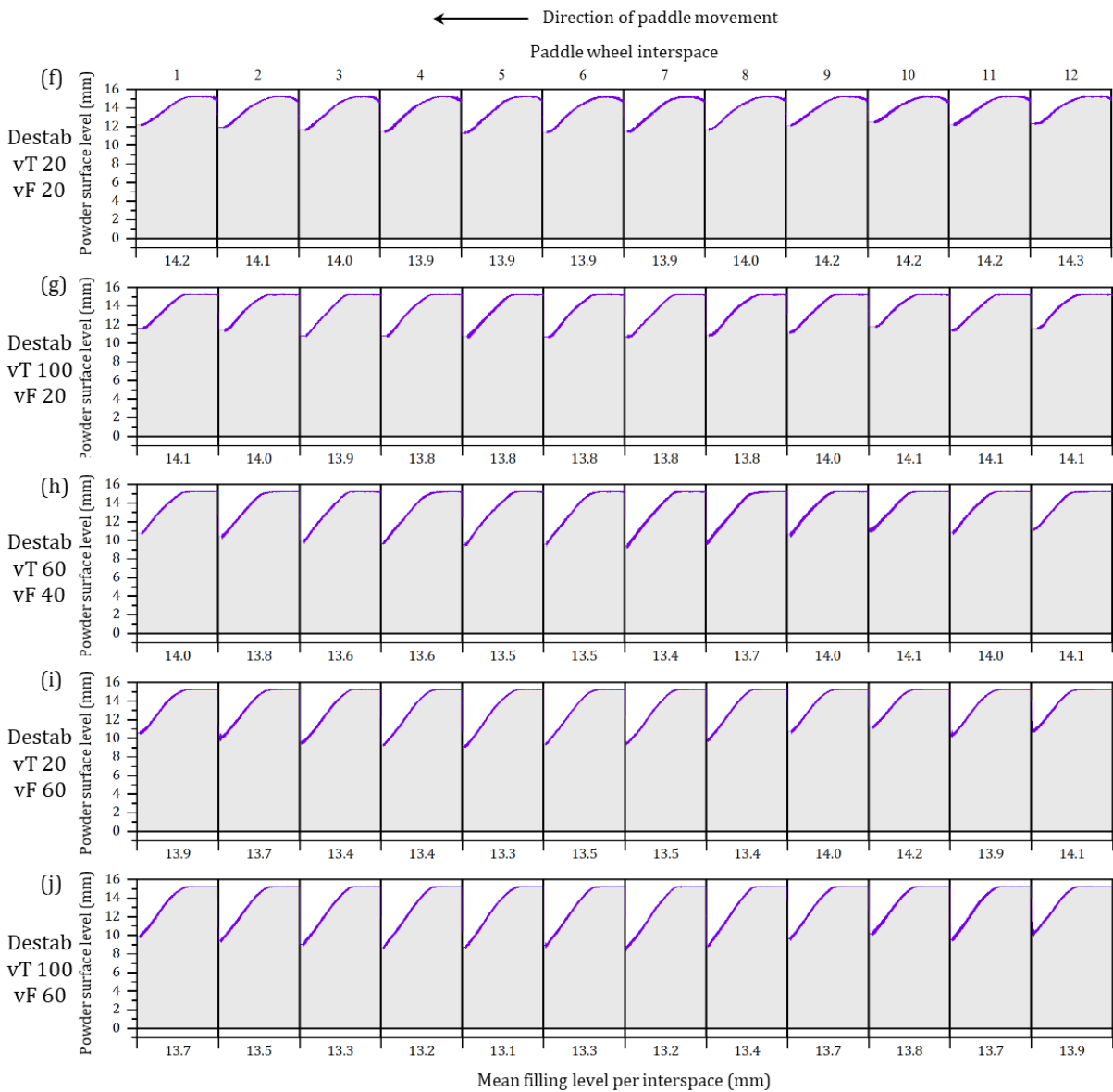


Fig. 36: Mean powder surface profiles obtained at 59 mm distance to the filling chambers' center from 30 s to 60 s of monitoring during the steady state powder supply. The purple band around the average profile represents the standard deviation of the layered profiles. The height of the filling chamber is 15.3 mm. The INT filling levels decrease in direction from the paddle wheel interspaces #1 to #7 and then increase in direction to the paddle wheel interspace #12.

3.4.2 Filling level of the feed frame and the resulting tablet masses

Under the experimental conditions the filling chamber of the feed frame was relatively full at all tableting runs at the selected monitoring position of the powder surface because only small amounts of powder were consumed by the 102i tablet press comparatively to the performance of the feed frame. In Fig. 37 the trends of the PWR filling levels and tablet masses of the individual tableting experiments in which the turret speed, the paddle wheel speed and the powder used for tableting were varied, are shown. To compare the PWR filling levels of the individual experiments, the 30 - 60 s of each experimental run were defined as steady state PWR filling levels and were highlighted by a gray background within the respective plots. This time range does not correspond to the total steady-state ranges of the individual experiments. It only serves to calculate the steady-state filling levels to improve the comparability of these values. The standard deviation of the 12 INT filling levels is plotted as a red band around the PWR filling level. The average tablet masses corresponding to the PWR filling levels are shown as blue dots within the plots at the respective sampling time. The tablet mass samples used for comparison of the experiments are shown as blue stars instead of dots.

The monitoring position of the powder surface is located between the inflow area, i.e. the partition plate orifice through which the powder flows into the filling chamber, and the powder consumption area where the dies are filled with powder. Therefore, the calculated PWR filling level does not represent the filling level of the entire chamber. Depending on how much powder is consumed by the tableting process, the filling level behind the die filling area varies. If the powder consumption is completely compensated by inflowing powder, the measured PWR filling level appears constant, although the total level inside the chamber differs. If more powder flows into the chamber than is consumed, the measured PWR filling level rises and vice versa. By this means, the filling level in the

feed frame which is crucial to the filling process of the dies is determined. As only one spot of the powder surface inside the chamber is monitored, the determined PWR filling level can only be transmitted radially to a limited extent to the remaining interspace, although the INT filling levels and therefore the PWR fillings level usually increase in the direction from the chambers' center to the side wall because of centrifugal effects. The increase of the powder surface from the center to the wall does not follow a general relationship because it depends on the rotational speed and the INT filling level. In addition, because of different powder properties, the forces acting on the powders might affect the radial powder distribution inside the chamber differently, which makes it difficult to compare different powders or rotational speeds. Depending on the INT filling level, the paddle wheel speed and the powder characteristics, powders are subject to a different degree of compression leading to density variations, which cannot be detected by a volumetric determination of the filling level. Therefore, the measurement of a filling level referring to a certain spot inside the chamber with regard to different powders or rotational speeds might stand for different powder volumes and masses which must be considered in a comparison of filling levels obtained at different process settings. Considering these limitations, the steady state range of the PWR filling level is analysed in the following chapter 3.4.2.1. The subsequent chapter 3.4.2.2 focuses on the trends of the PWR filling levels after the steady state range, while chapter 3.4.2.3 deals with the standard deviations of the 12 individual INT filling levels. Finally, effects of the PWR and INT filling level within the filling chamber on the die filling process based on the obtained tablet mass samples are discussed in chapter 3.4.2.4.

3.4.2.1 Steady state PWR filling levels during the tableting runs

In all experiments, the PWR filling levels reach a steady state span within a few paddle wheel revolutions. In one of the experiments containing Av102, the PWR filling level might rise slightly over the first few s (Fig. 37a). Much powder accumulates in the chamber and the powder inflow through the partition plate is limited by the back pressure of already present powder. During the fill-up process, precompacting effects may occur, which possibly manifest themselves volumetrically partly and/or delayed by a slight increase of the PWR filling level. In order for such initial fill-up effects to have no influence on the calculation of a steady state PWR filling level, data of the first 30 s were ignored in the calculation and only values of the following 30 - 60 s of each experimental run were considered. The steady state PWR filling levels which were calculated from the steady-state ranges presented in Figs. 36 and 37 are shown in Table 4.

The results show that all investigated factors, the paddle wheel speed, the turret speed, and the powder used for tableting affected the PWR filling level (Fig. 38a). The ANOVA for the response 'PWR filling level' may be found in the supplementary section. Most of the experiments carried out with Destab indicate a comparably less variable PWR filling level than those carried out with Av102, probably resulting from the better flow behavior of Destab (Fig. 37). Comparing experiments which were carried out at the same paddle wheel speed, the PWR filling level differences that result from varying the turret speed are higher with Av102 than with Destab (Table 4). The same time period is available for both powders to flow through the partition plate orifice and to refill the interspaces. The poorly flowing Av102 probably cannot compensate for the increased powder consumption within the available time period as much as Destab can and therefore shows a significantly larger difference in the PWR filling level if the powder consumption is increased by an enhancement of the turret speed. By increasing the paddle wheel speed,

the powders compared in this study showed opposite shifts of the INT and PWR filling level at least at the investigated monitoring position (Fig. 38a). At 60 rpm paddle wheel speed, the PWR filling level rises with Av102 and lowers with Destab compared to the respective PWR filling levels at 20 rpm paddle wheel speeds. These opposite effects on the PWR filling level occur at both, high and low turret speed. As already mentioned, if INT or PWR filling levels of different powders are compared with each other, it must be considered that different powders might react differently to a variation of the paddle wheel speed in terms of changes in their density and/or radial distribution. The decrease of the PWR filling level with increasing paddle wheel speed in experiments performed with Destab might be caused by its comparatively high density. Because of the high mass and the excellent flow properties of Destab, the centrifugal forces resulting from the rotational movement of the paddle wheel might cause a stronger shift of the powder towards the edge region of the chamber. A pronounced accumulation in this region might also prevent protruding powder from entering the chamber through the partition plate orifice by blocking the orifice. About the causes of this different behavior of both powders at the selected position of monitoring can only be speculated. These causes need to be investigated in futur studies.

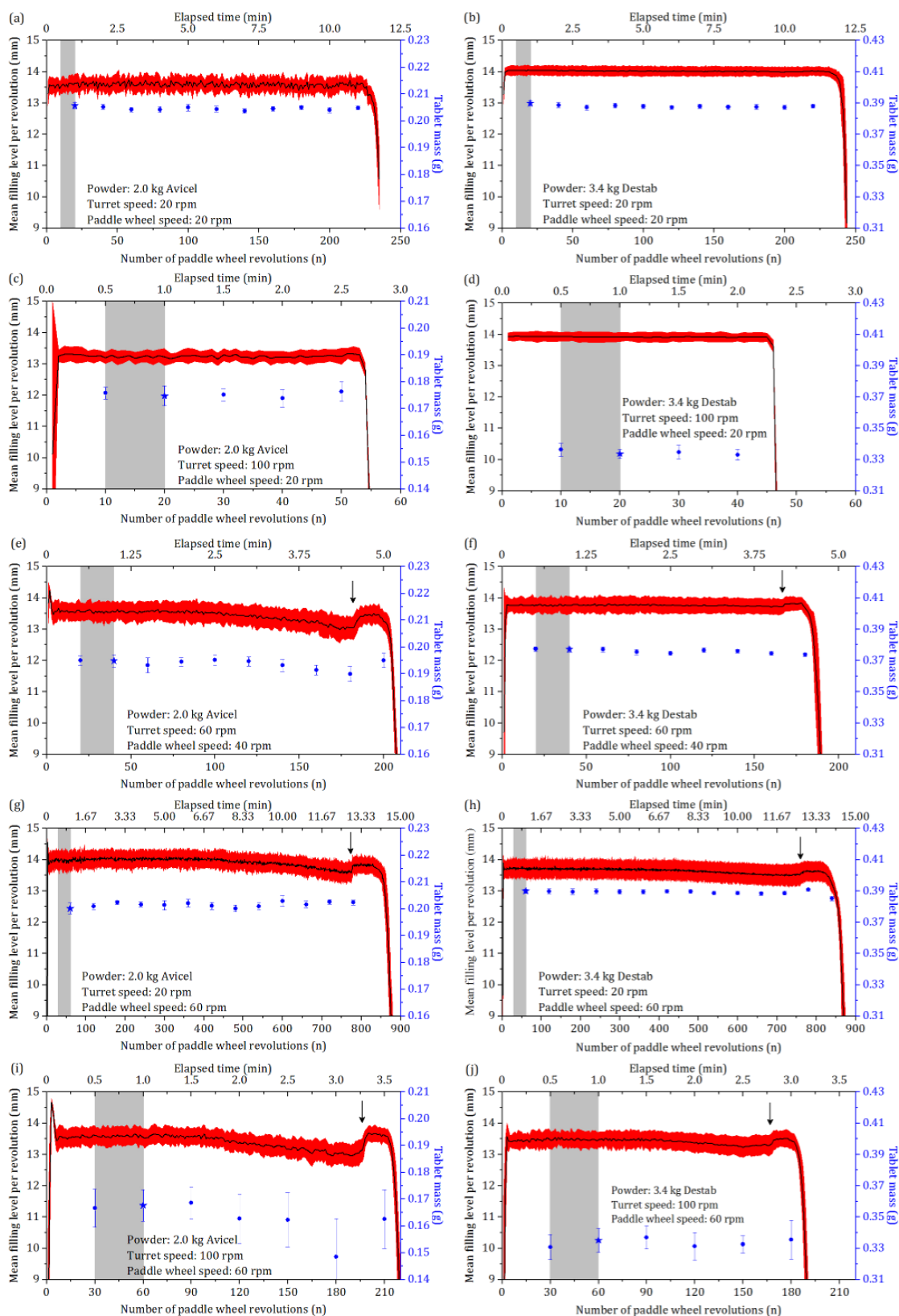
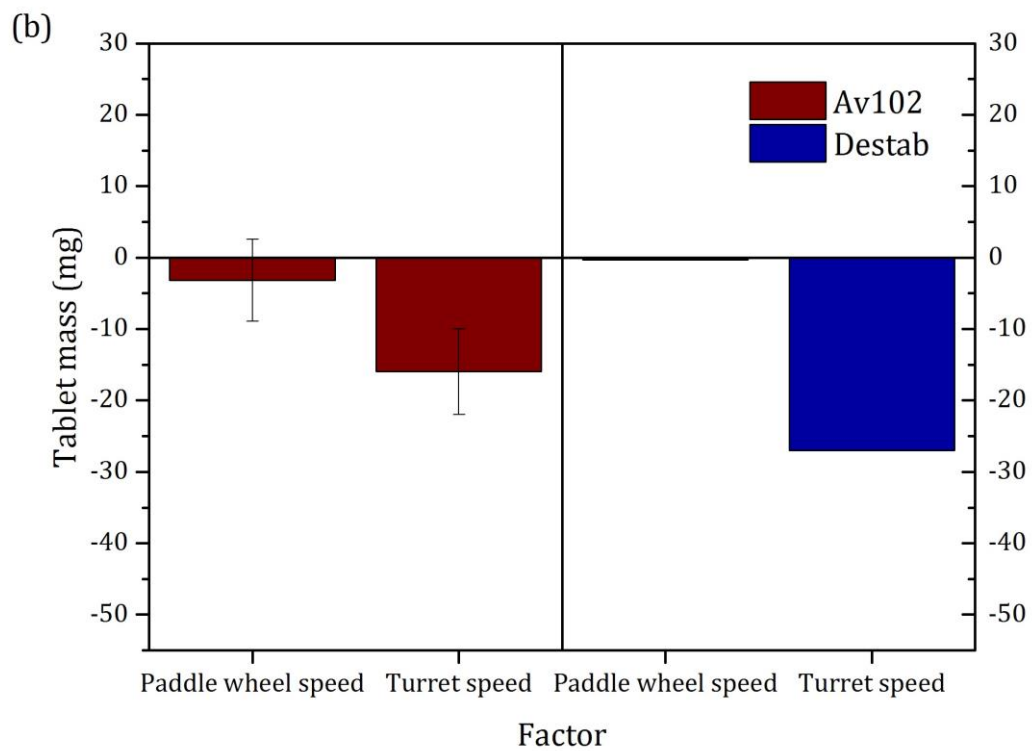
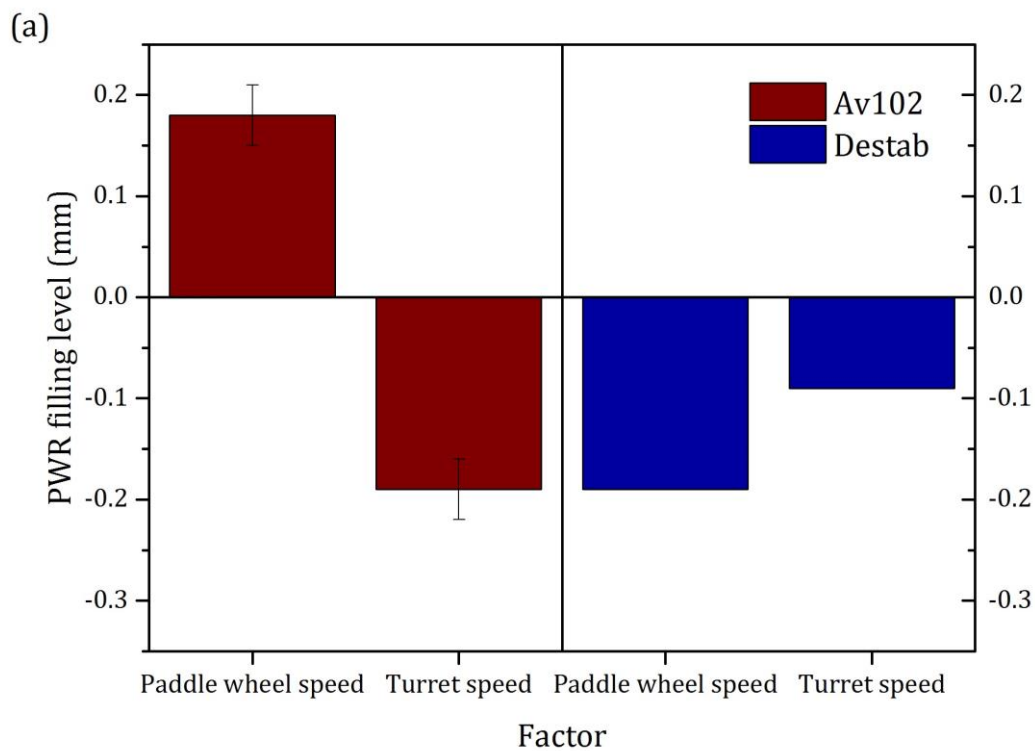


Fig. 37: Mean filling levels within the filling chamber of the feed frame per paddle wheel revolution (PWR filling level). The standard deviation of the filling levels of the 12 individual paddle wheel interspaces per paddle wheel revolution (INT filling levels) is shown as a red band around the mean filling level. The time period which was used for the calculation of the steady state filling level (30 - 60 s of each tableting experiment) is highlighted in gray. The tablet masses with standard deviations corresponding to the PWR filling level are shown as blue dots. The tablet samples ($n = 20$) used for comparisons of the individual experiments are shown as blue stars. Refill time points of the chamber are marked with an arrow. The run-time of the tableting process is shown as elapsed time on the upper x axis.



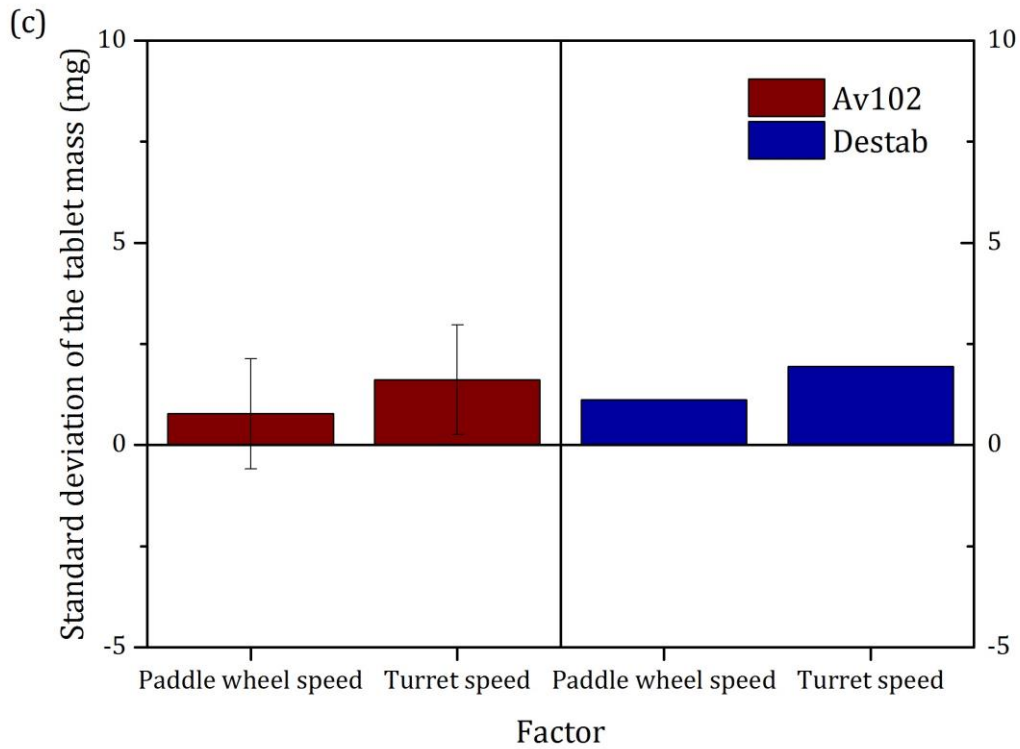


Fig. 38: Effect plots of the investigated factors paddle wheel speed (rpm), turret speed (rpm), and powder (Av102 or Destab) on the response (a) PWR filling level, (b) absolute tablet mass and (c) standard deviation of the tablet mass. Error bars are 95% confidence intervals (Av102).

Table 4: Factor settings with responses of all experiments. The arithmetic mean of the PWR filling levels were calculated within the steady state range of the respective tableting runs (means \pm SD, n = 30 for 60 rpm, n = 20 for 40 rpm, n = 10 for 20 rpm). The tablet samples collected after 60 s were used to calculate the average tablet masses (means \pm SD; (RSD), n = 20).

Turret speed (rpm)	Paddle wheel speed (rpm)	Investigated powder	Filling level (mm)	Tablet mass (mg \pm SD); (RSD %)
20	20	Destab	14.04 \pm 0.01	389.8 \pm 1.6; (0.41 %)
20	60	Destab	13.72 \pm 0.03	389.87 \pm 1.18; (0.30 %)
60	40	Destab	13.76 \pm 0.02	377.1 \pm 1.67; (0.44 %)
100	20	Destab	13.92 \pm 0.01	333.61 \pm 2.85; (0.85 %)
100	60	Destab	13.48 \pm 0.03	335.06 \pm 7.71; (2.30 %)
20	20	Av102	13.60 \pm 0.05	205.7 \pm 1.1; (0.53 %)
20	60	Av102	13.97 \pm 0.04	200.14 \pm 2.03; (1.01 %)
60	40	Av102	13.56 \pm 0.03*	194.83 \pm 2.34*; (1.20 %)
60	40	Av102	13.58 \pm 0.03*	193.06 \pm 1.17*; (0.61 %)
60	40	Av102	13.57 \pm 0.03*	191.24 \pm 2.34*; (1.22 %)
100	20	Av102	13.23 \pm 0.04	174.73 \pm 3.71; (2.12 %)
100	60	Av102	13.58 \pm 0.03	167.64 \pm 5.86; (3.50 %)

*Centerpoint experiment, performed in triplicate to determine the reproducibility of the PWR filling level.

3.4.2.2 Decrease of the PWR filling levels during the tableting runs

Based on the steady state section of the PWR filling level discussed in chapter 3.4.2.1, the experiments performed at 60 rpm paddle wheel speed (with Av102 already at 40 rpm paddle wheel speed) led to a decrease of the PWR filling level in the further course of the tableting runs (Fig. 37e, g-j). This effect indicates a decrease of powder inflow into the filling chamber and occurs independent of the powder consumption by variation of the turret speed.

In a die feeding system as used in this study, the powder inside the hopper above the feed frame causes a vertical pressure due to gravity onto the powder within the feed frame and thus the filling chamber. This pressure decreases if the powder level inside the hopper declines. Thereby it can be assumed that the powder density also decreases. Both, a reduced density as well as vertical pressure may lead to a decrease of the powder inflow through the partition plate orifice to the filling chamber. The distributing chamber and the partition plate are intended to reduce the transfer of these pressure effects on the die filling process by intercepting the pressure with the partition plate. However, the decrease of the PWR filling level indicates that these pressure effects may still have an influence on the filling level within the filling chamber.

The onset of the PWR filling level decrease begins after the consumption of approximately half of the powder volume of both powders. Destab is much denser than Av102 and thus its remaining volume in the hopper is heavier when the decrease of the PWR filling level begins. However, the absolute mass of the powders and therefore the pressure acting on the powder inside the distributing chamber appears to be of minor importance for the beginning of this effect. If the absolute mass was of major importance, the PWR filling levels in experiments carried out with Av102 would lower much earlier than those carried

out with Destab. Instead of the absolute powder mass, the remaining powder volume seems to be of importance for the begin of the PWR filling level decrease, as it represents a pressure relative to the powder density and therefore a minimum limit of vertical pressure which is necessary to exert no measurable effect (by the device) on the chambers' filling process.

Nevertheless, the decrease in the PWR filling level was more pronounced in experiments performed with Av102 which is most likely caused by its cohesive properties. A high paddle wheel speed might lead to a decrease in flowability by precompaction of the powders in the distributing chamber which might therefore increase the influence of the vertical pressure on the powder stream through the partition plate orifice into the filling chamber. Possibly, the better flowability of Destab compensates for the counteracting effects on the powder inflow into the filling chamber more efficiently. These counteracting effects caused by centrifugal forces occur horizontally and therefore lower effects by vertical forces on the powder movement in the direction of the partition plate orifice.

A sudden refill of the chamber at the end of the tableting experiments shortly before the powder is used up was observed leading to a PWR filling level which is approximately the same as before the level decrease began (Fig. 37e-j). It appears that a critical condition is reached which triggers an accelerated powder inflow into the chamber. Moreover, the position of the transition orifice inside the partition plate might play a critical role. However, the effect of refilling needs to be investigated in futur studies.

3.4.2.3 Initial inhomogeneities in the powder filling levels

Differences between the individual INT filling levels arose in all experiments during the initial filling of the chamber and persisted until the end of the tableting process. A comparably lower filling of interspaces during the initial fill-up of the filling chamber still showed the lowest INT filling levels at the end of the respective experiment (Fig. 39). In almost all experiments, these differences follow a similar pattern, which apparently can be assigned to the numbered physical 12 interspaces: The INT filling level decreases in the direction from paddle wheel interspaces number 1 to number 5-7 and then increases in direction to paddle wheel interspace number 12 (Fig. 36). These differences in the powder distribution between the paddle wheel interspaces were always less pronounced in experiments carried out with Destab compared to Av102 at otherwise the same process settings. With both powders these differences were less pronounced in experiments run at the low paddle wheel speed of 20 rpm. They might result from the already mentioned manufacturing and/or mounting inaccuracies, e.g. geometric deviations of the paddle wheel heights within the chamber. Consequently, the distance between the individual paddles and the ground plate may vary, by which different amounts of powder may be captured by the paddles and may thus accumulate to different extents in front of the respective paddle. This effect might be less pronounced at low paddle wheel speeds and with better flowing materials than Av102.

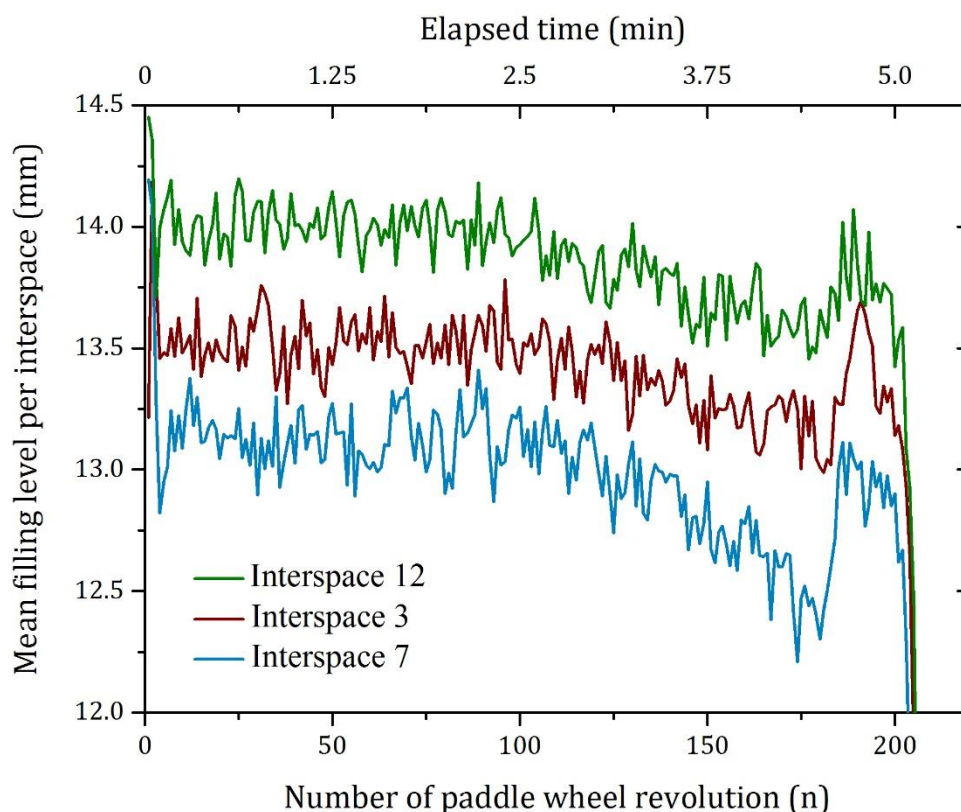


Fig. 39: INT filling levels of 3 out of the 12 individual paddle wheel interspaces within the filling chamber of the feed frame during the tableting experiment with Av102 at a turret speed of 60 rpm and a paddle wheel speed of 40 rpm. Initial filling level differences persist until the end of the tableting experiment.

In this study only the filling chamber was used and the dosing chamber was deactivated by an acrylic lid. To find out whether the differences between the INT filling levels are compensated by the dosing chamber as both chambers are connected to each other to a small extent, in a further experiment both chambers were employed and the resulting differences were determined. This experiment was carried out with Av102. It was found that the differences in the powder distribution were lower but still remained from the beginning until the end of the experiment (Fig. 40). The cause of such INT filling level

differences and whether these occur and/or vanish during commercial production need to be clarified by futur studies.

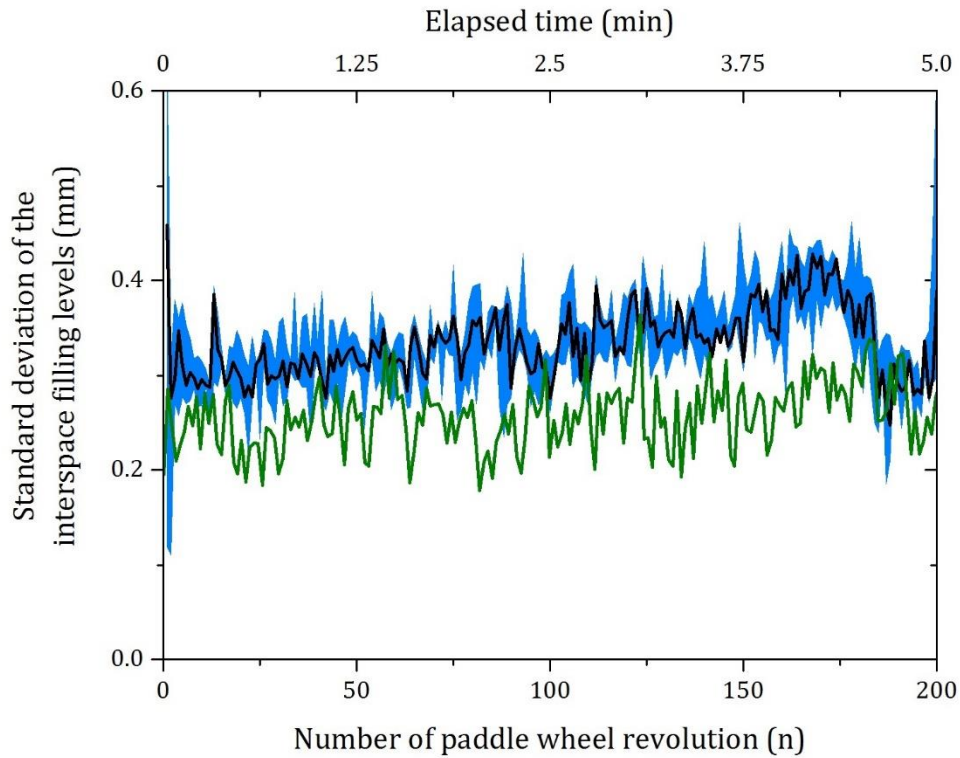


Fig. 40: Comparison of the standard deviations of the 12 interspace filling levels (INT-filling levels) of the tableting experiments in which only the filling chamber was used and the dosing chamber was deactivated ($n = 3$, black curve) and the experiment in which both chambers were used ($n = 1$, green curve). The span of the standard deviations of the tableting experiments containing only the filling chamber is shown as a blue band around the median.

3.4.2.4 Factor influences on the feed frames' filling level and the tablet masses

The presented results show that a variation of the powder used for tableting and / or the turret speed lead to significantly different tablet masses and their corresponding standard deviations (Table 4, Fig. 37). It can be assumed that the tablet masses of the Av102 and Destab tablets differ mainly because of the different specific densities of the Av102 and Destab powders. Destab is more densely packed than Av102 and leads to the heavier tablets. The relative standard deviations of Destab tablets are significantly lower, which is mainly a consequence of its excellent flow behavior.

As expected, an increase in the turret speed led to a significant reduction in the tablet masses of both powders (Fig. 38b). The ANOVA for the response 'tablet mass' may be found in the supplementary section. Usually, the faster the turret speed, the lower the weight of the tablets and the larger the mass deviations [81]. A reduction in the tablet mass results from the decreased filling time, which is available to fill the dies with powder [18]. The result might be an incomplete filling or a lower filling density of the dies. Also, at high turret speeds, increased centrifugal forces may eject some of the powder back out of the dies within the region between the scraper and the precompaction station. With an increase in the turret speed the absolute decrease of the tablet masses is more pronounced in the experiments performed with Destab than in those performed with Av102, mainly resulting from the higher density of the Destab powder. However, the percentage decrease in tablet mass, which is more meaningful than absolute values regarding comparisons of powders with different densities, was slightly higher in the experiments with Av102, presumably because of the poorer flow behavior of Av102 than that of Destab and therefore a higher influence of the filling time of the dies on their filling with Av102. With an increase in the turret speed a significant increase in the standard

deviation of the tablet masses was observed ($p = 0.03$) (Fig. 38c). The ANOVA for the response 'standard deviation of the tablet mass' may be found in the supplementary section. However, because of the large variation in the response 'standard deviation of the tablet mass' during the center point experiment (40 rpm paddle wheel speed, 60 rpm turret speed, 2 kg of Av102 powder, $n = 3$), no significant effect of the paddle wheel speed on the standard deviation of the tablet mass could be determined with a significance threshold of $p = 0.05$. According to the analysis of variance the F value of the model of 6.61 implies that there is a 5.4 % chance that an F value of the model this large could occur because of noise if the insignificant factor paddle wheel speed is considered within the model. In the literature it is described that an increase of the paddle wheel speed usually leads to a decrease of the standard deviation of the tablet mass [212]. However, in this study a contrary but nonsignificant effect was found ($p = 0.054$). A comparison of the standard deviations of the tablet masses at a paddle wheel speed of 20 and 60 rpm and at 100 rpm turret speed showed that an increase of the paddle wheel speed led to an increase of the standard deviations of the tablet masses with both powders (Fig. 37c vs. 37i, 37d vs. 37j). No significant effect on the tablet masses was observed with increasing paddle wheel speed in the experiments carried out with Av102 ($p = 0.2$), although it is described in the literature that an increase of the paddle wheel speed may lead to an increase of the tablet masses [81]. Peeters et al. suggest, that the paddles may exert a force-feeding effect, which assists especially poorly flowing materials during filling of the dies [81]. Presumably, for these materials force-feeding makes a larger contribution to the filling process than other filling effects such as suction and / or gravity-feeding [81]. The evaluation of the INT filling levels showed that the paddle wheel interspaces are filled to different degrees with powder. These deviations might lead to variations in the die filling and thus to deviations in the resulting tablet masses [27]. A decrease of the PWR

and therefore INT filling levels in the feed frame may be accompanied by changes in the average masses of the tablets. At the turret speed of 60 and 100 rpm, a decrease of the PWR filling level can be associated with a decrease of the average tablet masses (Fig. 37e and i). As already mentioned, the pressure of the remaining powder resulting from its weight in the hopper above the feed frame mostly likely reduces the powder inflow into the filling chamber which subsequently leads to a lower filling degree of the dies. Additionally, the deviation of the tablet masses increases with a decrease of the PWR filling level in the experiment with Av102 at 100 rpm turret and 60 rpm paddle wheel speed, suggesting that the powder supply might become more irregular. The irregular powder supply during die filling is also reflected by a slight increasing standard deviation of the 12 INT filling levels, which is shown as a red band around the mean filling level (Fig. 37i).

The sudden increase of the PWR filling levels, which was discussed in chapter 3.4.2.2, were accompanied by an increase in the mean tablet masses (Fig. 37e, 37h, 37i). This observed phenomenon indicates that the extent of die filling may be dependent on the filling level of the feed frame as already suggested by experimental simulations of die filling [27]. However, in the experiment with Destab at 60 rpm paddle wheel speed and 100 rpm turret speed (Fig. 37j) the tablet mass varies much more over the course of the experiment than the powder filling level within the feed frame. Therefore, it is assumed that further factors influence the tablet mass, for example variations in the powder density or flowability within the die filling area of the feed frame, which were not considered in this study.

3.4.3 Conclusion

The presented method enables an in-line monitoring of the filling level in the filling chamber of the feed frame of rotary tablet presses. The experiments show that the turret speed, the paddle wheel speed and the powder characteristics may all affect the filling level within the filling chamber. An increase of the turret speed may reduce the filling level within the filling chamber because more powder is consumed by the dies whereas the dynamics of the filling level caused by an increase of the paddle wheel speed are more complex and affect the filling level in both directions, depending on the respective monitoring and process conditions, such as the position of the laser for monitoring of the filling level and the type of powder used for tableting.

Moreover, the device is suitable to provide information on the homogeneity of the powder supply for die filling during the tableting process by calculating the standard deviation of the filling levels of the individual paddle wheel interspaces per paddle wheel revolution. The method allows to detect a decrease of the filling level and / or a sudden refill effect in the filling chamber, which is often observed at the end of tablet productions and may influence the tablet mass.

The powders used in this study showed differences in the corresponding mean powder surface profiles which are monitored in the filling chamber. This is probably related to the different flow properties and might provide useful information on the influence of the rotational movement of the paddle wheel on differences in the accumulation behavior of powders in front of the pushing paddles. The powder surface profiles also provide information on variations in the availability of powders for die filling within the interspaces which might be used to optimize paddle wheel geometries for improvement

of the powder distribution homogeneity within the interspaces of paddle wheels or to select a suitable wheel geometry for a specific application.

Initial differences between the filling levels of the individual paddle wheel interspaces were detected by the presented method. Moreover, the results show that these initial differences persisted until the end of the tableting experiments. Additionally, it was observed that in some of the performed experiments the tablet mass varies more than the powder filling level in the filling chamber. Therefore, it is assumed that – besides the powder availability – further factors may also influence the tablet mass.

The one-point measurement used in this study is probably sufficient for production monitoring. However, a multi-point measurement may provide additional information on the radial distribution of bulk materials within the filling chamber which should be investigated in future studies.

3.5 Comparison of the paddle wheel geometries during tableting

The in-line monitoring of the powder surface profiles during the tableting process with the flat rod paddle wheel mounted results in a significantly lower filling level of the filling chamber than in the experiments described in study 3.4, in which the partition plate orifice was not downsized (Fig. 41). This downsizing thus effectively leads to a reduction of the powder flow into the filling chamber and thus to a reduction of the chambers' filling level. In contrast to this significantly reduced filling level with the flat rod paddle wheel, the in-line monitoring with the round rod paddle wheel showed a comparably high filling level despite the identical downsizing of the partition plate orifice (Fig. 41). The filling process of the filling chamber, i.e. the inflow of powder into the filling chamber through the partition plate orifice appears to be improved if using the round rod paddle wheel instead of that with flat rods, because the filling levels determined in the offline experiments with both paddle wheels at 60 rpm paddle wheel speed showed a significantly lower difference between the filling levels (Fig. 35b vs. 35e) compared to those determined in the in-line experiments (Fig. 41a vs. 41b). The cause for the improved filling process of the chamber could not be identified so far. A possible cause might be the higher number and lower displacement volume of the round rods compared to those of the flat rods. The round rods act at shorter intervals on the powder whereby the powder inflow might be improved and/or additional space for the succeeding powder might be available.

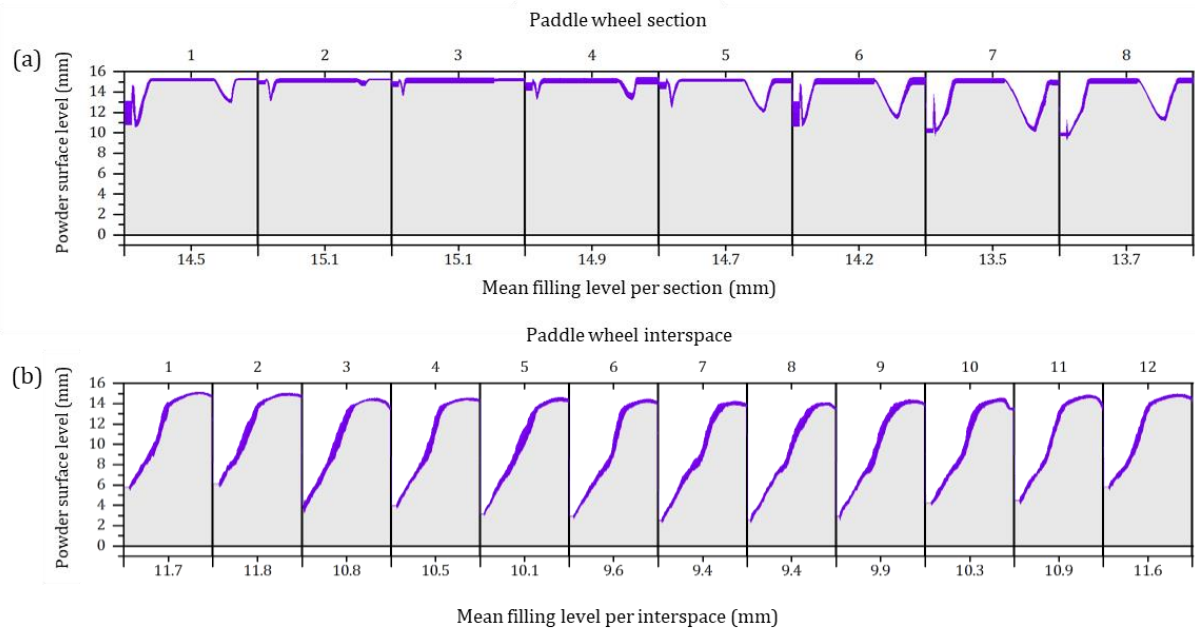


Fig. 41: Mean powder surface profiles obtained by 20 paddle wheel revolutions (from 100 to 120 s of monitoring) of the in-line tableting experiments (a) with the round rod paddle wheel and (b) with the flat rod paddle wheel at a turret speed and a paddle wheel speed of 60 rpm.

The comparison of the resulting tablet masses of the two tableting experiments shows that the choice of the paddle wheel significantly affects both, the absolute tablet masses and the relative standard deviation of the tablet masses over the entire time cause of the experiments. In the case of the round rod paddle wheel, the absolute masses of the produced tablets are significantly higher while the relative standard deviation of the tablet masses is significantly lower (Fig. 42). The powder thus appears to be more uniformly available for die filling if the round rod paddle wheel is mounted. Additionally, the flow behavior of the powder appears to be of advantage for the die filling process, as the dies were filled to a higher extent, which is reflected by the higher tablet masses. Possibly, the plowing behavior of the round rod paddle wheel reduces cohesive forces within the powder, so that it flows better into the dies. However, the increased tablet

masses might also result from the higher powder filling level within the filling chamber or from a combination of the mentioned phenomena [27].

The filling level, the tablet masses and the relative standard deviation of the tablet masses undergo a pronounced and simultaneous trend change at approximately 200 s after starting the tableting experiments, which illustrates the relationship between these factors (Fig. 42 and 43). With both paddle wheels, a decrease of the filling level may lead to a decrease of the absolute tablet masses with an increase of the relative standard deviation of the tablet masses. During the course of the experiments the tablet masses are reduced to a less extent if the round rod paddle wheel is installed compared to the tablet masses of the experiments with the flat rod paddle wheel (Fig. 42b). At the end of the experiments, because of the diminishing pressure of the remaining powder in the hopper, the powder transfer into the filling chamber and thus the powder availability for die filling decreases, which becomes apparent as a decrease in the PWR filling level in all tableting experiments (Fig. 43). With regard to the resulting tablet masses, a decrease of the PWR filling level within the filling chamber appears to be better compensated by the round rod paddle wheel.

The relative standard deviation of the tablet masses obtained with the flat rod paddle wheel varies over the time course of the experiments, while that of the experiments with the round rod paddle wheel keeps relatively constant (Fig. 42a). The cause of these variations has not yet been investigated. However, one possible cause might be the varying overlapping of the flat rod paddles with the dies during the individual die filling processes. Accordingly, the powder availability during die filling probably differs depending on whether the die is covered by a flat rod during filling, or if a critical part of

the filling process takes place within the paddle wheel interspaces with high or low powder accumulation.

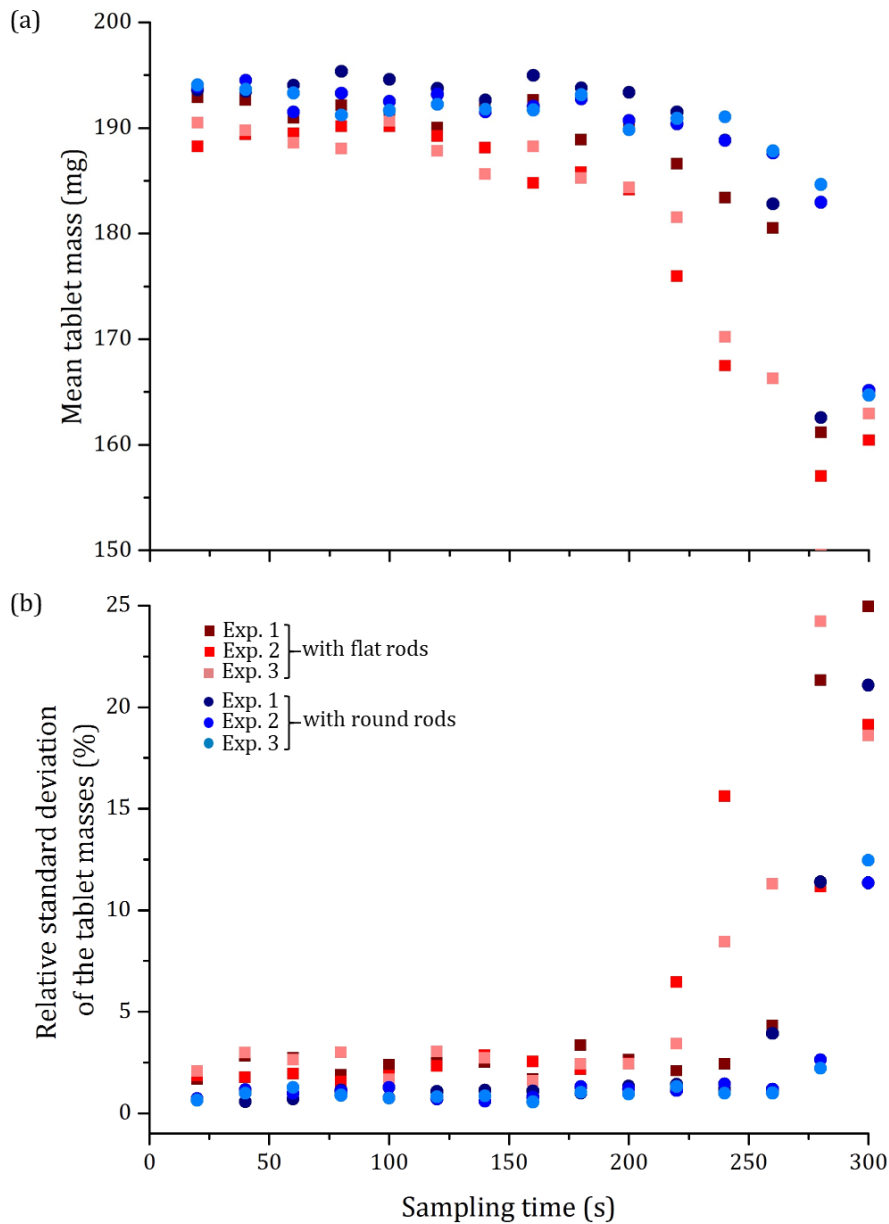


Fig. 42: (a) Mean tablet masses and (b) relative standard deviations of the tablet masses ($n = 3$) during the tableting experiments with Av102, which were performed with either the flat rod paddle wheel (squares) or the round rod paddle wheel (dots). The results of the individual experiments are shown in different colors. At each sample time point 10 tablets were collected, weighed and their weight averaged.

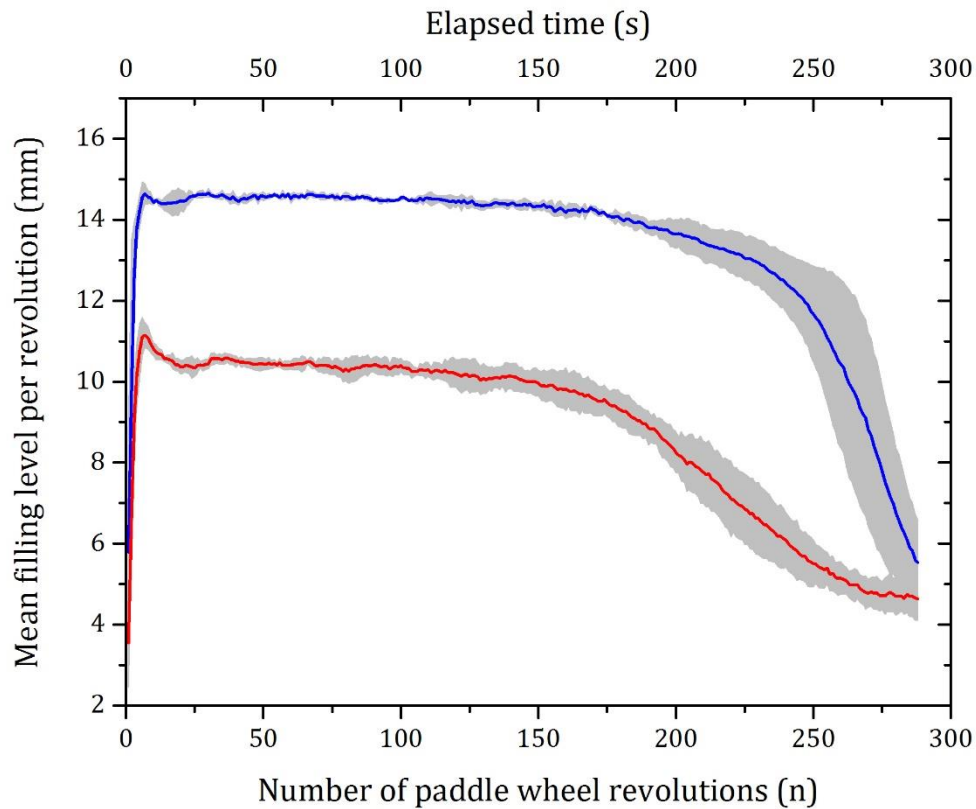


Fig. 43: Mean trend curves ($n = 3$) of the determined filling levels of the tableting experiments either with the round rod paddle wheel (blue line) or the flat rod paddle wheel (red line). The standard deviation of the individual trend curves is shown as a gray band around the means.

3.5.1 Conclusion

The PWR filling level, the tablet masses and the relative standard deviation of the tablet masses underwent a simultaneous trend change within the tableting experiments, which illustrates the relationship between these factors. With both paddle wheels, a decrease of the PWR filling level within the feed frame may lead to a decrease of the absolute tablet masses with an increase of their relative standard deviation. A significant influence of the paddle wheel geometry on both the tablet masses and their uniformity was observed. The tablets obtained with the round rod paddle wheel showed significantly higher masses and a lower standard deviation compared to tablets obtained with the flat rod paddle wheel under the same process conditions. Thus, the application of the paddle wheel with round rods may contribute to a more uniform and more effective die filling process compared to the flat rod paddle wheel. Additionally, the inflow of powder into the filling chamber through the partition plate orifice appeared to be improved if using the round rod paddle wheel instead of that with flat rods. An identification of the cause of this phenomenon might provide useful information for the optimization of the powder availability for the die filling process.

4 References

-
- [1] M. Jivraj, L.G. Martini, C.M. Thomson, An overview of the different excipients useful for the direct compression of tablets, *Pharm. Sci. Technol. Today* 3 (2000) 58–63.
- [2] W.A. Ritschel, A. Bauer-Brandl, *Die Tablette: Handbuch der Entwicklung, Herstellung und Qualitätssicherung*, 2nd ed., Aulendorf, Editio-Cantor-Verl. (2002).
- [3] B.D. Rohera, N.H. Parikh, Influence of plasticizer type and coat level on Surelease film properties, *Pharm. Dev. Technol.* 7 (2002) 407–420.
- [4] N. Pearnchob, J. Siepman, R. Bodmeier, Pharmaceutical applications of shellac: moisture-protective and taste-masking coatings and extended-release matrix tablets, *Drug Dev. Ind. Pharm.* 29 (2003) 925–938.
- [5] F. Siepman, A. Hoffmann, B. Leclercq, B. Carlin, J. Siepman, How to adjust desired drug release patterns from ethylcellulose-coated dosage forms, *J. Control. Release* 119 (2007) 182–189.
- [6] H. Sohi, Y. Sultana, R.K. Khar, Taste masking technologies in oral pharmaceuticals: recent developments and approaches, *Drug Dev. Ind. Pharm.* 30 (2004) 429–448.
- [7] Levina, M., Cunningham, C.R., The effect of core design and formulation on the quality of film coated tablets., *Pharm. Technol. Eur.* 17 (2005) 29–37.
- [8] M. Možina, D. Tomaževič, F. Pernuš, B. Likar, Real-time image segmentation for visual inspection of pharmaceutical tablets, *Mach. Vis. Appl.* 22 (2011) 145–156.
- [9] Food and Drug Administration, Code of Federal Regulations Title 21. Part 206. Imprinting of solid oral dosage form drug products for human use (2014 revised), http://academy.gmp-compliance.org/guidemgr/files/cfr_2016/cfr-2016-title21-vol4-part206.pdf. Accessed 11.06.2019.
-

-
- [10] S.S. Bharate, S.B. Bharate, A.N. Bajaj, Interactions and incompatibilities of pharmaceutical excipients with active pharmaceutical ingredients a comprehensive review, *J. Excip. Food Chem.* (2010) 3–26.
- [11] A. Delacourte, J.C. Guyot, P. Colombo, P.L. Catellani, Effectiveness of lubricants and lubrication mechanism in tablet technology, *Drug Dev. Ind. Pharm.* 21 (1995) 2187–2199.
- [12] T. Martinello, T.M. Kaneko, M.V.R. Velasco, M.E.S. Taqueda, V.O. Consiglieri, Optimization of poorly compactable drug tablets manufactured by direct compression using the mixture experimental design, *Int. J. Pharm.* 322 (2006) 87–95.
- [13] M.C. Gohel, P.D. Jogani, A review of co-processed directly compressible excipients, *J. Pharm. Pharm. Sci.* 8 (2005) 76–93.
- [14] G.K. Bolhuis, N.A. Armstrong, Excipients for direct compaction - an update, *Pharm. Dev. Technol.* 11 (2006) 111–124.
- [15] L.L. Augsburger, S.W. Hoag, *Pharmaceutical dosage forms: Tablets*, 3rd ed., Informa Healthcare USA (2008).
- [16] J. Li, Y. Wu, Lubricants in pharmaceutical solid dosage forms, *Lubricants* 2 (2014) 21–43.
- [17] M. Levina, A.R. Rajabi-Siahboomi, The influence of excipients on drug release from hydroxypropyl methylcellulose matrices, *J. Pharm. Sci.* 93 (2004) 2746–2754.
- [18] A. Mehrotra, B. Chaudhuri, A. Faqih, M.S. Tomassone, F.J. Muzzio, A modeling approach for understanding effects of powder flow properties on tablet weight variability, *Powder Technol.* 188 (2009) 295–300.
- [19] S.T. David, L.L. Augsburger, Plastic flow during compression of directly compressible fillers and its effect on tablet strength, *J. Pharm. Sci.* 66 (1977) 155–159.
-

-
- [20] C. Ufret, K. Morris, Modeling of powder blending using on-line near-infrared measurements, *Drug Dev. Ind. Pharm.* 27 (2001) 719–729.
- [21] M. Moakher, T. Shinbrot, F.J. Muzzio, Experimentally validated computations of flow, mixing and segregation of non-cohesive grains in 3D tumbling blenders, *Powder Technol.* 109 (2000) 58–71.
- [22] J.J. Fitzpatrick, T. Iqbal, C. Delaney, T. Twomey, M.K. Keogh, Effect of powder properties and storage conditions on the flowability of milk powders with different fat contents, *J. Food Eng.* 64 (2004) 435–444.
- [23] D.S. Parsons, Particle segregation in fine powders by tapping as simulation of jostling during transportation, *Powder Technol.* 13 (1976) 269–277.
- [24] A.U. Vanarase, J.G. Osorio, F.J. Muzzio, Effects of powder flow properties and shear environment on the performance of continuous mixing of pharmaceutical powders, *Powder Technol.* 246 (2013) 63–72.
- [25] V. Ganesan, K.A. Rosentrater, K. Muthukumarappan, Flowability and handling characteristics of bulk solids and powders – a review with implications for DDGS, *Biosyst. Eng.* 101 (2008) 425–435.
- [26] A.R. Fassihi, I. Kanfer, Effect of compressibility and powder flow properties on tablet weight variation, *Drug Dev. Ind. Pharm.* 12 (1986) 1947–1966.
- [27] L.A. Mills, I.C. Sinka, Effect of particle size and density on the die fill of powders, *Eur. J. Pharm. Biopharm.* 84 (2013) 642–652.
- [28] J. Visser, Van der Waals and other cohesive forces affecting powder fluidization, *Powder Technol.* 58 (1989) 1–10.
- [29] R. Furukawa, Y. Shiosaka, K. Kadota, K. Takagaki, T. Noguchi, A. Shimosaka, Y. Shirakawa, Size-induced segregation during pharmaceutical particle die filling assessed by response surface methodology using discrete element method, *J. Drug Deliv. Sci. Tech.* 35 (2016) 284–293.
-

-
- [30] Y. Guo, C.-Y. Wu, K.D. Kafui, C. Thornton, Numerical analysis of density-induced segregation during die filling, *Powder Technol.* 197 (2010) 111–119.
- [31] F. Lavoie, L. Cartilier, R. Thibert, New methods characterizing avalanche behavior to determine powder flow, *Pharm. Res.* 19 (2002) 887–893.
- [32] A.U. Vanarase, F.J. Muzzio, Effect of operating conditions and design parameters in a continuous powder mixer, *Powder Technol.* 208 (2011) 26–36.
- [33] S. Luding, Shear flow modeling of cohesive and frictional fine powder, *Powder Technol.* 158 (2005) 45–50.
- [34] A. Guo, J.K. Beddow, A.F. Vetter, A simple relationship between particle shape effects and density, flow rate and Hausner Ratio, *Powder Technol.* 43 (1985) 279–284.
- [35] P.W. Cleary, M.L. Sawley, DEM modelling of industrial granular flows: 3D case studies and the effect of particle shape on hopper discharge, *Appl. Math. Model.* 26 (2002) 89–111.
- [36] E. Emery, J. Oliver, T. Pugsley, J. Sharma, J. Zhou, Flowability of moist pharmaceutical powders, *Powder Technol.* 189 (2009) 409–415.
- [37] A. Santomaso, P. Lazzaro, P. Canu, Powder flowability and density ratios: the impact of granules packing, *Chem. Eng. Sci.* 58 (2003) 2857–2874.
- [38] Q. Li, V. Rudolph, B. Weigl, A. Earl, Interparticle van der Waals force in powder flowability and compactibility, *Int. J. Pharm.* 280 (2004) 77–93.
- [39] E.C. Abdullah, D. Geldart, The use of bulk density measurements as flowability indicators, *Powder Technol.* 102 (1999) 151–165.
- [40] R.E. Freeman, J.R. Cooke, L.C.R. Schneider, Measuring shear properties and normal stresses generated within a rotational shear cell for consolidated and non-consolidated powders, *Powder Technol.* 190 (2009) 65–69.
-

-
- [41] N.-O. Lindberg, M. Pålsson, A.-C. Pihl, R. Freeman, T. Freeman, H. Zetzener, G. Enstad, Flowability measurements of pharmaceutical powder mixtures with poor flow using five different techniques, *Drug Dev. Ind. Pharm.* 30 (2004) 785–791.
- [42] M. Peleg, Flowability of food powders and methods for its evaluation? A review, *J Food Process Eng.* 1 (1977) 303–328.
- [43] G. Lumay, F. Boschini, K. Traina, S. Bontempi, J.-C. Remy, R. Cloots, N. Vandewalle, Measuring the flowing properties of powders and grains, *Powder Technol.* 224 (2012) 19–27.
- [44] Y.S. Lee, R. Poynter, F. Podczec, J.M. Newton, Development of a dual approach to assess powder flow from avalanching behavior, *AAPS Pharm. Sci. Tech.* 1 (2000) E21.
- [45] A. Faqih, B. Chaudhuri, A.W. Alexander, C. Davies, F.J. Muzzio, M. Silvina Tomassone, An experimental/computational approach for examining unconfined cohesive powder flow, *Int. J. Pharm.* 324 (2006) 116–127.
- [46] L.C.R. Schneider, I.C. Sinka, A.C.F. Cocks, Characterisation of the flow behaviour of pharmaceutical powders using a model die–shoe filling system, *Powder Technol.* 173 (2007) 59–71.
- [47] I.C. Sinka, L.C.R. Schneider, A.C.F. Cocks, Measurement of the flow properties of powders with special reference to die fill, *Int. J. Pharm.* 280 (2004) 27–38.
- [48] P.D. Jager, T. Bramante, P.E. Luner, Assessment of pharmaceutical powder flowability using shear cell-based methods and application of Jenike's methodology, *J. Pharm. Sci.* 104 (2015) 3804–3813.
- [49] *Europäisches Arzneibuch 9.0 - 9.3: Amtliche deutsche Ausgabe*, 3rd ed., Deutscher Apotheker Verlag, Stuttgart (2018).
- [50] M.K. Taylor, J. Ginsburg, A. Hickey, F. Gheyas, Composite method to quantify powder flow as a screening method in early tablet or capsule formulation development, *AAPS Pharm. Sci. Tech.* 1 (2000) E18.
-

-
- [51] R.B. Shah, M.A. Tawakkul, M.A. Khan, Comparative evaluation of flow for pharmaceutical powders and granules, *AAPS Pharm. Sci. Tech.* 9 (2008) 250–258.
- [52] M.C. Sarraguça, A.V. Cruz, S.O. Soares, H.R. Amaral, P.C. Costa, J.A. Lopes, Determination of flow properties of pharmaceutical powders by near infrared spectroscopy, *J. Pharm. Biomed. Anal.* 52 (2010) 484–492.
- [53] M. Leturia, M. Benali, S. Lagarde, I. Ronga, K. Saleh, Characterization of flow properties of cohesive powders: A comparative study of traditional and new testing methods, *Powder Technol.* 253 (2014) 406–423.
- [54] M. Krantz, H. Zhang, J. Zhu, Characterization of powder flow: Static and dynamic testing, *Powder Technol.* 194 (2009) 239–245.
- [55] P. York, Application of Powder failure testing equipment in assessing effect of glidants on flowability of cohesive pharmaceutical powders, *J. Pharm. Sci.* 64 (1975) 1216–1221.
- [56] W.R. Ketterhagen, J.S. Curtis, C.R. Wassgren, B.C. Hancock, Predicting the flow mode from hoppers using the discrete element method, *Powder Technol.* 195 (2009) 1–10.
- [57] P.A. Langston, U. Tüzün, D.M. Heyes, Discrete element simulation of granular flow in 2D and 3D hoppers: Dependence of discharge rate and wall stress on particle interactions, *Chem. Eng. Sci.* 50 (1995) 967–987.
- [58] A.N. Faqih, A.W. Alexander, F.J. Muzzio, M.S. Tomassone, A method for predicting hopper flow characteristics of pharmaceutical powders, *Chem. Eng. Sci.* 62 (2007) 1536–1542.
- [59] D. Geldart, E.C. Abdullah, A. Verlinden, Characterisation of dry powders, *Powder Technol.* 190 (2009) 70–74.
- [60] R. Schmitt, H. Feise, Influence of tester geometry, speed and procedure on the results from a ring shear tester, *Part. Part. Syst. Charact.* 21 (2004) 403–410.
-

-
- [61] Y. Sheng, C.J. Lawrence, B.J. Briscoe, C. Thornton, Numerical studies of uniaxial powder compaction process by 3D DEM, *Eng. Computation*. 21 (2004) 304–317.
- [62] M.J. Adams, R. McKeown, Micromechanical analyses of the pressure-volume relationship for powders under confined uniaxial compression, *Powder Technol.* 88 (1996) 155–163.
- [63] D. Schulze, *Pulver und Schüttgüter*, Heidelberg, Springer (2014) 49-51.
- [64] Y.Q. D. Zhou, Understanding material properties in pharmaceutical product development and manufacturing: Powder flow and mechanical properties., *J. Validat. Technol.* 16 (2010) 65–77.
- [65] D. Schulze, *Fließeigenschaften von Schüttgütern*, Heidelberg, Springer (2014), 50-93.
- [66] J. Tomas, Fundamentals of cohesive powder consolidation and flow, *Granul. Matter* 6 (2004) 75–86.
- [67] L. Parrella, D. Barletta, R. Boerefijn, M. Poletto, Comparison between a uniaxial compaction tester and a shear tester for the characterization of powder flowability, *KONA* 26 (2008) 178–189.
- [68] L. Shi, S. Chattoraj, C.C. Sun, Reproducibility of flow properties of microcrystalline cellulose - Avicel PH102, *Powder Technol.* 212 (2011) 253–257.
- [69] S.V. Søgaaard, T. Pedersen, M. Allesø, J. Garnæs, J. Rantanen, Evaluation of ring shear testing as a characterization method for powder flow in small-scale powder processing equipment, *Int. J. Pharm.* 475 (2014) 315–323.
- [70] H. Hou, C.C. Sun, Quantifying effects of particulate properties on powder flow properties using a ring shear tester, *J. Pharm. Sci.* 97 (2008) 4030–4039.
- [71] C.C. Sun, Setting the bar for powder flow properties in successful high speed tableting, *Powder Technol.* 201 (2010) 106–108.
- [72] J. Schwedes, Review on testers for measuring flow properties of bulk solids, *Granul. Matter* 5 (2003) 1–43.
-

-
- [73] H. Kalman, Attrition of powders and granules at various bends during pneumatic conveying, *Powder Technol.* 112 (2000) 244–250.
- [74] M. Hirota, Y. Sogo, T. Marutani, M. Suzuki, Effect of mechanical properties of powder on pneumatic conveying in inclined pipe, *Powder Technol.* 122 (2002) 150–155.
- [75] S. Kamath, V.M. Puri, H.B. Manbeck, R. Hogg, Flow properties of powders using four testers - measurement, comparison and assessment, *Powder Technol.* 76 (1993) 277–289.
- [76] A. Fahr, R. Voigt, *Pharmazeutische Technologie*, 12th ed., Stuttgart, Deutscher Apotheker-Verlag (2015).
- [77] Fette Compacting, FE75 - Productivity redefined. <http://www.fette-compacting.com/fe75-productivity-redefined>. Accessed 5 February 2018.
- [78] Rundläuferpresse. <https://de.wikipedia.org/w/index.php?oldid=182955442>. Accessed 28 February 2019.
- [79] E. Nelson, S.M. Naqvi, L.W. Busse, T. Higuchi, The physics of tablet compression, *J. Am. Pharm. Ass.* 43 (1954) 596–602.
- [80] S. Jackson, I.C. Sinka, A.C.F. Cocks, The effect of suction during die fill on a rotary tablet press, *Eur. J. Pharm. Biopharm.* 65 (2007) 253–256.
- [81] E. Peeters, T. de Beer, C. Vervaet, J.-P. Remon, Reduction of tablet weight variability by optimizing paddle speed in the forced feeder of a high-speed rotary tablet press, *Drug Dev. Ind. Pharm.* 41 (2015) 530–539.
- [82] W. Grymonpré, V. Vanhoorne, B. van Snick, B. Blahova Prudilova, F. Detobel, J.P. Remon, T. de Beer, C. Vervaet, Optimizing feed frame design and tableting process parameters to increase die-filling uniformity on a high-speed rotary tablet press, *Int. J. Pharm.* 548 (2018) 54–61.
- [83] C.-Y. Wu, A.C.F. Cocks, O.T. Gillia, D.A. Thompson, Experimental and numerical investigations of powder transfer, *Powder Technol.* 138 (2003) 216–228.
-

-
- [84] M. Dülle, H. Özcoban, C.S. Leopold, Investigations on the residence time distribution of a three-chamber feed frame with special focus on its geometric and parametric setups, *Powder Technol.* 331 (2018) 276–285.
- [85] M. Dülle, H. Özcoban, C.S. Leopold, The effect of different feed frame components on the powder behavior and the residence time distribution with regard to the continuous manufacturing of tablets, *Int. J. Pharm.* 555 (2018) 220–227.
- [86] W.R. Vezin, H.M. Pang, K.A. Khan, S. Malkowska, The effect of precompression in a rotary machine on tablet strength, *Drug Dev. Ind. Pharm.* 9 (1983) 1465–1474.
- [87] D.M. Kremer, A numerical investigation of air flow during tablet compression, *Chem. Eng. Sci.* 61 (2006) 7963–7978.
- [88] C. Al-Karawi, T. Cech, F. Bang, C.S. Leopold, Investigation of the tableting behavior of Ibuprofen DC 85 W, *Drug Dev. Ind. Pharm.* 44 (2018) 1262–1272.
- [89] T.M. Jones, Rotary machine instrumentation for production purposes with particular reference to quality assurance, *Drug Dev. Ind. Pharm.* 12 (1986) 53–70.
- [90] A.M. Salpekar, L.L. Augsburger, Magnesium lauryl sulfate in tableting: Effect on ejection force and compressibility, *J. Pharm. Sci.* 63 (1974) 289–293.
- [91] E.L. Knoechel, C.C. Sperry, H.E. Ross, C.J. Lintner, Instrumented rotary tablet machines, *J. Pharm. Sci.* 56 (1967) 109–115.
- [92] K.T. Mitrevej, L.L. Augsburger, Adhesion of tablets in a rotary tablet press II. Effects of blending time, running time, and lubricant concentration, *Drug Dev. Ind. Pharm.* 8 (1982) 237–282.
- [93] I. Saniocki, A. Sakmann, C.S. Leopold, How suitable is the measurement of take-off forces for detection of sticking during direct compression of various ibuprofen tablet formulations?, *Pharmaceutical development and technology* 18 (2013) 257–265.
-

-
- [94] B.C. Lippold, C. Müller-Goymann, R. Schubert, *Pharmazeutische Technologie: Mit Einführung in Biopharmazie und Biotechnologie*, 10th ed., Stuttgart, Wissenschaftliche Verlagsgesellschaft (2017).
- [95] P.J. Owen, P.W. Cleary, Prediction of screw conveyor performance using the Discrete Element Method (DEM), *Powder Technol.* 193 (2009) 274–288.
- [96] G. Hu, J. Chen, B. Jian, H. Wan, L. Liu, Modeling and simulation of transportation system of screw conveyors by the Discrete Element Method, *IEEE*, (2010), 927–930.
- [97] D. Natoli, M. Levin, L. Tsygan, L. Liu, Development, optimization, and scale-up of process parameters, in: Y. Qiu, Y. Chen, G.G.Z. Zhang, L.X. Yu, R.V. Mantri (Eds.), *Developing solid oral dosage forms*. Amsterdam, Academic Press (2016) 917–951.
- [98] P.L. Catellani, P. Santi, E. Gasperini, S. Ciceri, G. Dondi, P. Colombo, Centrifugal die filling system in a new rotary tablet machine, *Int. J. Pharm.* 88 (1992) 285–291.
- [99] Y. Qiu, Y. Chen, G.G.Z. Zhang, L.X. Yu, R.V. Mantri (Eds.), *Developing solid oral dosage forms: Pharmaceutical theory & practice*, Academic Press, Amsterdam, 2016.
- [100] D. Mateo-Ortiz, R. Méndez, Relationship between residence time distribution and forces applied by paddles on powder attrition during the die filling process, *Powder Technol.* 278 (2015) 111–117.
- [101] R. Mendez, C. Velazquez, F.J. Muzzio, Effect of feed frame design and operating parameters on powder attrition, particle breakage, and powder properties, *Powder Technol.* 229 (2012) 253–260.
- [102] Y. Guo, K.D. Kafui, C.-Y. Wu, C. Thornton, J.P.K. Seville, A coupled DEM/CFD analysis of the effect of air on powder flow during die filling, *AIChE J* 55 (2009) 49–62.
-

-
- [103] R. Mendez, F.J. Muzzio, C. Velazquez, Powder hydrophobicity and flow properties: Effect of feed frame design and operating parameters, *AIChE J.* 58 (2012) 697–706.
- [104] A.S. Narang, V.M. Rao, H. Guo, J. Lu, D.S. Desai, Effect of force feeder on tablet strength during compression, *Int. J. Pharm.* 401 (2010) 7–15.
- [105] A. Mehrotra, M. Llusa, A. Faqih, M. Levin, F.J. Muzzio, Influence of shear intensity and total shear on properties of blends and tablets of lactose and cellulose lubricated with magnesium stearate, *Int. J. Pharm.* 336 (2007) 284–291.
- [106] P.J. Sheskey, R.T. Robb, R.D. Moore, B.M. Boyce, Effects of lubricant level, method of mixing, and duration of mixing on a controlled-release matrix tablet containing hydroxypropyl methylcellulose, *Drug Dev. Ind. Pharm.* 21 (1995) 2151–2165.
- [107] M. Perrault, F. Bertrand, J. Chaouki, An experimental investigation of the effect of the amount of lubricant on tablet properties, *Drug Dev. Ind. Pharm.* 37 (2011) 234–242.
- [108] I.C. Sinka, F. Motazedian, A.C.F. Cocks, K.G. Pitt, The effect of processing parameters on pharmaceutical tablet properties, *Powder Technol.* 189 (2009) 276–284.
- [109] G. Morin, L. Briens, The effect of lubricants on powder flowability for pharmaceutical application, *AAPS Pharm. Sci. Tech.* 14 (2013) 1158–1168.
- [110] A.C. Shah, A.R. Mlodozieniec, Mechanism of surface lubrication: Influence of duration of lubricant-exciipient mixing on processing characteristics of powders properties of compressed tablets, *J. Pharm. Sci.* 66 (1977) 1377–1382.
- [111] H.J. Venables, J.I. Wells, Powder mixing, *Drug Dev. Ind. Pharm.* 27 (2001) 599–612.
- [112] P.R. Wahl, G. Fruhmann, S. Sacher, G. Straka, S. Sowinski, J.G. Khinast, PAT for tableting: Inline monitoring of API and excipients via NIR spectroscopy, *Eur. J. Pharm. Biopharm.* 87 (2014) 271–278.
-

-
- [113] D. Mateo-Ortiz, F.J. Muzzio, R. Méndez, Particle size segregation promoted by powder flow in confined space: The die filling process case, *Powder Technol.* 262 (2014) 215–222.
- [114] H.W. Ward, D.O. Blackwood, M. Polizzi, H. Clarke, Monitoring blend potency in a tablet press feed frame using near infrared spectroscopy, *J. Pharm. Biomed. Anal.* 80 (2013) 18–23.
- [115] S. Šašić, D. Blackwood, A. Liu, H.W. Ward, H. Clarke, Detailed analysis of the online near-infrared spectra of pharmaceutical blend in a rotary tablet press feed frame, *J. Pharm. Biomed. Anal.* 103 (2015) 73–79.
- [116] E.M. Hetrick, Z. Shi, L.E. Barnes, A.W. Garrett, R.G. Rupard, T.T. Kramer, T.M. Cooper, D.P. Myers, B.C. Castle, Development of near infrared spectroscopy-based process monitoring methodology for pharmaceutical continuous manufacturing using an offline calibration approach, *Anal. Chem.* 89 (2017) 9175–9183.
- [117] F. de Leersnyder, E. Peeters, H. Djalabi, V. Vanhoorne, B. van Snick, K. Hong, S. Hammond, A.Y. Liu, E. Ziemons, C. Vervaet, T. de Beer, Development and validation of an in-line NIR spectroscopic method for continuous blend potency determination in the feed frame of a tablet press, *J. Pharm. Biomed. Anal.* 151 (2018) 274–283.
- [118] L. Manley, Z. Shi, Characterizing drug product continuous manufacturing residence time distributions of major/minor excipient step changes using near infrared spectroscopy and process parameters, *Int. J. Pharm.* 551 (2018) 60–66.
- [119] D. Mateo-Ortiz, Y. Colon, R.J. Romañach, R. Méndez, Analysis of powder phenomena inside a Fette 3090 feed frame using in-line NIR spectroscopy, *J. Pharm. Biomed. Anal.* 100 (2014) 40–49.
- [120] European Medicines Agency, Directive 2003/94/EC for medicines and investigational medicines for human use (2003). <https://eur-lex.europa.eu/legal-content/EN/TXT/?uri=celex:32003L0094>. Accessed 4 November 2018.
-

-
- [121] Food and Drug Administration, Code of federal regulations title 21. Part 211. Current Good Manufacturing Practice for finished pharmaceuticals (2014). <https://www.accessdata.fda.gov/scripts/cdrh/cfdocs/cfcr/CFRSearch.cfm?CFRPart=211&showFR=1>. Accessed 4 November 2018.
- [122] Food and Drug Administration, Code of federal regulations title 21. Part 210. Current Good Manufacturing Practice in manufacturing, processing, packing, or holding of drugs (2014). <https://www.accessdata.fda.gov/scripts/cdrh/cfdocs/cfcr/CFRSearch.cfm?CFRPart=210&showFR=1>. Accessed 4 November 2018.
- [123] ICH, Good manufacturing practice guide for active pharmaceutical ingredients Q7 (2000). <https://www.ich.org/products/guidelines/quality/quality-single/article/questions-and-answers-good-manufacturing-practice-guide-for-active-pharmaceutical-ingredients.html>. Accessed 4 November 2018.
- [124] J.D. Nally, Good manufacturing practices for pharmaceuticals, 6th ed., Hoboken, Taylor and Francis (2013).
- [125] Food and Drug Administration, Guidance for industry: Changes to an approved NDA or ANDA (2004). <http://www.fda.gov/downloads/drugs/guidancecomplianceregulatoryinformation/guidances/ucm077097>. Accessed 4 November 2018.
- [126] L.X. Yu, Pharmaceutical quality by design: Product and process development, understanding, and control, *Pharm. Res.* 25 (2008) 2463.
- [127] D.C. Hinz, Process analytical technologies in the pharmaceutical industry: the FDA's PAT initiative, *Anal. Bioanal. Chem.* 384 (2006) 1036–1042.
- [128] T. de Beer, A. Burggraeve, M. Fonteyne, L. Saerens, J.P. Remon, C. Vervaet, Near infrared and Raman spectroscopy for the in-process monitoring of pharmaceutical production processes, *Int. J. Pharm.* 417 (2011) 32–47.
- [129] Food and Drug Administration, Guidance for Industry: PAT - a framework for innovative pharmaceutical development, manufacturing, and quality assurance
-

-
- (2004), <http://www.fda.gov/downloads/Drugs/Guidances/ucm070305>. Accessed 4 November 2018.
- [130] Food and Drug Administration, Pharmaceutical CGMPs for the 21st Century: a risk-based approach (2004).
<http://www.fda.gov/downloads/Drugs/DevelopmentApprovalProcess/Manufacturing/QuestionsandAnsweronCurrentGoodManufacturingPracticescGMPforDrugs/UCM176374>. Accessed 4 November 2018.
- [131] ICH, Guideline on pharmaceutical development Q8 (2009).
<http://www.ich.org/products/guidelines/quality/quality-single/article/pharmaceutical-development.html>. Accessed 4 November 2018.
- [132] R.A. Lionberger, S.L. Lee, L. Lee, A. Raw, L.X. Yu, Quality by design: Concepts for ANDAs, *AAPS J* 10 (2008) 268–276.
- [133] K.A. Bakeev (Ed.), *Process analytical technology: Spectroscopic tools and implementation strategies for the chemical and pharmaceutical industries*, Oxford, Blackwell Pub (2005).
- [134] R. Guenard, G. Thureau, Implementation of process analytical technologies, in: K.A. Bakeev (Ed.), *Process analytical technology. Spectroscopic tools and implementation strategies for the chemical and pharmaceutical industries*, Blackwell Pub, Oxford, UK, Ames, Iowa, (2005), 13–38.
- [135] J.E. Dickens, Overview of process analysis and PAT, in: K.A. Bakeev (Ed.), *Process analytical technology. Spectroscopic tools and implementation strategies for the chemical and pharmaceutical industries*, vol. 3, 2nd ed., Wiley, Chichester, West Sussex, (2010), 1–15.
- [136] J. Munson, C.F. Stanfield, B. Gujral, A review of process analytical technology (PAT) in the U.S. pharmaceutical industry, *Curr. Pharm. Anal.* 2 (2006) 405–414.
- [137] E.W. Richmond, B.R. Buchanan, M.A. Baxter, A. Duff, O.M. Tully, S.A. Thornton, Method and system for determining the homogeneity of tablets: US Patent, (1994).
-

-
- [138] J. Hinzpeter, Method and apparatus for monitoring the compression force of pelleting press rams.: US Patent, (1977).
- [139] J. Hinzpeter, I. Schmidt, H.J. Pierags, Method and apparatus for determining the force-displacement diagram of the pairs of punches of a rotary pelleting machine: US Patent, (1995).
- [140] S.D.A. Wenning, Press production monitoring system and method: US Patent (2000).
- [141] T. Becker, Prozesse in Produktion und Supply Chain optimieren, 2nd ed., Heidelberg, Springer Verl. (2008).
- [142] E. Levi, R. Bojoi, F. Profumo, H.A. Toliyat, S. Williamson, Multiphase induction motor drives - a technology status review, IET Electr. Power Appl. 1 (2007) 489.
- [143] C.M.F.S. Reza, M.D. Islam, S. Mekhilef, A review of reliable and energy efficient direct torque controlled induction motor drives, Renew. Sust. Energ. Rev. 37 (2014) 919–932.
- [144] J.J. Williams, Force measurement and analysis particularly relating to rotary tablet presses, US Patent, (1978).
- [145] D.A. Lewis, Tablet press monitoring and controlling method and apparatus.: U.S. Patent, (1998).
- [146] T.R.M. de Beer, C. Bodson, B. Dejaegher, B. Walczak, P. Vercruysse, A. Burggraeve, A. Lemos, L. Delattre, Y.V. Heyden, J.P. Remon, C. Vervaet, W.R.G. Baeyens, Raman spectroscopy as a process analytical technology (PAT) tool for the in-line monitoring and understanding of a powder blending process, J. Pharm. Biomed. Anal. 48 (2008) 772–779.
- [147] J.D. Kirsch, J.K. Drennen, Near-Infrared spectroscopy: Applications in the analysis of tablets and solid pharmaceutical dosage forms, Appl. Spectrosc. Rev. 30 (1995) 139–174.
-

-
- [148] G. Reich, Near-infrared spectroscopy and imaging: basic principles and pharmaceutical applications, *Adv. Drug Deliver. Rev.* 57 (2005) 1109–1143.
- [149] J. Rantanen, Process analytical applications of Raman spectroscopy, *J. Pharm. Pharmacol.* 59 (2007) 171–177.
- [150] M. Blanco, M. Alcalá, Content uniformity and tablet hardness testing of intact pharmaceutical tablets by near infrared spectroscopy., *Anal. Chim. Acta.* 557 (2006) 353–359.
- [151] M. Klukkert, J.X. Wu, J. Rantanen, J.M. Carstensen, T. Rades, C.S. Leopold, Multispectral UV imaging for fast and non-destructive quality control of chemical and physical tablet attributes, *Eur. J. Pharm. Sci.* 90 (2016) 85–95.
- [152] M. Klukkert, J.X. Wu, J. Rantanen, S. Rehder, J.M. Carstensen, T. Rades, C.S. Leopold, Rapid assessment of tablet film coating quality by multispectral UV imaging, *AAPS Pharm. Sci. Tech.* 17 (2016) 958–967.
- [153] A. Novikova, J.M. Carstensen, T. Rades, C.S. Leopold, Multispectral UV imaging for surface analysis of MUPS tablets with special focus on the pellet distribution, *Int. J. Pharm.* 515 (2016) 374–383.
- [154] A. Novikova, J.M. Carstensen, T. Rades, C.S. Leopold, UV imaging of multiple unit pellet system (MUPS) tablets: A case study of acetylsalicylic acid stability, *Eur. J. Pharm. Biopharm.* 119 (2017) 447–453.
- [155] S.H. Tabasi, R. Fahmy, D. Bensley, C. O'Brien, S.W. Hoag, Quality by design, part I: application of NIR spectroscopy to monitor tablet manufacturing process, *J. Pharm. Sci.* 97 (2008) 4040–4051.
- [156] D. Mateo-Ortiz, F.J. Muzzio, R. Méndez, Particle size segregation promoted by powder flow in confined space: The die filling process case, *Powder Technol.* 262 (2014) 215–222.
- [157] M. Dülle, H. Özcoban, C.S. Leopold, Analysis of the powder behavior and the residence time distribution within a production scale rotary tablet press, *Eur. J. Pharm. Sci.* 125 (2018) 205–214.
-

-
- [158] S.R. Gopireddy, C. Hildebrandt, N.A. Urbanetz, Numerical simulation of powder flow in a pharmaceutical tablet press lab-scale gravity feeder, *Powder Technol.* 302 (2016) 309–327.
- [159] Data acquisition - Wikipedia.
<https://en.wikipedia.org/w/index.php?oldid=878093586>. Accessed 12 February 2019.
- [160] T. Beier, T. Mederer, *Messdatenverarbeitung mit LabVIEW*, München, Carl Hanser Verl. (2015).
- [161] M. Kofler, C. Kühnast, C. Scherbeck, *Raspberry Pi: Das umfassende Handbuch*, 4th ed., Bonn, Rheinwerk Verlag (2018).
- [162] A. Ellin, G. Dolsak, The design and application of rotary encoders, *Sensor Rev.* 28 (2008) 150–158.
- [163] A.C. Negrea, M. Imecs, I.I. Incze, A. Pop, C. Szabo, Error compensation methods in speed identification using incremental encoder, *Electr. Power Eng.* (2012) 441–445.
- [164] W. Blacharski, Monitoring of velocity of manufacturing machines subassemblies by means of a DAQ system, *SSP 164* (2010) 207–211.
- [165] M. Norgia, G. Giuliani, S. Donati, Absolute distance measurement with improved accuracy using laser diode self-mixing interferometry in a closed loop, *IEEE Trans. Instrum. Meas.* 56 (2007) 1894–1900.
- [166] T. Bosch, Laser ranging: a critical review of usual techniques for distance measurement, *Opt. Eng.* 40 (2001) 10.
- [167] Y. Salvadé, N. Schuhler, S. Lévêque, S. Le Floch, High-accuracy absolute distance measurement using frequency comb referenced multiwavelength source, *Appl. Opt.* 47 (2008) 2715.
- [168] F. Blais, Review of 20 years of range sensor development, *Appl. Opt.* 13 (2004) 231.
-

-
- [169] F. Gouaux, N. Servagent, T. Bosch, Absolute distance measurement with an optical feedback interferometer, *Appl. Opt.* 37 (1998) 6684.
- [170] F. Gueuning, M. Varlan, C. Eugene, P. Dupuis, Accurate distance measurement by an autonomous ultrasonic system combining time-of-flight and phase-shift methods, *IEEE IMTC. P.* (1996) 399–404.
- [171] M. Buzinski, A. Levine, W.H. Stevenson, Laser triangulation range sensors: A study of performance limitations, *J. Laser App.* 4 (1992) 29–36.
- [172] K.B. Smith, Y.F. Zheng, Accuracy analysis of point laser triangulation probes using simulation, *J. Manuf. Sci. Eng.* 120 (1998) 736.
- [173] K.H. Goh, N. Phillips, R. Bell, The applicability of a laser triangulation probe to non-contacting inspection, *Int. J. Prod. Res.* 24 (1986) 1331–1348.
- [174] R.R. Lathrop, Solder paste print qualification using laser triangulation, *IEEE Trans. Comp., Packag., Manufact. Technol. C* 20 (1997) 174–182.
- [175] J. Molleda, Real-time flatness inspection of rolled products based on optical laser triangulation and three-dimensional surface reconstruction, *J. Electron. Imaging* 19 (2010) 31206.
- [176] J. Santolaria, D. Guillomía, C. Cajal, J.A. Albajez, J.J. Aguilar, Modelling and calibration technique of laser triangulation sensors for integration in robot arms and articulated arm coordinate measuring machines, *Sensors* 9 (2009) 7374–7396.
- [177] C.P. Keferstein, M. Marxer, Testing bench for laser triangulation sensors, *Sensor Rev.* 18 (1998) 183–187.
- [178] H. Rothe, Improved accuracy in laser triangulation by variance-stabilizing transformations, *Opt. Eng.* 31 (1992) 1538.
- [179] W.Q. Liu, R.X. Jiang, Y.P. Wang, Y.X. Xia, Experimental study of the laser retroreflection of various surfaces, *Proc. SPIE* (1991), 240–243.
-

-
- [180] M. Daneshpanah, K. Harding, Surface sensitivity reduction in laser triangulation sensors, *Proc. SPIE* (2011), 813300.
- [181] R.G. Dorsch, G. Häusler, J.M. Herrmann, Laser triangulation: fundamental uncertainty in distance measurement, *Appl. Optics* 33 (1994) 1306–1314.
- [182] Z. Ji, M.C. Leu, Design of optical triangulation devices, *Opt. Laser Technol.* 21 (1989) 339–341.
- [183] J. Sun, J. Jiang, Laser triangulation measurement of the level in a coal silo, *Min. Sci. Technol. (China)* 21 (2011) 881-884.
- [184] S. Singh, Refractive index measurement and its applications, *Phys. Scr.* 65 (2002) 167–180.
- [185] A.S. Tanenbaum, H. Bos, *Moderne Betriebssysteme*, 4th ed., Hallbergmoos, Pearson (2016).
- [186] H. Herold, B. Lurz, J. Wohlrab, M. Hopf, *Grundlagen der Informatik*, 3rd ed., Hallbergmoos, Pearson (2017).
- [187] P.J. Moriarty, B.L. Gallagher, C.J. Mellor, R.R. Baines, Graphical computing in the undergraduate laboratory: Teaching and interfacing with LabVIEW, *Am. J. Phys.* 71 (2003) 1062–1074.
- [188] W. Georgi, E. Metin, *Einführung in LabVIEW*, 5th ed., München, Hanser (2012).
- [189] P. Orduna, J. Garcia-Zubia, L. Rodriguez-Gil, J. Irurzun, D. Lopez-de-Ipina, F. Gazzola, Using LabVIEW remote panel in remote laboratories: Advantages and disadvantages, *IEEE* (2012) 1–7.
- [190] A. Stefik, S. Siebert, An empirical investigation into programming language syntax, *Trans. Comput. Educ.* 13 (2013) 1–40.
- [191] M.J. Anderson, P.J. Whitcomb, *DOE simplified: Practical tools for effective experimentation*, 2nd ed., CRC Press, Boca Raton (2007).
-

-
- [192] W. Kleppmann, Taschenbuch Versuchsplanung: Produkte und Prozesse optimieren, 7th ed., München, Hanser Verl. (2011).
- [193] K. Siebertz, D. van Bebber, T. Hochkirchen, Statistische Versuchsplanung: Design of Experiments (DoE), 2nd ed., Heidelberg, Springer (2017).
- [194] Burghaus, R., Mogk, G., Mrziglod, T., Hübl, P., Method and system for the automatic design of experiments (2006).
- [195] P.A. Keller, Six sigma demystified, 2nd ed., New York, McGraw-Hill Education (2011).
- [196] P.A. Keller, Statistical process control demystified, New York, McGraw-Hill Education (2012).
- [197] S.C. Cotter, A screening design for factorial experiments with interactions, *Biometrika* 66 (1979) 317–320.
- [198] L.X. Yu, G. Amidon, M.A. Khan, S.W. Hoag, J. Polli, G.K. Raju, J. Woodcock, Understanding pharmaceutical quality by design, *AAPS J.* 16 (2014) 771–783.
- [199] J.T. Carstensen, C. Ertell, Physical and chemical properties of calcium phosphates for solid state pharmaceutical formulations, *Drug. Dev. Ind. Pharm.* 16 (1990) 1121–1133.
- [200] JRS Pharma, Emcompress. <https://www.jrspharma.com/pharmawAssets/docs/brochures/emcompress.pdf>. Accessed 17 August 2018.
- [201] Particle Dynamics, Destab. <http://pdhllc.com/products/destab>. Accessed 17 August 2018.
- [202] Avicel for Solid Dose Forms - DuPont, Danisco, 2018. <http://www.danisco.com/pharmaceuticals/pharmaceutical-products/avicelr-for-solid-dose-forms>. Accessed 17 August 2018.
- [203] J. Rojas, A. Lopez, S. Guisao, C. Ortiz, Evaluation of several microcrystalline celluloses obtained from agricultural by-products, *J. Adv. Pharm. Technol. Res.* 2 (2011) 144–150.
-

-
- [204] Foremost Fast Flo 316. http://www.sheffieldbioscience.com/Fast_Flo_316. Accessed 17 August 2018.
- [205] J. Wang, H. Wen, D. Desai, Lubrication in tablet formulations, *Eur. J. Pharm. Biopharm.* 75 (2010) 1–15.
- [206] L. Shi, Y. Feng, C.C. Sun, Origin of profound changes in powder properties during wetting and nucleation stages of high-shear wet granulation of microcrystalline cellulose, *Powder Technol.* 208 (2011) 663–668.
- [207] H.-G. Maas, On the Accuracy potential in underwater/multimedia photogrammetry, *Sensors* 15 (2015) 18140–18152.
- [208] W. Grymonpré, B. Blahova Prudilova, V. Vanhoorne, B. van Snick, F. Detobel, J.P. Remon, T. de Beer, C. Vervaet, Downscaling of the tableting process: Feasibility of miniaturized forced feeders on a high-speed rotary tablet press, *Int. J. Pharm.* 550 (2018) 477–485.
- [209] D. Mateo-Ortiz, R. Méndez, Microdynamic analysis of particle flow in a confined space using DEM: The feed frame case, *Adv. Powder Technol.* 27 (2016) 1597–1606.
- [210] L.Y. Leung, C. Mao, I. Srivastava, P. Du, C.-Y. Yang, Flow function of pharmaceutical powders is predominantly governed by cohesion, not by friction coefficients, *J. Pharm. Sci.* 106 (2017) 1865–1873.
- [211] B. van Snick, W. Grymonpré, J. Dhondt, K. Pandelaere, G. Di Pretoro, J.P. Remon, T. de Beer, C. Vervaet, V. Vanhoorne, Impact of blend properties on die filling during tableting, *Int. J. Pharm.* 549 (2018) 476–488.
- [212] X. Xie, V.M. Puri, Uniformity of powder die filling using a feed shoe: A review, *Particul. Sci. Technol.* 24 (2006) 411–426.
-

5 Appendix

A Supplementary data**A.1 Design matrix evaluation (Study 2.3.4.1)**

3 Factors: A, B, C (A = Paddle wheel speed, b = Mass of Emc, c = Monitoring position)

Design Matrix Evaluation for Response Surface Quadratic Model:

Degrees of Freedom for Evaluation

Model	9
Residuals	215
Lack Of Fit	65
Pure Error	150
Corr Total	224

A recommendation is a minimum of 3 lack of fit df and 4 df for pure error.

This ensures a valid lack of fit test.

Fewer df will lead to a test that may not detect lack of fit.

Power at 5 % alpha level to detect signal/noise ratios of

Term	StdErr**	VIF	Ri-Squared	0.5 Std. Dev.	1 Std. Dev.	2 Std. Dev.
A	0.094	1.00	0.0000	75.2 %	99.9 %	99.9 %
B	0.094	1.00	0.0000	75.2 %	99.9 %	99.9 %
C	0.082	1.00	0.0000	86.2 %	99.9 %	99.9 %
AB	0.13	1.00	0.0000	46.3 %	96.2 %	99.9 %
AC	0.12	1.00	0.0000	57.7 %	99.1 %	99.9 %
BC	0.12	1.00	0.0000	57.7 %	99.1 %	99.9 %
A^2	0.16	1.00	0.0000	87.8 %	99.9 %	99.9 %
B^2	0.16	1.00	0.0000	87.8 %	99.9 %	99.9 %
C^2	0.14	1.00	0.0000	94.1 %	99.9 %	99.9 %

**Basis Std. Dev. = 1.0

Standard errors should be similar within type of coefficient. Smaller is better. Ideal VIF is 1.0. VIFs above 10 are cause for alarm, indicating coefficients are poorly estimated due to multicollinearity.

Measures Derived From the $(X'X)^{-1}$ Matrix

Std	Leverage	Point Type
1	0.0883	Unknown
2	0.0883	Unknown
3	0.0883	Unknown
4	0.0616	Unknown
5	0.0616	Unknown
6	0.0616	Unknown
7	0.0883	Unknown
8	0.0883	Unknown
9	0.0883	Unknown
10	0.0535	Unknown
11	0.0535	Unknown
12	0.0535	Unknown
13	0.0368	Unknown
14	0.0368	Unknown
15	0.0368	Unknown
16	0.0535	Unknown
17	0.0535	Unknown
18	0.0535	Unknown
19	0.0483	Unknown
20	0.0483	Unknown
21	0.0483	Unknown
22	0.0349	Unknown
23	0.0349	Unknown
24	0.0349	Unknown
25	0.0483	Unknown
26	0.0483	Unknown
27	0.0483	Unknown
28	0.0535	Unknown
29	0.0535	Unknown
30	0.0535	Unknown

31	0.0368 Unknown
32	0.0368 Unknown
33	0.0368 Unknown
34	0.0535 Unknown
35	0.0535 Unknown
36	0.0535 Unknown
37	0.0883 Unknown
38	0.0883 Unknown
39	0.0883 Unknown
40	0.0616 Unknown
41	0.0616 Unknown
42	0.0616 Unknown
43	0.0883 Unknown
44	0.0883 Unknown
45	0.0883 Unknown
46	0.0535 Unknown
47	0.0535 Unknown
48	0.0535 Unknown
49	0.0368 Unknown
50	0.0368 Unknown
51	0.0368 Unknown
52	0.0535 Unknown
53	0.0535 Unknown
54	0.0535 Unknown
55	0.0287 Unknown
56	0.0287 Unknown
57	0.0287 Unknown
58	0.0221 Unknown
59	0.0221 Unknown
60	0.0221 Unknown
61	0.0287 Unknown
62	0.0287 Unknown

63	0.0287 Unknown
64	0.0268 Unknown
65	0.0268 Unknown
66	0.0268 Unknown
67	0.0235 Unknown
68	0.0235 Unknown
69	0.0235 Unknown
70	0.0268 Unknown
71	0.0268 Unknown
72	0.0268 Unknown
73	0.0287 Unknown
74	0.0287 Unknown
75	0.0287 Unknown
76	0.0221 Unknown
77	0.0221 Unknown
78	0.0221 Unknown
79	0.0287 Unknown
80	0.0287 Unknown
81	0.0287 Unknown
82	0.0535 Unknown
83	0.0535 Unknown
84	0.0535 Unknown
85	0.0368 Unknown
86	0.0368 Unknown
87	0.0368 Unknown
88	0.0535 Unknown
89	0.0535 Unknown
90	0.0535 Unknown
91	0.0483 Unknown
92	0.0483 Unknown
93	0.0483 Unknown
94	0.0349 Unknown

95	0.0349	Unknown
96	0.0349	Unknown
97	0.0483	Unknown
98	0.0483	Unknown
99	0.0483	Unknown
100	0.0268	Unknown
101	0.0268	Unknown
102	0.0268	Unknown
103	0.0235	Unknown
104	0.0235	Unknown
105	0.0235	Unknown
106	0.0268	Unknown
107	0.0268	Unknown
108	0.0268	Unknown
109	0.0260	Unknown
110	0.0260	Unknown
111	0.0260	Unknown
112	0.0260	Unknown
113	0.0260	Unknown
114	0.0260	Unknown
115	0.0260	Unknown
116	0.0260	Unknown
117	0.0260	Unknown
118	0.0268	Unknown
119	0.0268	Unknown
120	0.0268	Unknown
121	0.0235	Unknown
122	0.0235	Unknown
123	0.0235	Unknown
124	0.0268	Unknown
125	0.0268	Unknown
126	0.0268	Unknown

127	0.0483	Unknown
128	0.0483	Unknown
129	0.0483	Unknown
130	0.0349	Unknown
131	0.0349	Unknown
132	0.0349	Unknown
133	0.0483	Unknown
134	0.0483	Unknown
135	0.0483	Unknown
136	0.0535	Unknown
137	0.0535	Unknown
138	0.0535	Unknown
139	0.0368	Unknown
140	0.0368	Unknown
141	0.0368	Unknown
142	0.0535	Unknown
143	0.0535	Unknown
144	0.0535	Unknown
145	0.0287	Unknown
146	0.0287	Unknown
147	0.0287	Unknown
148	0.0221	Unknown
149	0.0221	Unknown
150	0.0221	Unknown
151	0.0287	Unknown
152	0.0287	Unknown
153	0.0287	Unknown
154	0.0268	Unknown
155	0.0268	Unknown
156	0.0268	Unknown
157	0.0235	Unknown
158	0.0235	Unknown

159	0.0235	Unknown
160	0.0268	Unknown
161	0.0268	Unknown
162	0.0268	Unknown
163	0.0287	Unknown
164	0.0287	Unknown
165	0.0287	Unknown
166	0.0221	Unknown
167	0.0221	Unknown
168	0.0221	Unknown
169	0.0287	Unknown
170	0.0287	Unknown
171	0.0287	Unknown
172	0.0535	Unknown
173	0.0535	Unknown
174	0.0535	Unknown
175	0.0368	Unknown
176	0.0368	Unknown
177	0.0368	Unknown
178	0.0535	Unknown
179	0.0535	Unknown
180	0.0535	Unknown
181	0.0883	Unknown
182	0.0883	Unknown
183	0.0883	Unknown
184	0.0616	Unknown
185	0.0616	Unknown
186	0.0616	Unknown
187	0.0883	Unknown
188	0.0883	Unknown
189	0.0883	Unknown
190	0.0535	Unknown

191	0.0535	Unknown
192	0.0535	Unknown
193	0.0368	Unknown
194	0.0368	Unknown
195	0.0368	Unknown
196	0.0535	Unknown
197	0.0535	Unknown
198	0.0535	Unknown
199	0.0483	Unknown
200	0.0483	Unknown
201	0.0483	Unknown
202	0.0349	Unknown
203	0.0349	Unknown
204	0.0349	Unknown
205	0.0483	Unknown
206	0.0483	Unknown
207	0.0483	Unknown
208	0.0535	Unknown
209	0.0535	Unknown
210	0.0535	Unknown
211	0.0368	Unknown
212	0.0368	Unknown
213	0.0368	Unknown
214	0.0535	Unknown
215	0.0535	Unknown
216	0.0535	Unknown
217	0.0883	Unknown
218	0.0883	Unknown
219	0.0883	Unknown
220	0.0616	Unknown
221	0.0616	Unknown
222	0.0616	Unknown

223 0.0883 Unknown

224 0.0883 Unknown

225 0.0883 Unknown

Average = 0.0444

A.2 ANOVA of Emc PWR filling level (Study 2.3.4.1)

Response: PWR_filling_level

ANOVA for Response Surface Reduced Quadratic Model

Analysis of variance table [Partial sum of squares - Type III]

(A = paddle wheel speed, b = Mass of Emc, c = monitoring position)

Source	Sum of Squares	df	Mean Square	F Value	p-value Prob > F	
Model	1896.45	7	270.92	3048.81	< 0.0001	significant
A-vFOM	11.38	1	11.38	128.12	< 0.0001	
B-mDCP	761.33	1	761.33	8567.62	< 0.0001	
C-LP	1003.58	1	1003.58	11293.77	< 0.0001	
AB	3.76	1	3.76	42.36	< 0.0001	
AC	95.32	1	95.32	1072.72	< 0.0001	
BC	14.03	1	14.03	157.91	< 0.0001	
C^2	7.03	1	7.03	79.16	< 0.0001	
Residual	19.28	217	0.089			
Lack of Fit	19.15	67	0.29	321.62	< 0.0001	significant
Pure Error	0.13	150	8.887E-004			
Cor Total	1915.73	224				

The Model F-value of 3048.81 implies the model is significant. There is only a 0.01% chance that a "Model F-Value" this large could occur due to noise.

Values of "Prob > F" less than 0.0500 indicate model terms are significant.

In this case A, B, C, AB, AC, BC, C++2+- are significant model terms.

Values greater than 0.1000 indicate the model terms are not significant.

If there are many insignificant model terms (not counting those required to support hierarchy), model reduction may improve the model.

The "Lack of Fit F-value" of 321.62 implies the Lack of Fit is significant. There is only a 0.01% chance that a "Lack of Fit F-value" this large could occur due to noise.

Std. Dev.	0.30	R-Squared	0.9899
Mean	6.91	Adj R-Squared	0.9896
C.V. %	4.31	Pred R-Squared	0.9890
PRESS	20.98	Adeq Precision	233.913

The "Pred R-Squared" of 0.9890 is in reasonable agreement with the "Adj R-Squared" of 0.9896.

"Adeq Precision" measures the signal to noise ratio. A ratio greater than 4 is desirable. The ratio of 233.913 indicates an adequate signal. This model can be used to navigate the design space.

Factor	Coefficient Estimate	df	Standard Error	95% CI Low	95% CI High	VIF
Intercept	6.66	1	0.034	6.59	6.73	
A-vFOM	-0.32	1	0.028	-0.37	-0.26	1.00
B-mDCP	2.60	1	0.028	2.55	2.66	1.00
C-LP	2.59	1	0.024	2.54	2.63	1.00
AB	0.26	1	0.040	0.18	0.34	1.00
AC	1.13	1	0.034	1.06	1.20	1.00
BC	0.43	1	0.034	0.36	0.50	1.00
C^2	0.38	1	0.042	0.29	0.46	1.00

Final equation in terms of coded factors:

$$\begin{aligned} \text{PWR filling level} &= \\ &+6.66 \\ &-0.32 * A \\ &+2.60 * B \\ &+2.59 * C \\ &+0.26 * A * B \\ &+1.13 * A * C \\ &+0.43 * B * C \\ &+0.38 * C^2 \end{aligned}$$

Final equation in terms of actual factors:

$$\begin{aligned} \text{PWR filling level} &= \\ &+8.80505 \\ &-0.14573 * \text{vFOM} \\ &+9.91801\text{E-}003 * \text{mDCP} \\ &-0.25377 * \text{LP} \\ &+1.61680\text{E-}004 * \text{vFOM} * \text{mDCP} \\ &+2.01317\text{E-}003 * \text{vFOM} * \text{LP} \\ &+7.72392\text{E-}004 * \text{mDCP} * \text{LP} \\ &+1.91372\text{E-}003 * \text{LP}^2 \end{aligned}$$

A.3 Design matrix evaluation (Study 2.3.4.2)

(Design Matrix Evaluation for the Response Surface Quadratic Model)

3 Factors: A = Rotational speed (rpm), B = Monitoring position (mm), C = Powder volume (ml)

Degrees of Freedom for Evaluation

Model	9
Residuals	41
Lack Of Fit	35
Pure Error	6
Corr Total	50

Power at 5 % alpha level to detect signal/noise ratios of

Term	StdErr**	VIF	Ri-Squared	0.5 Std. Dev.	1 Std. Dev.	2 Std. Dev.
A	0.20	1.05	0.0434	23.5 %	69.5 %	99.9 %
B	0.17	1.05	0.0459	29.1 %	80.3 %	99.9 %
C	0.18	1.04	0.0416	28.4 %	79.2 %	99.9 %
AB	0.24	1.04	0.0415	17.4 %	52.7 %	98.2 %
AC	0.25	1.05	0.0463	16.7 %	50.5 %	97.6 %
BC	0.21	1.06	0.0554	21.1 %	63.7 %	99.6 %
A^2	0.33	1.02	0.0176	31.0 %	83.4 %	99.9 %
B^2	0.30	1.02	0.0201	36.0 %	89.3 %	99.9 %
C^2	0.30	1.04	0.0345	36.5 %	89.8 %	99.9 %

**Basis Std. Dev. = 1.0

Measures Derived From the $(X'X)^{-1}$ Matrix

Std Leverage Point Type

1	0.1918	Unknown
2	0.1459	Unknown
3	0.2384	Unknown
4	0.1265	Unknown
5	0.1134	Unknown
6	0.1393	Unknown
7	0.1338	Unknown
8	0.1340	Unknown
9	0.1355	Unknown
10	0.1426	Unknown
11	0.1254	Unknown
12	0.1330	Unknown
13	0.2489	Unknown
14	0.1720	Unknown
15	0.2048	Unknown
16	0.3166	Unknown
17	0.2362	Unknown
18	0.3657	Unknown
19	0.2014	Unknown
20	0.1436	Unknown
21	0.2092	Unknown
22	0.1860	Unknown
23	0.1369	Unknown
24	0.1861	Unknown
25	0.2069	Unknown
26	0.1412	Unknown
27	0.2100	Unknown
28	0.3672	Unknown
29	0.2481	Unknown
30	0.3611	Unknown

31	0.3397 Unknown
32	0.2384 Unknown
33	0.3521 Unknown
34	0.2045 Unknown
35	0.1393 Unknown
36	0.1773 Unknown
37	0.1874 Unknown
38	0.1335 Unknown
39	0.1323 Unknown
40	0.2100 Unknown
41	0.1312 Unknown
42	0.1159 Unknown
43	0.3607 Unknown
44	0.2093 Unknown
45	0.1159 Unknown
46	0.1936 Unknown
47	0.1936 Unknown
48	0.1918 Unknown
49	0.1459 Unknown
50	0.1323 Unknown
51	0.1936 Unknown

Average = 0.1961

A.4 ANOVA of Emc PWR filling level (Study 2.3.4.2)

(Response Surface Reduced Quadratic Model)

(vFOM = paddle wheel speed, SP = monitoring position, PVolume = Powder volume)

Source	Sum of Squares	df	Mean Square	F	p-value Value	Prob > F
Model	292.95	7	41.85	652.28	< 0.0001	significant
A-vFOM	2.17	1	2.17	33.81	< 0.0001	
B-SP	212.11	1	212.11	3305.98	< 0.0001	
C-PVolume	53.40	1	53.40	832.37	< 0.0001	
AB	22.44	1	22.44	349.73	< 0.0001	
AC	0.30	1	0.30	4.63	0.0379	
BC	1.24	1	1.24	19.36	< 0.0001	
B^2	1.29	1	1.29	20.08	< 0.0001	
Residual	2.37	37	0.064			
Cor Total	295.32	44				

Std. Dev.	0.25	R-Squared	0.9920
Mean	6.90	Adj R-Squared	0.9904
C.V. %	3.67	Pred R-Squared	0.9874
PRESS	3.73	Adeq Precision	100.320

Factor	Coefficient Estimate	df	Standard Error	95% CI Low	95% CI High	VIF
Intercept	6.66	1	0.065	6.53	6.79	
A-vFOM	-0.31	1	0.053	-0.42	-0.20	1.00
B-SP	2.66	1	0.046	2.57	2.75	1.00
C-PVolume	1.33	1	0.046	1.24	1.43	1.00
AB	1.22	1	0.065	1.09	1.36	1.00
AC	0.14	1	0.065	8.264E-003	0.27	1.00
BC	0.25	1	0.057	0.13	0.36	1.00
B^2	0.36	1	0.080	0.20	0.52	1.00

Final Equation in Terms of Coded Factors:

PWR filling level =

+6.66

-0.31 * A

+2.66 * B

+1.33 * C

+1.22 * A * B

+0.14 * A * C

+0.25 * B * C

+0.36 * B²**Final Equation in Terms of Actual Factors:**

PWR filling level =

+1.41900

-0.059457 * vFOM

-0.099189 * SP

+0.043692 * PVolume

+2.18406E-003 * vFOM * SP

+1.75974E-004 * vFOM * PVolume

+8.90030E-004 * SP * PVolume

+1.83110E-003 * SP²

A.5 ANOVA of Destab PWR filling level (Study 2.3.4.2)

(Response Surface Reduced Quadratic Model)

(vFOM = paddle wheel speed, SP = monitoring position, PVolume = Powder volume)

Source	Sum of Squares	df	Mean Square	F Value	p-value Prob > F	
Model	332.00	6	55.33	739.95	< 0.0001	significant
A-vFOM	3.59	1	3.59	48.05	< 0.0001	
B-SP	224.40	1	224.40	3000.83	< 0.0001	
C-PVolume	43.70	1	43.70	584.31	< 0.0001	
AB	48.32	1	48.32	646.12	< 0.0001	
B^2	6.20	1	6.20	82.89	< 0.0001	
C^2	5.80	1	5.80	77.50	< 0.0001	
Residual	2.84	38	0.075			
Cor Total	334.85	44				

Std. Dev.	0.27	R-Squared	0.9915
Mean	6.59	Adj R-Squared	0.9902
C.V. %	4.15	Pred R-Squared	0.9879
PRESS	4.06	Adeq Precision	106.377

Factor	Coefficient Estimate	df	Standard Error	95% CI Low	95% CI High	VIF
Intercept	5.56	1	0.091	5.38	5.75	
A-vFOM	-0.40	1	0.058	-0.52	-0.28	1.00
B-SP	2.73	1	0.050	2.63	2.84	1.00
C-PVolume	1.21	1	0.050	1.11	1.31	1.00
AB	1.79	1	0.071	1.65	1.94	1.00
B^2	0.79	1	0.086	0.61	0.96	1.00
C^2	0.76	1	0.086	0.59	0.94	1.00

Final Equation in Terms of Coded Factors:

PWR filling level =

+5.56

-0.40 * A

+2.73 * B

+1.21 * C

+1.79 * A * B

+0.79 * B²+0.76 * C²**Final Equation in Terms of Actual Factors:**

PWR filling level =

+27.07024

-0.054860 * vFOM

-0.10941 * SP

-0.39644 * PVolume

+3.20491E-003 * vFOM * SP

+4.01689E-003 * SP²+1.90325E-003 * PVolume²

A.6 ANOVA of Av200 PWR filling level (Study 2.3.4.2)

(Response Surface Reduced 2FI Model)

(vFOM = paddle wheel speed, SP = monitoring position, PVolume = Powder volume)

Source	Sum of Squares	df	Mean Square	F	p-value Value	Prob > F
Model	314.88	5	62.98	510.61	< 0.0001	significant
A-vFOM	6.39	1	6.39	51.79	< 0.0001	
B-SP	214.82	1	214.82	1741.69	< 0.0001	
C-PVolume	58.89	1	58.89	477.43	< 0.0001	
AB	34.18	1	34.18	277.12	< 0.0001	
AC	0.62	1	0.62	5.00	0.0311	
Residual	4.81	39	0.12			
Cor Total	319.70	44				

Std. Dev.	0.35	R-Squared	0.9850
Mean	7.06	Adj R-Squared	0.9830
C.V. %	4.98	Pred R-Squared	0.9785
PRESS	6.88	Adeq Precision	90.289

Factor	Coefficient Estimate	df	Standard Error	95% CI Low	95% CI High	VIF
Intercept	7.06	1	0.052	6.95	7.16	
A-vFOM	-0.53	1	0.074	-0.68	-0.38	1.00
B-SP	2.68	1	0.064	2.55	2.81	1.00
C-PVolume	1.40	1	0.064	1.27	1.53	1.00
AB	1.51	1	0.091	1.33	1.69	1.00
AC	0.20	1	0.091	0.019	0.39	1.00

Final Equation in Terms of Coded Factors:

$$\begin{aligned} \text{Av200} = & \\ & +7.06 \\ & -0.53 * A \\ & +2.68 * B \\ & +1.40 * C \\ & +1.51 * A * B \\ & +0.20 * A * C \end{aligned}$$

Final Equation in Terms of Actual Factors:

$$\begin{aligned} \text{Av200} = & \\ & +0.86321 \\ & -0.081476 * \text{vFOM} \\ & +0.029403 * \text{SP} \\ & +0.054842 * \text{PVolume} \\ & +2.69557\text{E-}003 * \text{vFOM} * \text{SP} \\ & +2.53483\text{E-}004 * \text{vFOM} * \text{PVolume} \end{aligned}$$

A.7 ANOVA of FFL PWR filling level (Study 2.3.4.2)

(Response Surface 2FI Model)

(vFOM = paddle wheel speed, SP = monitoring position, PVolume = Powder volume)

Source	Sum of Squares	df	Mean Square	F	p-value Value	Prob > F
Model	415.98	6	69.33	415.42	< 0.0001	significant
A-vFOM	7.93	1	7.93	47.50	< 0.0001	
B-SP	236.75	1	236.75	1418.59	< 0.0001	
C-PVolume	61.23	1	61.23	366.90	< 0.0001	
AB	41.11	1	41.11	246.35	< 0.0001	
AC	0.75	1	0.75	4.51	0.0396	
BC	0.74	1	0.74	4.43	0.0414	
Residual	7.01	42	0.17			
Lack of Fit	6.41	38	0.17	1.13	0.5183	not significant
Pure Error	0.60	4	0.15			
Cor Total	422.99	48				

Std. Dev. 0.41 R-Squared 0.9834

Mean 7.37 Adj R-Squared 0.9811

C.V. % 5.55 Pred R-Squared 0.9758

PRESS 10.22 Adeq Precision 76.090

Factor	Coefficient Estimate	df	Standard Error	95% CI		VIF
				Low	High	
Intercept	6.96	1	0.059	6.84	7.08	
A-vFOM	-0.58	1	0.084	-0.74	-0.41	1.03
B-SP	2.70	1	0.072	2.56	2.85	1.04
C-PVolume	1.37	1	0.072	1.23	1.52	1.04
AB	1.58	1	0.10	1.38	1.79	1.04
AC	0.21	1	0.10	0.011	0.42	1.04
BC	0.18	1	0.086	7.448E-003	0.36	1.05

Final Equation in Terms of Coded Factors:

$$\begin{aligned} \text{TL FFL} = & \\ & +6.96 \\ & -0.58 * A \\ & +2.70 * B \\ & +1.37 * C \\ & +1.58 * A * B \\ & +0.21 * A * C \\ & +0.18 * B * C \end{aligned}$$

Final Equation in Terms of Actual Factors:

$$\begin{aligned} \text{TL FFL} = & \\ & +2.25568 \\ & -0.086073 * \text{vFOM} \\ & -0.054109 * \text{SP} \\ & +0.043621 * \text{PVolume} \\ & +2.82530\text{E-}003 * \text{vFOM} * \text{SP} \\ & +2.67617\text{E-}004 * \text{vFOM} * \text{PVolume} \\ & +6.47404\text{E-}004 * \text{SP} * \text{PVolume} \end{aligned}$$

A.8 ANOVA of Av102 PWR filling level (Study 2.3.4.2)

(Response Surface Reduced Quadratic Model)

(vFOM = paddle wheel speed, SP = monitoring position, PVolume = Powder volume)

Source	Sum of Squares	df	Mean Square	F Value	p-value Prob > F	
Model	384.51	5	76.90	319.24	< 0.0001	significant
A-vFOM	7.72	1	7.72	32.04	< 0.0001	
B-SP	266.04	1	266.04	1104.45	< 0.0001	
C-PVolume	60.19	1	60.19	249.85	< 0.0001	
AB	60.41	1	60.41	250.78	< 0.0001	
B^2	1.59	1	1.59	6.61	0.0138	
Residual	9.88	41	0.24			
Lack of Fit	9.87	39	0.25	60.06	0.0165	significant
Pure Error	8.426E-003	2	4.213E-003			
Cor Total	394.38	46				

Std. Dev.	0.49	R-Squared	0.9750
Mean	7.33	Adj R-Squared	0.9719
C.V. %	6.70	Pred R-Squared	0.9659
PRESS	13.43	Adeq Precision	71.863

Factor	Coefficient Estimate	df	Standard Error	95% CI Low	95% CI High	VIF
Intercept	7.07	1	0.12	6.82	7.31	
A-vFOM	-0.56	1	0.100	-0.76	-0.36	1.00
B-SP	2.94	1	0.088	2.76	3.11	1.00
C-PVolume	1.42	1	0.090	1.24	1.60	1.00
AB	1.95	1	0.12	1.70	2.20	1.00
B^2	0.39	1	0.15	0.084	0.69	1.00

Final Equation in Terms of Coded Factors:

$$\begin{aligned} \text{TL Av102} &= \\ &+7.07 \\ &-0.56 * A \\ &+2.94 * B \\ &+1.42 * C \\ &+1.95 * A * B \\ &+0.39 * B^2 \end{aligned}$$

Final Equation in Terms of Actual Factors:

$$\begin{aligned} \text{TL Av102} &= \\ &-0.21066 \\ &-0.062811 * \text{vFOM} \\ &-0.054711 * \text{SP} \\ &+0.070820 * \text{PVolume} \\ &+3.48055\text{E-}003 * \text{vFOM} * \text{SP} \\ &+1.98400\text{E-}003 * \text{SP}^2 \end{aligned}$$

A.9 Design matrix evaluation (Study 2.3.4.3)

Design Matrix Evaluation for Response Surface Quadratic Model

3 Factors: A, B, C (A = Powder mass, B = Paddle wheel speed, C = Position of monitoring)

Degrees of Freedom for Evaluation

Model	9
Residuals	37
Lack Of Fit	35
Pure Error	2
Corr Total	46

A recommendation is a minimum of 3 lack of fit df and 4 df for pure error.

This ensures a valid lack of fit test. Fewer df will lead to a test that may not detect lack of fit.

Power at 5 % alpha level to detect signal/noise ratios of

Term	StdErr**	VIF	Ri-Squared	0.5 Std. Dev.	1 Std. Dev.	2 Std. Dev.
A	0.18	1.00	0.0000	26.6 %	76.0 %	99.9 %
B	0.21	1.00	0.0000	21.1 %	63.7 %	99.6 %
C	0.18	1.00	0.0000	26.6 %	76.0 %	99.9 %
AB	0.26	1.00	0.0000	15.6 %	47.1 %	96.5 %
AC	0.22	1.00	0.0000	19.3 %	58.6 %	99.2 %
BC	0.26	1.00	0.0000	15.6 %	47.1 %	96.5 %
A^2	0.31	1.01	0.0100	35.8 %	89.1 %	99.9 %
B^2	0.35	1.01	0.0083	28.9 %	80.0 %	99.9 %
C^2	0.31	1.01	0.0100	35.8 %	89.1 %	99.9 %

**Basis Std. Dev. = 1.0

Standard errors should be similar within type of coefficient. Smaller is better.

Ideal VIF is 1.0. VIFs above 10 are cause for alarm, indicating coefficients are poorly estimated due to multicollinearity. Ideal Ri-squared is 0.0. High Ri-squared means terms are correlated with each other, possibly leading to poor models. Power is an inappropriate tool to evaluate response surface designs.

Measures Derived From the $(X'X)^{-1}$ Matrix

Std	Leverage	Point Type
1	0.3661	Unknown
2	0.2134	Unknown
3	0.1927	Unknown
4	0.2134	Unknown
5	0.3661	Unknown
6	0.2537	Unknown
7	0.1412	Unknown
8	0.1338	Unknown
9	0.1412	Unknown
10	0.2537	Unknown
11	0.3661	Unknown
12	0.2134	Unknown
13	0.1927	Unknown
14	0.2134	Unknown
15	0.3661	Unknown
16	0.2537	Unknown
17	0.1412	Unknown
18	0.1338	Unknown
19	0.1412	Unknown
20	0.2537	Unknown
21	0.1775	Unknown
22	0.1051	Unknown
23	0.1111	Unknown
24	0.1051	Unknown
25	0.1775	Unknown
26	0.2537	Unknown
27	0.1412	Unknown
28	0.1338	Unknown
29	0.1412	Unknown
30	0.2537	Unknown

31	0.3661	Unknown
32	0.2134	Unknown
33	0.1927	Unknown
34	0.2134	Unknown
35	0.3661	Unknown
36	0.2537	Unknown
37	0.1412	Unknown
38	0.1338	Unknown
39	0.1412	Unknown
40	0.2537	Unknown
41	0.3661	Unknown
42	0.2134	Unknown
43	0.1927	Unknown
44	0.2134	Unknown
45	0.3661	Unknown
46	0.1111	Unknown
47	0.1111	Unknown

Average = 0.2128

A.10 ANOVA of Av102 PWR filling level - flat rod paddle wheel - (Study 2.3.4.3)**Response PWR filling level (Paddle wheel with flat rods)**

ANOVA for Response Surface Reduced Quadratic Model

Analysis of variance table [Partial sum of squares - Type III]

Source	Sum of Squares	df	Mean Square	F Value	p-value Prob > F	
Model	381.12	5	76.22	318.66	< 0.0001	significant
A-Powder mass	59.75	1	59.75	249.79	< 0.0001	
B-Paddle wheel speed	7.31	1	7.31	30.54	< 0.0001	
C-Pos. of monitoring	256.42	1	256.42	1071.97	< 0.0001	
BC	56.12	1	56.12	234.61	< 0.0001	
C ²	1.53	1	1.53	6.38	0.0155	
Residual	9.81	41	0.24			
Lack of Fit	9.76	39	0.25	10.95	0.0871	not significant
Pure Error	0.046	2	0.023			
Cor Total	390.93	46				

The Model F-value of 318.66 implies the model is significant. There is only a 0.01% chance that a "Model F-Value" this large could occur due to noise. Values of "Prob > F" less than 0.0500 indicate model terms are significant. In this case A, B, C, BC, C² are significant model terms. Values greater than 0.1000 indicate the model terms are not significant. If there are many insignificant model terms (not counting those required to support hierarchy), model reduction may improve the model. The "Lack of Fit F-value" of 10.95 implies there is a 8.71% chance that a "Lack of Fit F-value" this large could occur due to noise.

Std. Dev.	0.49	R-Squared	0.9749
Mean	7.32	Adj R-Squared	0.9719
C.V. %	6.68	Pred R-Squared	0.9654
PRESS	13.53	Adeq Precision	71.751

The "Pred R-Squared" of 0.9654 is in reasonable agreement with the "Adj R-Squared" of 0.9719.

"Adeq Precision" measures the signal to noise ratio. A ratio greater than 4 is desirable. The ratio of 71.751 indicates an adequate signal. This model can be used to navigate the design space.

Factor	Coefficient Estimate	df	Standard Error	95% CI		95% CI VIF
				Low	High	
Intercept	7.08	1	0.12	6.84	7.32	
A-Powder mass	1.41	1	0.089	1.23	1.59	1.00
B-Paddle wheel speed	-0.57	1	0.10	-0.78	-0.36	1.00
C-Pos. of monitoring	2.92	1	0.089	2.74	3.10	1.00
BC	1.93	1	0.13	1.68	2.19	1.00
C^2	0.38	1	0.15	0.075	0.68	1.00

Final Equation in Terms of Coded Factors:

$$\begin{aligned} \text{PWR filling level flatrod} &= \\ &+7.08 \\ &+1.41 * A \\ &-0.57 * B \\ &+2.92 * C \\ &+1.93 * B * C \\ &+0.38 * C^2 \end{aligned}$$

Final Equation in Terms of Actual Factors:

$$\begin{aligned} \text{PWR filling level flatrod} &= \\ &+6.39311 \\ &+0.17641 * \text{Powder mass} \\ &-0.21803 * \text{Paddle wheel speed} \\ &-0.22428 * \text{Position of monitoring} \\ &+3.45403\text{E-}003 * \text{Paddle wheel speed} * \text{Position of monitoring} \\ &+1.91410\text{E-}003 * \text{Position of monitoring}^2 \end{aligned}$$

A.11 ANOVA of Av102 PWR filling level - round rod paddle wheel - (Study 2.3.4.3)**Response PWR filling level (Paddle wheel with round rods)**

ANOVA for Response Surface Reduced 2FI Model

Analysis of variance table [Partial sum of squares - Type III]

Source	Sum of Squares	df	Mean Square	F	p-value Value	Prob > F
Model	232.29	5	46.46	144.67	< 0.0001	significant
A-Powder mass	46.58	1	46.58	145.07	< 0.0001	
B-Paddle wheel speed	2.55	1	2.55	7.93	0.0074	
C-Pos. of monitoring	147.12	1	147.12	458.12	< 0.0001	
AC	1.43	1	1.43	4.46	0.0409	
BC	34.61	1	34.61	107.78	< 0.0001	
Residual	13.17	41	0.32			
Lack of Fit	13.17	39	0.34	4308.60	0.0002	significant
Pure Error	1.567E-004	2	7.835E-005			
Cor Total	245.46	46				

The Model F-value of 144.67 implies the model is significant. There is only a 0.01% chance that a "Model F-Value" this large could occur due to noise. Values of "Prob > F" less than 0.0500 indicate model terms are significant. In this case A, B, C, AC, BC are significant model terms. Values greater than 0.1000 indicate the model terms are not significant. If there are many insignificant model terms (not counting those required to support hierarchy), model reduction may improve the model. The "Lack of Fit F-value" of 4308.60 implies the Lack of Fit is significant. There is only a 0.02% chance that a "Lack of Fit F-value" this large could occur due to noise.

Std. Dev.	0.57	R-Squared	0.9464
Mean	7.73	Adj R-Squared	0.9398
C.V. %	7.33	Pred R-Squared	0.9263
PRESS	18.09	Adeq Precision	49.188

The "Pred R-Squared" of 0.9263 is in reasonable agreement with the "Adj R-Squared" of 0.9398. "Adeq Precision" measures the signal to noise ratio. A ratio greater than 4 is desirable. The ratio of 49.188 indicates an adequate signal. This model can be used to navigate the design space.

Factor	Coefficient Estimate	df	Standard Error	95% CI Low	95% CI High	VIF
Intercept	7.73	1	0.083	7.56	7.90	
A-Powder mass	1.25	1	0.10	1.04	1.46	1.00
B-Paddle wheel speed	-0.34	1	0.12	-0.58	-0.095	1.00
C-Position of monitoring	2.21	1	0.10	2.01	2.42	1.00
AC	0.27	1	0.13	0.012	0.52	1.00
BC	1.52	1	0.15	1.22	1.81	1.00

Final Equation in Terms of Coded Factors:

$$\begin{aligned}
 \text{PWR filling level Roundrod} = & \\
 & +7.73 \\
 & +1.25 * A \\
 & -0.34 * B \\
 & +2.21 * C \\
 & +0.27 * A * C \\
 & +1.52 * B * C
 \end{aligned}$$

Final Equation in Terms of Actual Factors:

$$\begin{aligned}
 \text{PWR filling level Roundrod} = & \\
 & +7.82377 \\
 & +0.014821 * \text{Powder mass} \\
 & -0.16845 * \text{Paddle wheel speed} \\
 & -0.11446 * \text{Position of monitoring} \\
 & +2.38888\text{E-}003 * \text{Powder mass} * \text{Position of monitoring} \\
 & +2.71253\text{E-}003 * \text{Paddle wheel speed} * \text{Position of monitoring}
 \end{aligned}$$

A.12 Design matrix evaluation (Study 2.4.3.1)**Design Matrix Evaluation for Factorial Main effects Model**

2 Factors: A, B (A = paddle wheel speed, rpm; B = tableting speed, rpm)

No aliases found for Main effects Model

Degrees of Freedom for Evaluation

Model	2
Residuals	4
Lack Of Fit	2
Pure Error	2
Corr Total	6

Power at 5 % alpha level to detect signal/noise ratios of

Term	StdErr**	VIF	Ri-Squared	0.5 Std. Dev.	1 Std. Dev.	2 Std. Dev.
A	0.50	1.00	0.0000	6.8 %	12.2 %	33.6 %
B	0.50	1.00	0.0000	6.8 %	12.2 %	33.6 %

**Basis Std. Dev. = 1.0

Measures Derived From the $(X'X)^{-1}$ Matrix

Std	Leverage	Point Type
1	0.6429	Factorial
2	0.6429	Factorial
3	0.6429	Factorial
4	0.6429	Factorial
5	0.1429	Center
6	0.1429	Center
7	0.1429	Center

Average =0.4286

A.13 ANOVA of Av102 PWR filling level (Study 2.4.3.1)

Response: Av102_filling_level

ANOVA for selected factorial model

Analysis of variance table [Partial sum of squares - Type III]

Source	Sum of Squares	df	Mean Square	F Value	p-value Prob > F	
Model	0.27	2	0.14	399.58	< 0.0001	significant
A-paddle wheel speed	0.13	1	0.13	378.00	< 0.0001	
B-tabletting speed	0.14	1	0.14	421.17	< 0.0001	
Residual	1.371E-003	4	3.429E-004			
Lack of Fit	1.171E-003	2	5.857E-004	5.86	0.1458	not significant
Pure Error	2.000E-004	2	1.000E-004			
Cor Total	0.28	6				

The Model F-value of 399.58 implies the model is significant. There is only a 0.01% chance that a "Model F-Value" this large could occur due to noise. Values of "Prob > F" less than 0.0500 indicate model terms are significant. In this case A, B are significant model terms. Values greater than 0.1000 indicate the model terms are not significant. If there are many insignificant model terms (not counting those required to support hierarchy), model reduction may improve the model. The "Lack of Fit F-value" of 5.86 implies the Lack of Fit is not significant relative to the pure error. There is a 14.58% chance that a "Lack of Fit F-value" this large could occur due to noise.

Std. Dev.	0.019	R-Squared	0.9950
Mean	13.58	Adj R-Squared	0.9925
C.V. %	0.14	Pred R-Squared	0.9801
PRESS	5.490E-003	Adeq Precision	61.047

The "Pred R-Squared" of 0.9801 is in reasonable agreement with the "Adj R-Squared" of 0.9925. "Adeq Precision" measures the signal to noise ratio. A ratio greater than 4 is desirable. The ratio of 61.047 indicates an adequate signal. This model can be used to navigate the design space.

Factor	Coefficient Estimate	df	Standard Error	95% CI		95% CI VIF
				Low	High	
Intercept	13.58	1	6.999E-003	13.56	13.60	
A-paddle wheel speed	0.18	1	9.258E-003	0.15	0.21	1.00
B-tabletting speed	-0.19	1	9.258E-003	-0.22	-0.16	1.00

Final Equation in Terms of Coded Factors:

$$\begin{aligned} \text{FL Av102} &= \\ &+13.58 \\ &+0.18 * A \\ &-0.19 * B \end{aligned}$$

Final Equation in Terms of Actual Factors:

$$\begin{aligned} \text{FL Av102} &= \\ &+13.50929 \\ &+9.00000\text{E-}003 * \text{paddle wheel speed} \\ &-4.75000\text{E-}003 * \text{tabletting speed} \end{aligned}$$

A.14 ANOVA of Av102 tablet mass (Study 2.4.3.1)

Response: Av102_tablet_mass

ANOVA for selected factorial model

Analysis of variance table [Partial sum of squares - Type III]

Source	Sum of Squares	df	Mean Square	F Value	p-value Prob > F	
Model	1.007E-003	1	1.007E-003	46.38	0.0010	significant
B-tabletting speed	1.007E-003	1	1.007E-003	46.38	0.0010	
Residual	1.086E-004	5	2.171E-005			
Lack of Fit	1.021E-004	3	3.404E-005	10.56	0.0877	not significant
Pure Error	6.444E-006	2	3.222E-006			
Cor Total	1.116E-003	6				

The Model F-value of 46.38 implies the model is significant. There is only a 0.10% chance that a "Model F-Value" this large could occur due to noise. Values of "Prob > F" less than 0.0500 indicate model terms are significant. In this case B is a significant model term. Values greater than 0.1000 indicate the model terms are not significant. If there are many insignificant model terms (not counting those required to support hierarchy), model reduction may improve the model. The "Lack of Fit F-value" of 10.56 implies there is a 8.77% chance that a "Lack of Fit F-value" this large could occur due to noise.

Std. Dev.	4.660E-003	R-Squared	0.9027
Mean	0.19	Adj R-Squared	0.8832
C.V. %	2.46	Pred R-Squared	0.7864
PRESS	2.383E-004	Adeq Precision	12.741

The "Pred R-Squared" of 0.7864 is in reasonable agreement with the "Adj R-Squared" of 0.8832. "Adeq Precision" measures the signal to noise ratio. A ratio greater than 4 is desirable. The ratio of 12.741 indicates an adequate signal. This model can be used to navigate the design space.

Factor	Coefficient Estimate	df	Standard Error	95% CI Low	95% CI High	VIF
Intercept	0.19	1	1.761E-003	0.19	0.19	
B-tabletting speed	-0.016	1	2.330E-003	-0.022	-9.879E-003	1.00

Final Equation in Terms of Coded Factors:

$$\text{Mass Av102} = +0.19 - 0.016 * B$$

Final Equation in Terms of Actual Factors:

$$\text{Mass Av102} = +0.21342 - 3.96688\text{E-}004 * \text{tabletting speed}$$

A.15 ANOVA of Av102 tablet mass with nonsignificant factors included (Study 2.4.3.1)

Response Av102_tablet_mass_nonsignificant_factors_included

ANOVA for selected factorial model

Analysis of variance table [Partial sum of squares - Type III]

Source	Sum of Squares	df	Mean Square	F Value	p-value Prob > F
Model	1.047E-003	2	5.236E-004	30.55	0.0038 significant
A-paddle wheel speed	4.001E-005	1	4.001E-005	2.33	0.2013
B-tabletting speed	1.007E-003	1	1.007E-003	58.76	0.0016
Residual	6.856E-005	4	1.714E-005		
Lack of Fit	6.211E-005	2	3.106E-005	9.64	0.0940 not significant
Pure Error	6.444E-006	2	3.222E-006		
Cor Total	1.116E-003	6			

The Model F-value of 30.55 implies the model is significant. There is only a 0.38% chance that a "Model F-Value" this large could occur due to noise. Values of "Prob > F" less than 0.0500 indicate model terms are significant. In this case B is a significant model term. Values greater than 0.1000 indicate the model terms are not significant. If there are many insignificant model terms (not counting those required to support hierarchy), model reduction may improve the model. The "Lack of Fit F-value" of 9.64 implies there is a 9.40% chance that a "Lack of Fit F-value" this large could occur due to noise.

Std. Dev.	4.140E-003	R-Squared	0.9386
Mean	0.19	Adj R-Squared	0.9078
C.V. %	2.18	Pred R-Squared	0.7598
PRESS	2.679E-004	Adeq Precision	14.043

The "Pred R-Squared" of 0.7598 is in reasonable agreement with the "Adj R-Squared" of 0.9078. "Adeq Precision" measures the signal to noise ratio. A ratio greater than 4 is desirable. The

ratio of 14.043 indicates an adequate signal. This model can be used to navigate the design space.

Factor	Coefficient Estimate	df	Standard Error	95% CI Low	95% CI High	VIF
Intercept	0.19	1	1.565E-003	0.19	0.19	
A-paddle wheel speed	-3.163E-003	1	2.070E-003	-8.910E-003	2.585E-003	1.00
B-tabletting speed	-0.016	1	2.070E-003	-0.022	-0.010	1.00

Final Equation in Terms of Coded Factors:

$$\begin{aligned} \text{Mass Av102} &= \\ &+0.19 \\ &-3.163\text{E-}003 * A \\ &-0.016 * B \end{aligned}$$

Final Equation in Terms of Actual Factors:

$$\begin{aligned} \text{Mass Av102} &= \\ &+0.21975 \\ &-1.58125\text{E-}004 * \text{paddle wheel speed} \\ &-3.96688\text{E-}004 * \text{tabletting speed} \end{aligned}$$

A.16 ANOVA of Av102 tablet mass SD (Study 2.4.3.1)

Response: Av102_SD_tablet_mass

ANOVA for selected factorial model

Analysis of variance table [Partial sum of squares - Type III]

Source	Sum of Squares	df	Mean Square	F Value	p-value Prob > F
Model	10.37	1	10.37	8.32	0.0344 significant
B-tabletting speed	10.37	1	10.37	8.32	0.0344
Residual	6.23	5	1.25		
Lack of Fit	5.32	3	1.77	3.88	0.2115 not significant
Pure Error	0.91	2	0.46		
Cor Total	16.60	6			

The Model F-value of 8.32 implies the model is significant. There is only a 3.44% chance that a "Model F-Value" this large could occur due to noise. Values of "Prob > F" less than 0.0500 indicate model terms are significant. In this case B is a significant model term. Values greater than 0.1000 indicate the model terms are not significant. If there are many insignificant model terms (not counting those required to support hierarchy), model reduction may improve the model. The "Lack of Fit F-value" of 3.88 implies the Lack of Fit is not significant relative to the pure error. There is a 21.15% chance that a "Lack of Fit F-value" this large could occur due to noise.

Std. Dev.	1.12	R-Squared	0.6247
Mean	2.65	Adj R-Squared	0.5496
C.V. %	42.12	Pred R-Squared	0.1759
PRESS	13.68	Adeq Precision	5.397

The "Pred R-Squared" of 0.1759 is not as close to the "Adj R-Squared" of 0.5496 as one might normally expect. This may indicate a large block effect or a possible problem with the model and/or data. Things to consider are model reduction, response transformation, outliers, etc. "Adeq Precision" measures the signal to noise ratio. A ratio greater than 4 is desirable. The

ratio of 5.397 indicates an adequate signal. This model can be used to navigate the design space.

Factor	Coefficient Estimate	df	Standard Error	95% CI Low	95% CI High	VIF
Intercept	2.65	1	0.42	1.57	3.73	
B-tabletting speed	1.61	1	0.56	0.18	3.04	1.00

Final Equation in Terms of Coded Factors:

$$\text{SD Mass Av102} = +2.65 + 1.61 * B$$

Final Equation in Terms of Actual Factors:

$$\text{SD Mass Av102} = +0.23500 + 0.040250 * \text{tableting speed}$$

A.17 ANOVA of Av102 tablet mass SD with nonsignificant factors included (Study 2.4.3.1)

Response: Av102_SD_tablet_mass_nonsignificant_factors_included

ANOVA for selected factorial model

Analysis of variance table [Partial sum of squares - Type III]

Source	Sum of Squares	df	Mean Square	F Value	p-value Prob > F	
Model	12.74	2	6.37	6.61	0.0540	not significant
A-paddle wheel speed	2.37	1	2.37	2.46	0.1919	
B-tabletting speed	10.37	1	10.37	10.75	0.0305	
Residual	3.86	4	0.96			
Lack of Fit	2.94	2	1.47	3.23	0.2366	not significant
Pure Error	0.91	2	0.46			
Cor Total	16.60	6				

The Model F-value of 6.61 implies there is a 5.40% chance that a "Model F-Value" this large could occur due to noise. Values of "Prob > F" less than 0.0500 indicate model terms are significant. In this case B is a significant model term. Values greater than 0.1000 indicate the model terms are not significant. If there are many insignificant model terms (not counting those required to support hierarchy), model reduction may improve the model. The "Lack of Fit F-value" of 3.23 implies the Lack of Fit is not significant relative to the pure error. There is a 23.66% chance that a "Lack of Fit F-value" this large could occur due to noise.

Std. Dev.	0.98	R-Squared	0.7676
Mean	2.65	Adj R-Squared	0.6514
C.V. %	37.06	Pred R-Squared	0.1081
PRESS	14.80	Adeq Precision	7.404

The "Pred R-Squared" of 0.1081 is not as close to the "Adj R-Squared" of 0.6514 as one might normally expect. This may indicate a large block effect or a possible problem with the model and/or data. Things to consider are model reduction, response transformation, outliers, etc.

"Adeq Precision" measures the signal to noise ratio. A ratio greater than 4 is desirable. The ratio of 7.404 indicates an adequate signal. This model can be used to navigate the design space.

Factor	Coefficient Estimate	df	Standard Error	95% CI Low	95% CI High	VIF
Intercept	2.65	1	0.37	1.62	3.68	
A-paddle wheel speed	0.77	1	0.49	-0.59	2.13	1.00
B-tabletting speed	1.61	1	0.49	0.25	2.97	1.00

Final Equation in Terms of Coded Factors:

$$\begin{aligned} \text{SD Mass Av102} &= \\ &+2.65 \\ &+0.77 * A \\ &+1.61 * B \end{aligned}$$

Final Equation in Terms of Actual Factors:

$$\begin{aligned} \text{SD Mass Av102} &= \\ &-1.30500 \\ &+0.038500 * \text{paddle wheel speed} \\ &+0.040250 * \text{tabletting speed} \end{aligned}$$

A.18 ANOVA of Destab PWR filling level (Study 2.4.3.1)

Response: Destab_filling_level

ANOVA for selected factorial model

Analysis of variance table [Partial sum of squares - Type III]

Source	Sum of Squares	df	Mean Square	F Value	p-value Prob > F	
Model	0.14	1	0.14	11.80	0.0414	significant
A-paddle wheel speed	0.14	1	0.14	11.80	0.0414	
Residual	0.037	3	0.012			
Cor Total	0.18	4				

The Model F-value of 11.80 implies the model is significant. There is only a 4.14% chance that a "Model F-Value" this large could occur due to noise. Values of "Prob > F" less than 0.0500 indicate model terms are significant. In this case A is a significant model term. Values greater than 0.1000 indicate the model terms are not significant. If there are many insignificant model terms (not counting those required to support hierarchy), model reduction may improve the model.

Std. Dev.	0.11	R-Squared	0.7973
Mean	13.78	Adj R-Squared	0.7297
C.V. %	0.80	Pred R-Squared	0.3353
PRESS	0.12	Adeq Precision	5.431

The "Pred R-Squared" of 0.3353 is not as close to the "Adj R-Squared" of 0.7297 as one might normally expect. This may indicate a large block effect or a possible problem with the model and/or data. Things to consider are model reduction, response transformation, outliers, etc. "Adeq Precision" measures the signal to noise ratio. A ratio greater than 4 is desirable. The ratio of 5.431 indicates an adequate signal. This model can be used to navigate the design space.

Factor	Coefficient Estimate	df	Standard Error	95% CI Low	95% CI High	VIF
Intercept	13.78	1	0.049	13.63	13.94	
A-paddle wheel speed	-0.19	1	0.055	-0.37	-0.014	1.00

Final Equation in Terms of Coded Factors:

$$\text{FL Destab} = +13.78 - 0.19 * A$$

Final Equation in Terms of Actual Factors:

$$\text{FL Destab} = +14.16400 - 9.50000\text{E-}003 * \text{paddle wheel speed}$$

A.19 ANOVA of Destab PWR filling level nonsignificant factors included (Study 2.4.3.1)

Response: Destab_filling_level_nonsignificant_factors_included

ANOVA for selected factorial model

Analysis of variance table [Partial sum of squares - Type III]

Source	Sum of Squares	df	Mean Square	F Value	p-value Prob > F	
Model	0.18	2	0.088	40.93	0.0239	significant
A-paddle wheel speed	0.14	1	0.14	66.85	0.0146	
B-tabletting speed	0.032	1	0.032	15.00	0.0607	
Residual	4.320E-003	2	2.160E-003			
Cor Total	0.18	4				

The Model F-value of 40.93 implies the model is significant. There is only a 2.39% chance that a Model F-Value" this large could occur due to noise. Values of "Prob > F" less than 0.0500 indicate model terms are significant. In this case A is a significant model term. Values greater than 0.1000 indicate the model terms are not significant. If there are many insignificant model terms (not counting those required to support hierarchy), model reduction may improve the model.

Std. Dev.	0.046	R-Squared	0.9761
Mean	13.78	Adj R-Squared	0.9523
C.V. %	0.34	Pred R-Squared	0.7653
PRESS	0.042	Adeq Precision	15.556

The "Pred R-Squared" of 0.7653 is in reasonable agreement with the "Adj R-Squared" of 0.9523. "Adeq Precision" measures the signal to noise ratio. A ratio greater than 4 is desirable. The ratio of 15.556 indicates an adequate signal. This model can be used to navigate the design space.

Factor	Coefficient Estimate	df	Standard Error	95% CI Low	95% CI High	VIF
Intercept	13.78	1	0.021	13.69	13.87	
A-paddle wheel speed	-0.19	1	0.023	-0.29	-0.090	1.00
B-tabletting speed	-0.090	1	0.023	-0.19	9.985E-003	1.00

Final Equation in Terms of Coded Factors:

$$\begin{aligned} \text{FL Destab} &= \\ &+13.78 \\ &-0.19 * A \\ &-0.090 * B \end{aligned}$$

Final Equation in Terms of Actual Factors:

$$\begin{aligned} \text{FL Destab} &= \\ &+14.29900 \\ &-9.50000\text{E-}003 * \text{paddle wheel speed} \\ &-2.25000\text{E-}003 * \text{tabletting speed} \end{aligned}$$

A.20 ANOVA of Destab tablet mass (Study 2.4.3.1)

Response: Destab_tablet_mass

ANOVA for selected factorial model

Analysis of variance table [Partial sum of squares - Type III]

Source	Sum of Squares	df	Mean Square	F Value	p-value Prob > F	
Model	2.977E-003	2	1.489E-003	13.52	0.0689	not significant
A-paddle wheel speed	4.229E-007	1	4.229E-007	3.840E-003	0.9562	
B-tabletting speed	2.977E-003	1	2.977E-003	27.03	0.0351	
Residual	2.203E-004	2	1.101E-004			
Cor Total	3.198E-003	4				

The Model F-value of 13.52 implies there is a 6.89% chance that a "Model F-Value" this large could occur due to noise. Values of "Prob > F" less than 0.0500 indicate model terms are significant. In this case B is a significant model term. Values greater than 0.1000 indicate the model terms are not significant. If there are many insignificant model terms (not counting those required to support hierarchy), model reduction may improve the model.

Std. Dev.	0.010	R-Squared	0.9311
Mean	0.36	Adj R-Squared	0.8622
C.V. %	2.88	Pred R-Squared	0.7413
PRESS	8.273E-004	Adeq Precision	6.792

The "Pred R-Squared" of 0.7413 is in reasonable agreement with the "Adj R-Squared" of 0.8622. "Adeq Precision" measures the signal to noise ratio. A ratio greater than 4 is desirable. The ratio of 6.792 indicates an adequate signal. This model can be used to navigate the design space.

Factor	Coefficient Estimate	df	Standard Error	95% CI Low	95% CI High	VIF
Intercept	0.36	1	4.693E-003	0.34	0.38	
A-paddle wheel speed	-3.251E-004	1	5.247E-003	-0.023	0.022	1.00
B-tabletting speed	-0.027	1	5.247E-003	-0.050	-4.704E-003	1.00

Final Equation in Terms of Coded Factors:

$$\begin{aligned} \text{Mass Destab} &= \\ &+0.36 \\ &-3.251\text{E-}004 * A \\ &-0.027 * B \end{aligned}$$

Final Equation in Terms of Actual Factors:

$$\begin{aligned} \text{Mass Destab} &= \\ &+0.40569 \\ &-1.62569\text{E-}005 * \text{paddle wheel speed} \\ &-6.82003\text{E-}004 * \text{tabletting speed} \end{aligned}$$

A.21 ANOVA of Destab tablet mass SD (Study 2.4.3.1)

Response: Destab_SD_tablet_mass

ANOVA for selected factorial model

Analysis of variance table [Partial sum of squares - Type III]

Source	Sum of Squares	df	Mean Square	F Value	p-value Prob > F	
Model	20.06	2	10.03	2.18	0.3141	not significant
A-paddle wheel speed	4.93	1	4.93	1.07	0.4091	
B-tabletting speed	15.13	1	15.13	3.29	0.2112	
Residual	9.19	2	4.59			
Cor Total	29.25	4				

The "Model F-value" of 2.18 implies the model is not significant relative to the noise. There is a 31.41 % chance that a "Model F-value" this large could occur due to noise. Values of "Prob > F" less than 0.0500 indicate model terms are significant. In this case there are no significant model terms. Values greater than 0.1000 indicate the model terms are not significant.

Std. Dev.	2.14	R-Squared	0.6859
Mean	3.00	Adj R-Squared	0.3718
C.V. %	71.40	Pred R-Squared	-1.9110
PRESS	85.14	Adeq Precision	3.680

A negative "Pred R-Squared" implies that the overall mean is a better predictor of the response than the current model. "Adeq Precision" measures the signal to noise ratio. A ratio of 3.68 indicates an inadequate signal and therefore this model should not be used to navigate the design space.

Factor	Coefficient Estimate	df	Standard Error	95% CI Low	95% CI High	VIF
Intercept	3.00	1	0.96	-1.12	7.13	
A-paddle wheel speed	1.11	1	1.07	-3.50	5.72	1.00
B-tabletting speed	1.94	1	1.07	-2.67	6.56	1.00

Final Equation in Terms of Coded Factors:

$$\begin{aligned} \text{SD Mass Dest} &= \\ &+3.00 \\ &+1.11 * A \\ &+1.94 * B \end{aligned}$$

Final Equation in Terms of Actual Factors:

$$\begin{aligned} \text{SD Mass Dest} &= \\ &-2.13550 \\ &+0.055500 * \text{paddle wheel speed} \\ &+0.048625 * \text{tabletting speed} \end{aligned}$$

B Curriculum vitae

The CV is not published for reasons of data protection.

C Conference contributions and publications

In context with this work, the following contributions have been presented at conferences and journal articles have been published.

Conference contribution - poster presentation*






Dülmeyer, K.P., Özcoban, H., Leopold, C.S.
A novel method for determination of the filling level in the feed frame of a rotary
tablet press
11th PBP World Meeting, Granada, Spain (2018)

*Conference contributions were not permitted due to non-disclosure agreement until September 2017.

Journal articles with authors contributions and reference chapters.

Title	Journal	Authors	Contribution to the work	Percentage	Reference chapters
A novel method for determination of the filling level in the feed frame of a rotary tablet press	Drug Development and Industrial Pharmacy (accepted)	Dühlmeyer, K.P. Özcoban, H. Leopold, C.S.	Project plan, experiments, data analysis, publication Supervisor Supervisor	95 % 5%	3.1
Comparison of two paddle wheel geometries within the filling chamber of a rotary tablet press feed frame with regard to the distribution behavior of a model powder and the influence on the resulting tablet mass	Drug Development and Industrial Pharmacy (accepted)	Dühlmeyer, K.P. Özcoban, H. Leopold, C.S.	Project plan, experiments, data analysis, publication Supervisor Supervisor	95 % 5%	3.3, 3.5
Inline monitoring of the powder filling level within a rotary tablet press feed frame	Powder Technology (accepted)	Dühlmeyer, K.P. Özcoban, H. Leopold, C.S.	Project plan, experiments, data analysis, publication Supervisor Supervisor	95 % 5%	3.4
Investigation of the distribution behavior of different powders within the filling chamber of a rotary tablet press feed frame	Pharmazeutische Industrie (accepted)	Dühlmeyer, K.P. Leopold, C.S.	Project plan, experiments, data analysis, publication Supervisor	100 %	3.2

D Hazardous materials

Substance	Supplier	Danger symbol	Hazard statements	Precautionary statements
Benzoyl peroxide*	Motip Dupli		H241, H317, H319, H410	P101, P102, P210, P261, P273, P280, P305+351+338, P333+313, P420, P501
Ethylene glycol*	Motip Dupli		H302, H373	P101, P102, P301+P312+P330
Fumed silica*	Motip Dupli		H319, H335	P101, P102, P280
Vinyltoluene*	Motip Dupli		H226, H304, H332, H315, H319	P101, P102, P280, P302, P352, P501
Styrene*	Motip Dupli		H226, H332, H315, H319, H361d, H372	P101, P102, P210, P302+352, P305+351+338, P314

* Component of polyester filling putty used for the enclosure of the sealing segment of the feed frame.

E Declaration on oath / Eidesstattliche Versicherung

Hiermit erkläre ich an Eides statt, dass ich die vorliegende Dissertationsschrift selbst verfasst und keine als die angegebenen Quellen und Hilfsmittel benutzt habe. Ich versichere zudem, keinen weiteren Promotionsversuch an einer anderen Einrichtung unternommen zu haben.

Hamburg, den _____

Kym Patrick Dühlmeier
